Lawrence Berkeley Laboratory
UNIVERSITY OF CALIFORNIA

Presented at the IX Workshop on Nuclear Physics,
Buenos Aires, Argentina, June 23 - July 4, 1986;
and to be published in the Proceedings

HIGH-SPIN NUCLEAR SPECTROSCOPY

R.M. Diamond

July 1986

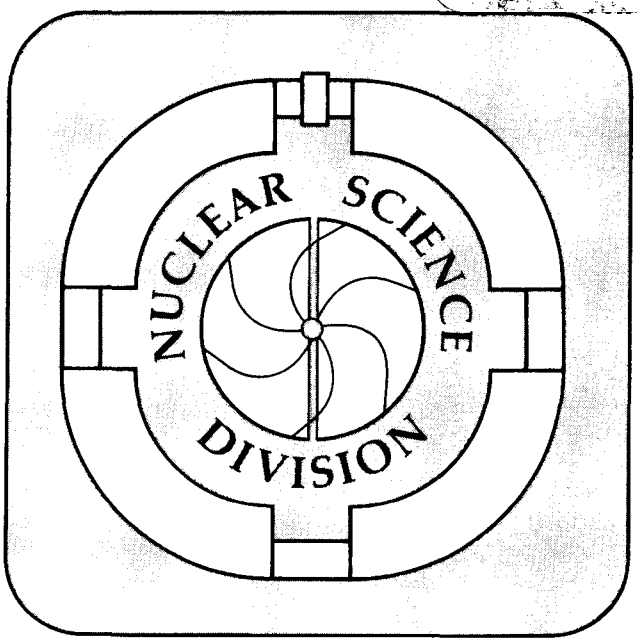

Prepared for the U.S. Department of Energy under Contract DE-AC03-76SF00098

DISCLAIMER

LBL-21863

High-Spin Nuclear Spectroscopy

Richard M. Diamond

Nuclear Science Division
Lawrence Berkeley Laboratory
University of California
Berkeley, California 94720

This work was supported by the Director, Office of Energy Research, Division of Nuclear Physics of the Office of High Energy and Nuclear Physics of the U.S. Department of Energy under Contract DE-AC03-76SF00098.

HIGH-SPIN NUCLEAR SPECTROSCOPY

Richard M. Diamond

Nuclear Science Division, Lawrence Berkeley Laboratory
University of California, Berkeley, California 94720
USA

ABSTRACT

High-spin spectroscopy is the study of the changes in nuclear structure, properties, and behavior with increasing angular momentum. It involves the complex interplay between collective and single-particle motion, between shape and deformation changes, particle alignments, and changes in the pairing corrleations. By the use of new techniques, instruments, and theoretical calculations great strides have been made in the last few years, but much remains to be understood.

1. INTRODUCTION

High-spin nuclear physics is nuclear physics where the Coriolis and centrifugal interactions have become large enough to compare and compete with the pairing interactions and shell effects that dominate nuclear behavior at low spin. The limit to the amount of angular momentum a nucleus can hold is given when the Coriolis and centrifugal forces become so large as to cause the nucleus to fission. The variation of nuclear properties and behavior with the spin coordinate axis is as fundamental a study as that with the excitation energy or the neutron or proton number of a nucleus.

The full range of angular momentum possible in a nucleus can usually be produced in a heavy-ion fusion reaction (H.I.,xn). Neutrons carry off most of the product excitation energy, but little of its angular momentum. When not enough energy is left to emit

another particle, the remaining excitation energy and angular momentum is removed by γ-ray cascades, as shown schematically in fig. 1. There is a line below which no states of a given spin exist; this is the yrast line. After the initial particle evaporation, much of the area between the yrast line and the entry limit (approximately a neutron binding energy higher) is populated, and so there are a great number of pathways down towards the ground state. The initial transitions have too little intensity to be observed individually, even by the highest resolution detectors available today, and so these produce the "continuum" γ-ray spectrum. This consists of two main types of γ-rays: the "statistical" ones, a small number of transitions (represented by the vertical arrows in fig. 1) that carry off energy but little angular momentum; and the "yrast-like" transitions that run roughly parallel to the yrast line and remove the angular momentum and some excitation energy. Eventually the cascades lose enough energy so that they come to the region of low level density near the yrast line, and there they condense into a small enough number of pathways that the individual transitions can be detected, forming the discrete γ-ray spectrum. The latter has been the backbone of in-beam γ-ray spectroscopy. To give you some feeling for the relative intensities involved, discrete transitions, with one exception so far, can only be seen below about spin 46ħ, and their intensity is ~1% at spin 40ħ and 20-40% at spin 20ħ in rare-earth nuclei (where the highest spins are possible and where much of the experimental work has been concentrated). With increasingly better instruments and better statistics, we can push discrete γ-ray spectroscopy to still lower intensities and thus higher spins, but in general if we want to know about nuclear properties and behavior at very high spins, we must study the continuum spectra. Thus my discussion of experimental results and interpretation will be divided into two main sections: discrete and continuum γ-ray spectroscopy. Figure 2 shows a spectrum taken of the sum of these cascades; on average a cascade in this example has 20-25 transitions, and shows three components. The discrete transitions that are along and near the yrast line at the lower spins are obvious. Underneath these

peaks and extending above 1 MeV is the "yrast bump," the unresolved yrast-like transitions. At still higher energies is a tail that decreases exponentially with increasing γ-ray energy. This exponential fall-off is a signature of the statistical transitions, and comes from the exponential increase in the level density with excitation energy above the yrast line. The intensity of the spectrum above the yrast-bump edge corresponds to 1½-2 transitions per average cascade, but to determine the total number of statistical transitions, those that lie below 1.5 MeV must be estimated. The shape of the statistical component may be approximated by an expression of the form:

$$N_\gamma = N E_\gamma^n \exp[-(E_\gamma/T)] \quad , \qquad (1)$$

where N and T are constants to be fixed by fitting the spectrum above the edge of the yrast bump, and n is usually taken to be 3 (for dipole transitions). In this particular example, another 2 transitions can be estimated to lie below 1.5 MeV, giving a total of ~4 statistical transitions. This value is in agreement with other methods for estimating this number in this mass region, but the number of statistical transitions per average cascade does vary from 2-6 depending upon the cascade multiplicity itself. The current picture that has emerged from what little study of the high-energy statistical-tail region that has been performed is: the high-energy transitions are probably E1 (from angular distribution and correlation experiments[1-4] and conversion-electron measurements,[5,6] and the angular distribution is essentially isotropic, implying that the transitions are a mixture of approximately ½-⅝ stretched and ⅛-½ unstretched dipoles, thus carrying off little angular momentum.

However, it is the study of the discrete transitions that has given us in the past the most information about the nucleus, and so that is where we shall start. Their spectrum may show one of two limiting patterns, corresponding to the two principal ways that nuclei can take up angular momentum: by the collective rotation of a deformed nucleus as a whole and by the alignment of individual high-j nucleons along the rotation axis. For spherical (or near-spherical)

nuclei, the latter mode is the only one possible. On the right in fig. 3 the levels of ^{212}Rn illustrate a scheme of particle alignment[7]; it is quite irregular with transitions of a variety of electromagnetic types and with little apparent pattern to the level spacing (but in agreement with shell-model calculations). On the left, the yrast band of ^{238}U is shown,[8] a predominantly rotational scheme with only strongly enhanced electric quadrupole transitions and a level spacing that approximates that of a rigid rotor.

$$E = \frac{\hbar^2}{2J} I(I+1) \qquad (2a)$$

$$I = 0, 2, 4, \ldots$$

$$E_\gamma = \frac{\hbar^2}{2J} (4I - 2) \qquad (2b)$$

where J is the moment of inertia. Most nuclei, however, combine both types of motion, and it is this interplay between collective and single-particle motion that makes the behavior of nuclei along the angular momentum coordinate so fascinating and so rich in variety.

Consider, for example, the moment of inertia as defined by eq. (2b). If the nucleus were rigid, J would be a constant. But a nucleus is not rigid; the nucleons move throughout the nuclear volume, and values for the moments of inertia of deformed nuclei at low spin are smaller than rigid-body values by factors of ~3. This reduction is due to correlations in the nucleonic motion, in particular to the pairing interactions.[9] With an increase in either nuclear excitation or nuclear spin, the moment of inertia is expected to rise toward the rigid-body value. Figure 4 shows[10] at top a plot of $2J/\hbar^2$ vs $\hbar\omega$ for ^{158}Er where $\hbar\omega \approx \Delta E/\Delta I = E_\gamma/2$ and ω is often called the rotational frequency. For low values of ω there is a gradual, but smooth, rise in J. This occurs because the increase in ω increases the Coriolis interaction on the paired nucleons, weakening the pairing correlations (Coriolis anti-pairing) and so increasing the value of J. But since the Coriolis force is also proportional to the j of the particle, it acts most strongly on the high-j particles. Thus on the background of gradually increasing J there are occasional sharp, irregular increases, where the nucleus

finds it energetically more favorable to align a pair of high-j particles rather completely while essentially keeping the pairing correlations among the lower-j nucleons.[11,12] This process corresponds to a bandcrossing between the completely paired ground band and an excited band with two aligned particles (and a larger effective moment of inertia). Above the crossing the two-particle band becomes the yrast one, and the gain in aligned spin (bottom of fig. 4) allows the nucleus as a whole to slow down, to decrease its collective rotation. In the rare-earth region, it is the alignment of a pair of $i_{13/2}$ neutrons that causes the sudden jump in the value of J at $\hbar\omega \sim 0.25$ Mev.

Experimentally, the γ-ray transition energies at a bandcrossing may show a decrease, rather than the smooth increase with spin expected from eq. (2b), and this phenomenon has been called "backbending." Some nuclei in this region, e.g. ^{158}Er, show a second smaller irregularity at $\hbar\omega \sim 0.4$ MeV when a pair of protons or a second pair of neutrons align to make a four-particle band yrast. It has become customary to denote individual quasiparticles by letters. For example, A, B, C, and D represent the lowest-lying unique-parity orbitals in the valence shell, and E, F represent the lowest-lying normal-parity ones. For neutrons in the fifth shell, this corresponds to the $i_{13/2}$ orbitals and mixed $f_{7/2}$ and $h_{9/2}$ ones, respectively. Proton orbitals are indicated either by a subscript p, or the use of small letters, e.g., a, b, e.

A whole new spectroscopy of these backbends or alignments has developed over the last few years. Initially, most of the data were on the alignment of a pair of $i_{13/2}$ neutrons, which gave the first backbend in the rare-earth region, but by now there is information available on other high-j orbitals in other parts of the Periodic table (e.g., the $h_{11/2}$ protons and neutrons in the light rare-earth region and immediately below, and the $g_{9/2}$ protons and neutrons in the region below the tin isotopes) and about higher backbends. In fig. 5 the relative aligned spin, i, for the pairs of $i_{13/2}$ neutrons is plotted against rotational frequency for three bands.[13] The

solid line is for the lowest-energy band in the even-even nucleus ^{162}Yb, similar to that in ^{158}Er. The frequency of the crossing is about 0.26 MeV and the aligned angular momentum is ~10$\hbar$ (12$\hbar$ is the maximum for two $i_{13/2}$ neutrons). The dashed lines are for two bands in ^{163}Yb with the additional neutron located in an (predominantly $h_{9/2}$) orbital labeled E or F. In ^{162}Yb, this pair of states (E,F) is available for the pairing correlations, and, in particular, a pair of $i_{13/2}$ neutrons can scatter into it. On the other hand, in ^{163}Yb it is blocked by the odd nucleon for the bands based on either E or F. The pairing correlations are thereby weaker in general, and in particular for a pair of $i_{13/2}$ neutrons. It is then easier to unpair and align the $i_{13/2}$ neutrons, and this occurs at a lower rotational frequency, ~0.22 MeV, as seen in fig. 5. The shift, $\delta\hbar\omega_c$, is clear and also occurs in other nearby nuclei.[14] Thus, blocking just one orbital near the Fermi level reduces the pairing correlations appreciably, a result that is in agreement with transfers of pairs of nucleons and the odd-even mass difference.

But the analysis of data like that shown in fig. 5 can be carried even further. Most of the calculations of nuclear pairing correlations assume equal scattering for any orbital equally distant from the Fermi level ("monopole pairing"). This is, in fact, not very reasonable, since those orbitals that have better spatial overlap (are more similar) with the aligning nucleons (in this case, $i_{13/2}$ neutrons) will affect the pairing more (larger $\delta\hbar\omega_c$). One measure of the shape of an orbit is its quadrupole moment relative to the nuclear symmetry axis. The aligning $i_{13/2}$ neutrons have a large positive (prolate) quadrupole moment, and it has been found[15] that the magnitude of $\delta\hbar\omega_c$ is reasonably clearly correlated with the similarity of the quadrupole moment of the blocked state to this value (fig. 6). In fact, the $11/2^-[505]$ orbital is strongly oblate (very different), and blocking it produces no difference in the pairing behavior of the $i_{13/2}$ neutrons ($\delta\hbar\omega_c \sim 0$), while prolate orbitals do decrease $\hbar\omega_c$. These higher order effects[16] are referred to as "quadrupole pairing," and such studies can be extended to additional blocked orbitals and other aligning pairs. They are a

good example of the detailed nuclear structure information now becoming available from in-beam γ-ray spectroscopy, and described in recent reviews.[17-21] I shall return later to still newer developments. Now I would like to turn briefly to the new type of instrumentation that is making possible even more detailed investigations.

2. HERA, THE HIGH-ENERGY-RESOLUTION ARRAY

Nuclear spectroscopic studies are often limited, as are most types of spectroscopy, by either insufficient resolution or insufficient statistics, or both. Almost five years ago Frank Stephens and I began planning a high-resolution, high-statistics γ-ray system in order both to push discrete-line work to higher spins and to help with continuum studies.[22] Our three primary criteria for a high-resolution array were: high (good) energy resolution, good response function, and good efficiency. Three secondary features we desired were: capability of a total-energy spectrometer, capability as a multiplicity filter, and a prompt initial timing signal.

Germanium detectors provide the highest resolution for γ-rays (2 keV for a 1 MeV γ ray) possible with reasonable efficiency, so our system is based on an array of such detectors. Can we do better? With a single detector, no. If two γ rays fall on the same point (within the 2 keV resolution), they cannot be resolved by that detector. But the γ rays we are interested in are usually not single events; rather they are members of a cascade and are in coincidence with the other members. If two (or more) detectors are used, the coincidence relationships between the two overlapping γ rays and the other members of their individual cascades may serve to resolve them, as illustrated in fig. 7. The number of resolvable points in the 2-dimensional matrix is squared, and it is much less probable that the two pairs of γ rays coincide than the original single lines. Still higher order coincidences give still higher effective resolution for coincident cascades of γ rays by enormously increasing the number of possible resolvable points in the higher-dimensional space, e.g., a triple coincidence would cube the number of resolvable points. Thus, a desirable feature for our array

is to have as many detectors as close as is reasonably possible to the target, in order to favor high-order coincidences.

The second criterion is to have a good response function, i.e., every γ ray that strikes the detector should result in an output signal proportional to the original γ-ray energy. A Ge counter does not fulfill this requirement very well. It is a relatively low Z, moderately dense material that interacts with γ rays in the energy range of interest principally by Compton scattering. With a 5 x 5 cm Ge detector (approximately 20% the efficiency of a 7.6 x 7.6 cm NaI detector for 1.33 MeV γ rays) a 1.33 MeV γ ray has an absorption probability of ~3/4 and a peak to total (P/T) ratio of 15-20%. This means that ~1/4 of such γ rays do not interact at all with the detector, and that of those that do, only 15-20% give useful full-energy peaks. In a doubles coincidence measurement, only 2-4% of the events obtained are good peak-peak values; the remaining 96-98% are unwanted garbage. This is a very undesirable situation, and the solution has been known for some time; put Compton-suppression shields around the Ge detectors. This was done at Daresbury[23] four years ago. Large 20 x 25 cm NaI shields were placed on six Ge detectors placed around the target, giving a markedly improved peak/total ratio and creating TESSA2, which became the leading instrument for γ-ray spectroscopy in the world for the next two years. We, however, had decided to try for bismuth germanate (BGO) shields, for, if successful, they offered a great advantage over NaI. The material is considerably denser than NaI (7.13 to 3.67 g/cm^3) and of higher average Z, so that it has a γ-ray absorption length 2½ times smaller than NaI. This means more compact shields, so that more Compton-suppressed detectors can be placed near the target to give the higher order coincidences discussed in the previous paragraph. But bismuth germanate also has two serious handicaps. First, the light output is only 10-15% that of NaI. Second, at that time (1981) the companies that marketed it had not made BGO single crystals large enough to serve this purpose, as shields of the order of 13 cm or more in diameter and length were needed. We solved this latter problem by having the shield made out

of six pieces that fit together to form a cylindrical shell, each with its own photomultiplier tube. This was the first use of BGO as an anti-Compton shield, and I believe that all of the Compton-suppression shields that have been made since from BGO have been produced in this way.

A schematic drawing of our BGO shield (showing two of the six photomultiplier tubes) is given in fig. 8. It is a coaxial design, so that there is no shield material at the front opening where the γ rays come in to the Ge detector, nor at the rear where the snout of the Ge detector enters. Lack of coverage at the latter position means that Compton-scattered γ rays in the angular range of 0°-25° (multiple Compton scattering in the Ge crystal and primary interactions throughout the whole volume of the Ge smear these angles out) will not be caught by the shield, leaving the complementary non-full-energy transition in the resulting spectrum. We do not believe these low-energy transitions pose a serious problem, although their effect can be decreased by reducing the snout behind the Ge detector to a minimum diameter and then surrounding it with additional shield material. (Of course the transverse shields do not have this hole, but they have one at the side instead.) But the opening at the front is more disturbing, as the (low energy) γ rays Compton-scattered through about 135°-180° correspond to leaving in the spectrum the Compton edges just below the full energy peaks. The edges appear just where we are interested in having a clean, low-background region. By the addition of a NaI "cap" to the front of the BGO shield, as shown schematically in fig. 8, we can almost completely wipe out the Compton-edge peaks. Figure 9 shows two spectra of ^{60}Co taken with one of our Ge detectors, a Compton- suppressed one taken with the BGO shield and NaI cap and an unsuppressed one normalized to the same full-energy peak heights. The peak/total ratio for ^{60}Co above a 300 keV threshold improves from ~20% with the bare detector to 50% with the BGO shield and to 55% with the cap. Other designs using larger BGO shields can give P/T ratios of 60-70% for ^{60}Co, so tremendous improvement in the Ge response function is possible. For coincidence experiments this makes an enormous difference as shown in

Table I. Note, for example, that with bare Ge detectors full-energy triple coincidences are only 0.8% of the events, so that triple coincidences have not been used in in-beam spectroscopy. But with a 50% P/T ratio, 12.5% are good events making them quite useable. And still higher ratios are possible.

The system efficiency involves the questions of how many Ge detectors at what distance from the target. With the design shown in

TABLE I 20% Ge detector (counts above 300 keV).

	Ge^1	Ge^2	Ge^3	Ge^4
Peak/Total	0.2	0.04	0.008	0.0016
Compton-suppressed Peak/Total	0.5	0.25	0.13	0.06
Improvement factor	2.5	6	16	39

fig. 8 involving 13 x 13 cm shields, some units will touch at their tapered cones when 13-14 cm from the target. If we take 15 cm as the distance from the target to the face of the 5 x 5 cm Ge detector inside the BGO shield, we find we can place 21 detectors at this distance and still leave the top and bottom above the target clear. This will be necessary to accommodate the photomultiplier tubes for a small, central BGO ball between the target and the Ge modules.

It should be mentioned that γ-ray summing in the individual Ge detectors also limits their size and closeness to the target, but is ~5% for γ-ray cascades of multiplicity 20-25 in this arrangement. This is probably O.K. for most purposes; if not the geometric efficiency must be reduced. A final limitation on closeness is the magnitude of Doppler broadening for the detectors near 90° to the beam (product recoil) direction. This must be considered for each nuclear system studied, as the effect can be quite large in (H.I.,xn)

reactions where the recoils attain several percent the speed of light. For example, in a typical case, ~180 MeV ^{40}Ar on ^{124}Sn, the recoiling compound nucleus has a velocity ~2.5% that of light. The first-order Doppler shift for a γ ray emitted by such a moving source is

$$\frac{E - E_0}{E_0} = \frac{v}{c} \cos \theta \qquad (3)$$

where θ is the angle between the detector and the recoiling nucleus. So near 0° or 180° the Doppler shift is quite large, ~25 keV for a 1 MeV γ ray. But the broadening there due to the finite opening-half-angle ϕ of the detector

$$\frac{\Delta E}{E_0} \approx 2 \frac{v}{c} \sin \theta \sin \phi \qquad (4)$$

is quite small, $\leq$1/2 keV for $\phi = 9.5°$. By using a thin target or multiple thin targets, the full Doppler shift is obtained, but since this corresponds to a change in gain it can be corrected for in the amplifier or ADC or in the analysis program with no loss in resolution. On the other hand, for angles of θ near 90°, the Doppler shift becomes small, but the broadening becomes a maximum. For the 180 MeV ^{40}Ar + ^{124}Sn example, $\Delta E/E_0 \approx 0.8\%$ or 8 keV broadening for a 1 MeV transition. Such a smearing of the energy ruins the resolution of the detector, but can be reduced or avoided altogether under certain conditions. For example, if such a product nucleus recoils out of the target into a lead or gold backing, it will stop in the order of picoseconds. If the transitions are emitted after stopping, there will be no Doppler shift or broadening. Thus, nuclei that have some slow, non-collective transitions in their de-excitation cascades can, and do, take picoseconds to de-excite and do not present a problem. But if the γ rays are fast, something has to be done to alleviate the Doppler broadening; the detectors must be pulled back further, or collimated, or both, in order to decrease the detector opening angle, and thus the broadening.

With these considerations in mind, we designed the High-Energy-Resolution-Array to consist of 21 BGO-shielded Ge detectors arranged

(in three rings of seven detectors) around a small, central "ball" or "castle" of 40 BGO sectors. Some of the latter have holes through which the Ge detectors see the target, and the 40 together form a sum spectrometer and multiplicity filter around the target, as well as giving the angular pattern of the γ rays emitted. A sideview of the arrangement is given in fig. 10, which shows one detector from each ring. Not shown are the NaI caps on the BGO shields, nor are the photomultiplier tubes drawn in on either the shields or the central ball sectors. For the BGO sectors in the upper half of the central ball, the photomultiplier tubes go up from the top faces of the sectors, and for those in the lower half, the tubes go downwards from the bottom faces. A cut-away perspective drawing of the system is shown in fig. 11, and a photograph of the 21-detector array, without the central ball (not yet built) and without the 21 NaI nose cones, is shown in fig. 12. With 21 detectors at 15 cm from the target, an event rate of 10^5/second (the order of our usual rate in a (^{40}Ar,xn) reaction with a 1 mg/cm^2 target and a 2 pna beam), and an average γ-ray multiplicity of 20, we had estimated the double-, triple-, and quadrupole-coincidence rates to be 11 K/s, 2.2 K/s and 280/s, respectively. We have achieved these rates routinely and have even gone somewhat higher. The system performs well. Although it represents the state of the art today, it is not the last word, and it will be very exciting to see what directions instrumentation for nuclear spectroscopy takes in the next few years.

The 21-detector array (without the central ball or NaI cones) has been operating for a year-and-a-half, and I shall spend the rest of my time discussing experimental results obtained mainly with it and with TESSA2 and with TESSA3 (the new 12-detector, BGO-suppressed array now operating at Daresbury). This limitation is not meant in any way to deny the beautiful and significant work that is going on elsewhere in the world, but only that with my limited time I have chosen those results with which I am most familiar.

3. DISCRETE-LINE GAMMA-RAY SPECTROSCOPY

In our experiments so far, we have only recorded triple and higher coincidences on tape; double coincidences come too fast to be so handled. (In the future, they will go directly into a 2000 x 2000 matrix in a 4-megaword external memory.) But the triple and higher coincidences can be unpacked in sorting into double coincidences, and it is this two-dimensional matrix which is mainly used in working out the decay schemes. However, as mentioned in the previous section, when a transition is multiply degenerate, resolution of the problem may be accomplished by going to the triple coincidences. Or, as described below, use of the triple coincidences can give a rather clean spectrum for a particular band in a particular nucleus. Also, the requirement of at least three γ rays in coincidence discriminates efficiently against lower multiplicity processes such as Coulomb excitation and radioactivity.

In the introduction, the two limiting ways that nuclei carry angular momentum were described, and I would now like to consider some features of these cases further. Two good examples[24] of collective rotation that we have studied are ^{165,166}Yb. They were made by the reaction of 180 MeV ^{40}Ar from the Lawrence Berkeley Laboratory 88" cyclotron on ^{130}Te targets: one was two thin targets of ~0.3 mg/cm^2 on thin gold backing, and the other was ~1 mg/cm^2 on 13 mg/cm^2 gold foil. The unbacked-target data gave a (symmetrized) doubles matrix with 370 million coincidences, and the backed-target data gave a matrix with 920 million events. These matrices were used in the primary analyses of the data. But individual two-dimensional matrices for each product nucleus were also prepared by testing each γ ray in a triple or higher coincidence event against a series of discrete-line gates belonging to that nucleus and, if within any gate limit, then the other two coincident transitions were stored in the appropriate "gated ^{166}Yb" or "gated ^{165}Yb" matrix. A set of gates also produced a background matrix to be subtracted from the first two, after proper normalization. Total projections of the ^{165}Yb and ^{166}Yb gated matrices after subtraction of such an appropriate

background matrix are shown in fig. 13, together with the total projection of the full "doubles" matrix of the unbacked data. The amount of 4n in the ^{165}Yb matrix, and 5n in the ^{166}Yb matrix, is reduced considerably and the 6n channel is strongly suppressed in both matrices. The peak-to-background ratio is improved by a factor of three for energies above 450 keV in the projection derived from the gated matrices compared with that from the full matrix.

Of course this selectivity comes with a loss in statistics. The photopeaks derived from the gated matrix for ^{165}Yb contain about one tenth the number of counts in the photopeaks from the full matrix, and for ^{166}Yb, about one seventh the number. However, if one looks at spectra gated by high-spin transitions, the loss is relatively smaller for the photopeaks above the gate because of the better peak-to-background ratio in the gated matrices. To illustrate this point, the two spectra in fig. 14 are in coincidence with the same 490 keV gate, one taken in the full (top) and one in the gated matrix derived from ^{165}Yb lines (bottom). The structure of the E band in ^{165}Yb is clearly visible in the double-gated spectrum, whereas the single-gated spectrum looks confusing because of strong contamination by the 6n reaction channel. The loss in statistics of the gated matrices is partially compensated by the cleanliness of these matrices; a whole series of gates, in one band for example, can be summed in contrast to the case of the full matrix where typically only about three gates are sufficiently clean to sum. Whether the selectivity and simplicity obtained in these spectra compensate for the loss of statistics depends on the number and intensity of the photopeaks chosen as gates to create the matrix. Here the derived ^{165}Yb matrix was obtained by 19 gates (equivalent to 40% of the total feeding of the nucleus) resulting in 16 million counts in the background-subtracted matrix, and the ^{166}Yb matrix came from 35 gates (equivalent to 60% of the total feeding of the nucleus) resulting in 17 million counts.

The level schemes derived from these data are given in figs. 15 and 17 for ^{165}Yb and ^{166}Yb, and plots of I ($= \frac{I_i + I_f}{2} + 1/2$) vs. $\hbar\omega$

are shown in figs. 16 and 18. The following features may be noted.

In ^{165}Yb:

1) The lowest-lying negative-parity band, EAB, at the highest spins, crosses the lowest-lying positive-parity band, ABC, and becomes yrast.

2) The lowest positive-parity band A is observed beyond the BC crossing, we believe for the first time.

3) Because of 2) and the measurement of the branching ratios from the two $45/2^+$ states, the mixing matrix element between bands A and ABC was determined to be 47.5 keV. This compares well with the strength of the AB crossing in ^{166}Yb which is reported[25] to be 45-50 keV, but is in disagreement with cranked-shell-model (CSM) calculations that give a much larger value for the BC crossing. This is not an unusual difficulty for the calculations. However, they do usually give the right trend[26,27] with neutron number. Thus, this measurement and the calculations help predict values for nearby nuclei.

4) Band ABC and particularly band EAB appear to show the start of an upbend at the same frequency for the highest spins. We believe this may be the alignment of the first pair of protons (but see later), since they are expected to do so above $\hbar\omega$ = 0.5 MeV.

In ^{166}Yb:

1) The ground band is observed above the AB crossing and appears to undergo a different crossing, probably the BC. The gain in alignment, however, may be too large and may indicate an additional alignment of the AD neutrons to form the four-quasineutron band ABCD, as suggested[28] already for ^{164}Yb.

2) There is possible evidence for the start of an upbend at the top of the positive-parity AB band and the negative-parity AE band (see especially the upturn of $^{(2)}$ for AB in fig. 19). If this is the first proton alignment, it should occur at approximately the same frequency as in ^{165}Yb. Observation of the next couple of transitions in both nuclei would help resolve this problem.

3) But probably the most interesting feature of the high-spin states in this nucleus is that the plots of I vs $\hbar\omega$ in fig. 18 for the three two-quasineutron bands become essentially linear above $\hbar\omega \approx$

0.3 MeV (at least up to 0.55 MeV), and the lines pass through the origin.

The slope of the lines in this plot is related to the inverse of the moment of inertia of the nucleus in that configuration, and so what this means is that the bands are exhibiting a constant moment of inertia and obeying the rigid-rotor formula of eq. (2b) to an astonishing accuracy. The magnitude of this moment of inertia is about 80% of the value calculated for a rigid deformed prolate rotor with $\beta = 0.25$. This behavior is not unique to ^{166}Yb but occurs above a frequency of ~0.3 MeV for a number of nuclei,[29-35] particularly in this region. Three other examples are illustrated in fig. 19. When the first examples were found during the last three years, it was initially thought this was an illustration of the early and complete quenching of the neutron pairing by the high spin through the Coriolis interaction, and was the behavior to be expected. Indeed, there are several arguments that suggest the neutron pairing has been much reduced above $\hbar\omega \approx 0.3$ MeV. For example, in some nuclei at high frequency the yrast configuration has negative parity, e.g., ^{164}Hf, ^{165}Yb, ^{168}Yb, ^{160}Er. Cranked-shell-model calculations for these heavier rare-earth nuclei always give positive-parity configurations as yrast for neutron-pair gaps $\geq$0.3 MeV; only if the gap goes below 0.2 MeV are negative-parity yrast states possible,[30] depending upon where the Fermi surface lies. And estimates based on a model of equidistant two-fold degenerate levels indicate that the alignment of 3-4 quasineutrons in rare-earth nuclei is sufficient to destroy the neutron pair correlations.[36,37] However, the explanation for the linear regions of the plots of I vs $\hbar\omega$ does not appear to be the simple quenching of the neutron pairing, and to understand why I must digress and discuss moments of inertia in somewhat more detail first.

The problem is that there are several moments of inertia one can measure, and they are usually not constant. The first distinction to make is between kinematic and dynamic values.[38] The equation for the rotational energies of a symmetrical top is:

$$E(I) = \frac{\hbar^2}{2J} I(I+1) \quad , \tag{2a}$$

where J is the moment of inertia. Thus it may be defined from the first derivative of the energy with respect to spin:

$$\frac{J^{(1)}}{\hbar^2} = I\left(\frac{dE}{dI}\right)^{-1} = \frac{I}{\hbar\omega} \quad , \tag{5}$$

where $J^{(1)}$ is called the "kinematic" moment of inertia because it has to do with the motion of the system--the ratio of angular momentum to angular frequency and is an average over the spin range $0 \rightarrow I$. The second derivative also leads to a definition:

$$\frac{J^{(2)}}{\hbar^2} = \left(\frac{d^2E}{dI^2}\right)^{-1} = \frac{dI}{\hbar d\omega} \quad , \tag{6}$$

where $J^{(2)}$ is called the "dynamic" moment of inertia because it has to do with the way the system will respond to a force; it is a local value. If there is only the kinetic energy term as given in eq. (2a), these are equal. But, in general, when there are additional I-dependent terms in the Hamiltonian, these two moments of inertia will differ. In the present case, the Coriolis force perturbs the internal nuclear structure, giving rise, in lowest order, to an $(I \cdot j)$ term, so that $J^{(1)} \neq J^{(2)}$.

These two moments of inertia can be defined in principle for any sequence of states desired, but certain ones occur rather naturally in the decay processes. If the particle configuration is frozen, so that one is confined to a collective rotational band, the appropriate moment of inertia is $J^{(2)}_{band}$. When there is no perturbation (alignment, shape change, etc.) of the internal structure along this band, this corresponds to the true "collective" value, and this is an approximation often made. In general, however, a single decay pathway involves a sequence of bands having different alignments or shapes. It is then natural to define "effective" moments of inertia $J^{(1)}_{eff}$ and $J^{(2)}_{eff}$, which include <u>both</u> the collective spin contribution <u>and</u>, in addition, contributions caused by changes in particle alignment.

We can now go back to the straight-line behavior of the curves for I vs $\hbar\omega$ for $\hbar\omega > 0.3$ MeV (this is equivalent to saying that $\mathcal{J}^{(1)} = J^{(2)}$). Let us consider the expected properties of a system with no pairing correlations (the initially proposed explanation). If there are no shape or deformation changes, then $J^{(1)}$ should average to a particular deformed rigid-rotor value, but would not be constant due to the occurrence of particle alignments which cause jumps in $J^{(1)}$. Cranked-shell-model calculations of high-spin nuclear behavior[39,40] predict that part of the angular momentum will continue to come in these sudden alignments leaving significantly less available for the collective motion. Between alignments, $J^{(2)}_{band}$ should therefore be less than $J^{(1)}$ (around 1/2 to 2/3 on average), causing $J^{(1)}$ to drop slowly there. Thus $J^{(1)}$ is expected to oscillate around the rigid-rotor value.

This behavior is not very similar to that observed in fig. 19; we must explain the features that $J^{(2)}_{band} \approx J^{(1)}$ and that they are constant over a considerable range of frequency. There are several ways to increase the value of $J^{(2)}_{band}$. Since there have been no obvious proton alignments in the observed bands, the proton pairing correlations are almost surely not quenched. This means that the protons will contribute less angular momentum at a given frequency, resulting in an $J^{(1)}$ lower than the rigid-body value (as observed). It also means that the proton pairing will be continuously reduced by the Coriolis interaction (Coriolis anti-pairing) as $\hbar\omega$ increases. This will, by itself, contribute to an increased $J^{(2)}_{band}$ value. Also the existence of band crossings based on the alignment of an additional pair of $i_{13/2}$ quasineutrons in the positive-parity bands of odd-N nuclei and in the negative-parity bands of even-N ones argues that some neutron pair correlations must still be acting above a rotational frequency of 0.3 MeV, and their decrease will also increase $J^{(2)}_{band}$. In fact, some theorists have argued for years that the pair correlations decrease much more slowly with increasing rotational frequency than given by CSM calculations, and are only correctly given by particle-number projected calculations.[41,42] In the last year it has been recognized that even if the "static"

pairing correlations are quenched by rapid rotation, there remain "dynamic" pair correlations from the fluctuating pair gap[43] (pairing vibrations) which vary with the particle configuration, and are expected to persist to the highest frequencies observed so far, particularly with the lowest-lying positive-parity configuration. And finally, we must consider whether it is reasonable to think that the shape and deformation of the nucleus remain constant over the frequency range observed. Because $\mathcal{J}^{(1)} \approx \mathcal{J}^{(2)}$ and we appear to be dealing with a single band, that idea did seem reasonable, but lifetime measurements[44] performed recently on ^{166}Yb (described later) using the Doppler-shift attenuation method (DSAM), show that in going from spin 24^+ to 34^+ the reduced transition probabilities, B(E2)'s, decrease about 35%. This most likely occurs because of a shape and/or deformation change. If so, this by itself would cause a decrease in the moments of inertia, precisely in the region where constant values are observed. So it must be compensated by another change in the opposite direction. Particle alignment will increase the moment of inertia and will decrease the pairing correlations (as will the already mentioned Coriolis antipairing), both tending to increase $\mathcal{J}$. Hence alignments and pairing loss could compensate the shape and deformation changes and produce the locally constant effective moment of inertia which we observe. Selfconsistent cranking calculations for the ^{168}Hf case[41] reproduce the constancy of the moment of inertia after the first backbend fairly well and indicate at the same time gradual proton alignment above $I \approx 26^+$ in the yrast band. The smoothness is explained by the large interaction matrix element which one would expect for Z = 72.[27] Calculations for ^{166}Yb, which has the same neutron number but two protons less, seem to give very similar results.[45] However, these calculations do not yield a 20% decrease in β over the spin range 24 to 34, but rather a decrease of the order of a few percent to 10% while γ stays at small negative values (Lund convention). Still, no other explanation has been forthcoming, and so it remains surprising that such an apparently accidental compensation is realized over such a large frequency range in so many nuclei in the well-deformed

rare-earth region. It is an interesting problem, whether the shape change is due to the alignment of the same states in all those nuclei, and is thus systematically balanced to result in a constant effective moment of inertia. This whole question remains open today, and again illustrates how little we really know about the structure of nuclei at high spin, where shape changes, alignments, and a decrease in pairing correlations must all be considered simultaneously.

Next we will leave the region of good rotors and go to lighter transition nuclei between them and the doubly closed-shell ^{146}Gd. A number of interesting properties are predicted for nuclei in this region. Since their potential-energy surfaces are relatively shallow, small driving forces can produce different shapes. Thus the shape may change depending upon the spin, upon which valence orbitals are filled, and upon the degree of quenching of the pairing correlations through its effect on the orbital population. Band terminations are expected to occur; that is, with increasing spin a band becomes more and more triaxial (larger γ) and ends at $\gamma = 60°$ at an oblate shape. No collective rotation is left, only the angular momentum generated by the motion of the aligned particles themselves. And at very high spins ($\geq$50$\hbar$), superdeformed bands are predicted with a 2:1 axial ratio. I would like to illustrate examples of these features, and will start with a study of ^{156}Er which yielded the first example of a band termination in a medium or heavy nucleus.[46)]

This was done with nine Compton-suppressed Ge detectors (of the then incomplete HERA) in a two-day run with 170 MeV ^{40}Ar on ^{120}Sn. The target was ~1 mg/cm^2 ^{120}Sn on lead backing, and 1.2 x 10^8 γ-γ events were recorded on magnetic tape. The backing stopped the recoiling Er nuclei in ~2 psec. It was found that all the resolved γ-ray lines were emitted after stopping, due to the (previously known[47)]) long feeding times, and this improved the resolution from 3-4 keV (when thin targets were used) down to ~2 keV. No delayed transitions were observed with lifetimes longer than ~20 nsec, the electronic resolving time used.

The level scheme for ^{156}Er was constructed from the coincidence data and is shown in fig. 20. It consists of nearly 100 levels, connected by about 130 γ rays, which form five bands and pieces of two or three other bands, and has about twice the number of previously known transitions. All transitions of intensity greater than ~5% are placed in the scheme. There are a few unplaced transitions in the 2%-5% range, and many below this intensity. Because of the large number of connections among the various bands we consider the scheme reasonably certain. There are several cases, especially high in the scheme, where the ordering of transitions is not well defined, and a few uncertain assignments are included with dashed lines.

The spin assignments are based on angular correlation data. Six of the detectors were effectively at ~30° (two at ~30° and four at ~150°) and the other three at ~95°. Thus, about half of all events have one detector at ~30° and the other at ~95°. These were sorted into a two-dimensional spectrum (x,y) with the former along the x axis, and the latter along the y axis. A projection along the x axis (30°) from a γ-ray gate on the y axis (95°) can be compared with the inverse projection--the given γ-ray gate on the x axis (30°) and the projected spectrum on the y axis (95°). Gamma rays in the projected spectra that have the same character as the gate γ ray (multipolarity and spin change) appear equally intense in the two spectra, whereas those with different character are generally not the same. For the common situation of a stretched dipole ($\Delta I = 1$) and a stretched quadrupole ($\Delta I = 2$) transition, the resulting peak is about twice as large when the dipole is at 95° and the quadrupole at 30° as for the inverted situation. An example is shown in fig. 21. The selected gating transitions are three successive stretched quadrupole transitions (604, 509, and 434 keV) in band 3. They are added together to improve the statistics in order to characterize weak transitions. Most of the transitions in the two parts of fig. 21 are comparable, which indicates a consistency with stretched quadrupole character. Notable exceptions are the 291, 531, and 690 keV transitions, consistent with stretched dipole character, as was

known.[48] An important result is that the 627 and 748 keV transitions are also consistent with stretched dipole character, which confirms spins and parity for band 2. The apparent stretched dipole character of the 548 keV transition also ties together the spins in bands 3 and 5. Such assignments are, of course, not absolutely certain since nonstretched and mixed transitions can be indistinguishable from stretched ones. Nevertheless, stretched transitions are predominant in high-spin studies, and there are many interconnections among the observed bands that strengthen the assignments.

The lower part ($I \lesssim 30\hbar$) of the ^{156}Er level scheme is clearly rotational and resembles the heavier rare-earth nuclei. The lowest levels are probably weakly deformed prolate but soft toward deformation. Under rotation they appear (from the level spacings) to stretch out to typical deformations ($\epsilon \sim 0.2$-0.25) by spin 8 or $10\hbar$, as is seen for other nuclei in this part of the transition region.[49] The bandhead assignments seem reasonably clear: band 1, vacuum; band 2, EF; band 3, AE; band 5, AF; and band 4, mainly octupole. These bands seem to behave reasonably normally up to spin $\sim 30\hbar$. Band 1 has an AB crossing at $\sim 12\hbar$, and a second backbend at $\sim 24\hbar$, probably ABEF (see ^{158}Yb below), where it receives feeding from the 9.6-MeV 30^+ level, via three different paths.

Band 2 is not seen below spin 16, because of depopulation into band 3. This band is also not seen above the 9.6-MeV level, but whether it terminates there or is simply fed from there is not clear. Bands 3 and 5 have no AB backbend, but do have a backbend at spin 22 or 23 (very probably BC), and are not very regular above that. Nevertheless band 5 clearly continues up to $\sim 36\hbar$, far above the 9.6-MeV 30^+ state.

One new feature observed in bands 3, 4, 5, and the band fragment is the abundance of interband transitions at the backbends, presumably BC, around spin 22. All four of the bands participate in this cross feeding, and it is the only reason that the band fragment is seen. This cross feeding suggests that the integrity of the bands,

as indicated by a single predominant B(E2) value for the decay of each state, is broken. This is known to happen sometimes at band crossings due to mixing of the two bands, but in the present case bands having different signatures (odd and even spins) are involved, which requires a more general explanation. This suggests to us that the structure changes across this region. A structural change is supported by the fact that the bands are less regular above this region than below it. The nature of the change seems very likely to be related to the BC alignment, since the cross feeding occurs exactly at the associated backbend. It is reasonable that alignment of the third and fourth valence quasineutrons in ^{156}Er out of six total causes a large reduction of the neutron pairing which in turn might cause some change in shape. This seems to us a consistent explanation for the observed behavior. To our knowledge, this behavior has not previously been observed in a rotational nucleus, and the underlying origin of the effect has not yet been explained.

But the most interesting new feature of the ^{156}Er level scheme is the structure between the 9.6 MeV 30^+ and the 14.4 MeV 42^+ levels and the 42^+ level itself. The latter is almost surely the fully aligned configuration (relative to a ^{146}Gd core), $\pi(h_{11/2}^4)_{16}$; $\nu(f_{7/2})_6^2(h_{9/2})_8^2(i_{13/2})_{12}^2$, consistent with an oblate shape. However, the backbone of this structure (the 387-1368 and 704-918 branches are weak) is a sequence of six successive stretched E2 transitions, and, furthermore, of fifteen reasonably certain assignments between these spins, only the 219 and 721 keV cascade transitions are mainly dipole. We take this as evidence for some collectivity in the cascade. An interpretation consistent with all this evidence, as well as current theoretical calculations,[50,51] is that this is a triaxial band terminating in the oblate fully aligned 42^+ state. This is supported by the energy of these levels relative to that of a rotating liquid drop, shown in fig. 22. The gain in energy compared to the rigid rotor, especially for the 40^+ and 42^+ states, is characteristic of that calculated for such terminating bands based on fully aligned (energetically favorable) states. This low energy results in a large sudden population (nearly 10%) at spin 42ħ, whereas the only

continuation seen is a weak, high-energy (1058 keV) dipole transition. It is also interesting that the lowest member of this band, the 9.6 MeV 30^+ state, is distinctly different in character from the reasonably well developed rotational bands lying below it. This seems consistent with a shift (toward more triaxial shapes) to a level that is eventually related to the (essentially) oblate 42^+ state. The general agreement between experiment and calculation[52] in fig. 22 is impressive, showing the great strides that have been made in experiment and theory in the last year or two.

The next example is an isotone of ^{156}Er, namely ^{158}Yb, and together they illustrate the fact that in such soft nuclei small shape-driving forces, such as the change in occupation of particular quasiparticle orbitals at a band crossing, can produce marked shape changes depending upon which particles align. The ^{158}Yb was produced at the 88" cyclotron with 175 MeV ^{40}Ar on a 1 mg/cm^2 lead-backed target of ^{122}Te. By comparison with the results from an unbacked target, all of the assigned lines in ^{158}Yb are emitted after delays of $\geq$2 ps, implying that the decay has passed through regions of (relatively slow) non-collective behavior. Based on the data obtained, together with a knowledge of the level structures in ^{156}Er and ^{158}Er, where band terminations are observed, we reinterpret[53] the previously suggested structure[54] for the high-spin states of ^{158}Yb in terms of particular particle alignments rather than "quasivibrational behavior" and band terminations.[55]

The level scheme shown in fig. 23 was established from the coincidence relationships. Our ordering in band 1 is not completely unambiguous, but the main uncertainties are the location of the 793 keV transition relative to the two 786 keV ones, and the 725 keV transition relative to the two 733 keV ones. The small energy differences involved in any such interchanges will not affect the arguments made later. The spin assignments are based on the type of angular correlation studies already described for ^{156}Er. The assignments for bands 1, 2 and 3 are reasonably clear, as is the (second) 9^- assignment for the 2652 keV level. Band 4 is more difficult due to non-stretched dipoles connecting it with the ground

band, and mixed dipole-quadrupole transitions to the other negative-parity states. Rather lengthy arguments can be made showing that the spins in band 4 are very likely, and its negative parity probable. Although spin and parity assignments based solely on angular correlation measurements are never certain, we feel those in fig. 23 are rather good.

In the usual nomenclature, band 1 is initially the vacuum configuration, which undergoes a νAB alignment around spin 12ħ. Bands 2 and 4 are very likely νAE and νAF, respectively. Only band 3 presents any problem, and it can well be νBE, although this configuration is not often observed. Nuclear properties are mainly a function of neutron (rather than proton) number in the vicinity of ^{158}Yb. Thus the most similar well studied[47] nucleus should be ^{156}Er, and below spin 20 the similarity is quite striking as can be seen in fig. 24 where the spin, I, vs rotational frequency, $\hbar\omega$, is plotted for bands 1 (bottom) and 2 and 4 (top). Because of this, the differences between ^{158}Yb and ^{156}Er above spin 20 are more interesting. There are at least three of these. The first concerns the 30^+ levels in band 1. In ^{156}Er this level branches at least five ways, none of which carries more than ~1/3 of the total intensity. It is connected by three completely different routes to the lower part of band 1, but these account for only half the decay of the 30^+ level. The suggestion is strong that this 30^+ level in ^{156}Er is not closely related to the lower part of band 1, and has shifted to a more triaxial shape. By contrast, in ^{158}Yb there is no observed branching at all in this spin region. The population of this band falls gradually to ~5% at spin 34 and then drops suddenly by a factor of 5. Thus the relation of the top two transitions to the rest of the band is not so clear, but below spin 34 our tentative conclusion is that ^{158}Yb does <u>not</u> change shape like ^{156}Er.

A second related difference has to do with the second backbend (or upbend) in band 1. Figure 24 (bottom) shows that band 1 in ^{158}Yb bends strongly up at $\hbar\omega$ = 0.36, whereas in ^{156}Er it does not do so until $\hbar\omega$ = 0.41 MeV. Thus something about this backbend changes between the two nuclei. Above its backbend, ^{156}Er is

irregular and reaches the "triaxial" 30^+ state via several pathways. On the other hand ^{158}Yb behaves smoothly, apparently undergoing another (third) backbend (or upbend) at $\hbar\omega$ = 0.39 MeV, ending in the above-mentioned 34^+ state. Before discussing this further, we consider the sidebands. In ^{158}Yb both sidebands have backbends at $\hbar\omega$ = 0.36 or 0.37 MeV, extremely close to band 1 in that nucleus. They do not, however, show the "double upbend" behavior of band 1. In ^{156}Er, the sidebands are similar to those in ^{158}Yb, backbending a bit higher in frequency (~0.39 MeV), but pretty clearly below the band 1 frequency in ^{156}Er. There is, we believe, a simple and consistent interpretation of these characteristics, involving the three possible alignments in this frequency range for these nuclei: νBC, νEF, and πAB. In band 1, νBC is blocked (B is occupied) and, in the sidebands, νEF is blocked (E or F is occupied). Thus, if the simultaneous upbends in all bands of ^{158}Yb are due to the same alignment, it must be πAB. Conversely, band 1 of ^{156}Er does <u>not</u> seem to backbend where the sidebands do, suggesting that at least the lower of these (in the sidebands) is not πAB. It must then be νBC. If the upbend in band 1 of ^{156}Er were νEF, we could understand the dramatic behavior resulting, since alignment of the third and fourth neutron (out of six) will surely affect the neutron pairing drastically, and CSM calculations[56,57] show that in these nuclei the configuration νEF is strongly triaxial and oblate driving, whereas πAB and νBC are not. For similar reasons, if the second part of the double upbend in ^{158}Yb were νEF, we could understand why that band stops--the prolate shape has been destabilized. There is no good evidence as to the shape beyond spin 34, whereas at, and just below, this spin the regularity of the band and the lack of any branching argue that it is still reasonably collective.

The third difference is the absence in ^{158}Yb of the strong interband transitions that occur among the negative-parity bands in ^{156}Er at the $\hbar\omega$ = 0.39 backbend. This follows naturally from the above assignments. In ^{156}Er it is a νBC alignment, which will very likely quench the neutron pairing correlations (again only one pair

of neutrons is left above the N = 82 shell) as has been suggested.[47] What then happens to the shape is not clear, since νBC is not strongly triaxial driving, but, because of the quenching, some change in behavior is not surprising. In ^{158}Yb we have argued that this alignment is πAB, with no dramatic implications.

Both CSM calculations and empirical systematics suggest that the above-proposed alignments are reasonable. The πAB alignment decreases in frequency from 0.5 to 0.4 MeV as the neutron number decreases from 95 to 89 in Er and Yb nuclei,[58] and the calculations indicate that this is caused by a decrease in deformation. This alignment is, therefore, expected around 0.4 MeV for N = 88, though why it is somewhat lower in ^{158}Yb than ^{156}Er is not clear. The νBC alignment is generally found experimentally[59] between 0.3 and 0.4 MeV, and increases from 0.3 to 0.4 MeV between N = 92 and N = 89 and thus is also expected around 0.4 MeV for N = 88. Again the reason ^{156}Er has this alignment at slightly lower frequency than ^{158}Yb is not obvious. There are no very clear experimental data on the νEF alignment, but the CSM calculations[27] predict it at frequencies around 0.4 MeV for N = 88. Thus, although there are details to be understood, the alignments proposed here do seem plausible.

In summary, the evidence suggests to us that ^{158}Yb remains rather collective in the yrast band up to at least spin 34. The apparent reason it differs from ^{156}Er in this respect is that in ^{158}Yb the proton alignment (πAB) occurs before the neutron alignment (νEF) and, whereas νEF tends to induce both shape and pairing changes, πAB does not. A related effect appears to be that πAB in the ^{158}Yb sidebands also produces normal backbends, whereas νBC in ^{156}Er causes strong interband transitions, probably directly or indirectly due to the severe reduction or collapse of the neutron pairing correlations. If the interpretation given is correct, this behavior illuminates the fact that specific nucleon alignments imply specific shape and/or pairing changes. Thus relatively small shifts in alignment frequencies can replace one alignment by another,

producing larger differences in the band behavior. It will be interesting to study further the high-spin states in the third isotone, ^{154}Dy.

No discussion of high-spin states at this moment would do justice to the topic without mentioning the newest development on superdeformed bands. These are bands of nuclei with a ratio of axes approaching 2:1, and were first found in the actinide region. There they occur at low spin, and are the origin of the spontaneously fissioning isomers (from the second minimum). Since their discovery in the Pu-Am region,[60] it has been predicted by theoreticians that they occur in other regions of the Periodic table also, including just above N = 82 and Z = 64.[61-63] But in these rare-earth nuclei, superdeformed shapes would appear only at high spin, becoming yrast around spin 60ħ. However, if populated when yrast, appreciable intensity may well stay in the superdeformed band(s) to lower spins because the unique shape permits little interaction with more normal bands, at least until the superdeformed states' excitation energies above the yrast line become great enough for the out-of-band decays to compete with the very enhanced in-band E2 transitions. In fact such a band structure was observed in 1984 by a group at Daresbury[64] as a closely spaced pair of ridges along the diagonal valley in a two dimensional plot of γ-ray coincidence events in ^{152}Dy. A view of this matrix is shown in fig. 25; the width of the valley, or more accurately the distance between the two ridges, W, gives $\mathcal{J}^{(2)}_{band} = 8\hbar^2/W = (85 \pm 2)\hbar^2$ MeV^{-1} and the value of W/2 = (47 ± 1) keV is the change in energy for consecutive transitions in the band. Such a large moment of inertia is about 1.4 times the rigid-sphere value for mass 152 and corresponds to a deformation of $\varepsilon = 0.51$, not quite the $\varepsilon = 0.6$ for a 2:1 axial ratio. The superdeformed ridge structure was estimated to cover the spin range from about 34 to 58ħ, and a later experiment[65] (by comparison of a backed and unbacked target) set an upper limit on the lifetimes in that range that indicated very enhanced B(E2) values, much larger than those of a normal prolate band with $\varepsilon \approx 0.2$.

But the exciting new information announced in May at the Copenhagen workshop is that essentially the same group of workers using the same $^{108}Pd(^{48}Ca,4n)^{152}Dy$ reaction at 205 MeV have seen a band with 19 transitions going from 1449 to 602 keV with an average separation in neighboring transitions of 47 ± 1 keV (fig. 26).[66] Except for the first (highest) four and last (lowest) two transitions which are being populated and depopulated, respectively, all the transitions have the same intensity. It appears to be a weak band; its fraction of the total intensity is about 2%, and the authors think this is the total superdeformed shape intensity observed. This band decays from its last three states into the already well known oblate band structure between spins 25^- to 19^- via a few E1 transitions whose cascades are not yet worked out. This leaves an uncertainty of ±2ħ in the assignment of spins to the superdeformed band, but within that limitation they extend from 60ħ to 22ħ, with a constant moment of inertia to within a couple of percent, and represent the highest spin states so far observed. Much higher discrete states are not likely to be seen, as this is getting close to the spin limit for fission in this region.

The finding of this band of discrete, superdeformed states owes success both to the advances in theory that predicted superdeformed shapes, and to the advances in instrumentation that made the experiment possible. Possibly it raises more questions than it answers. For example, why the sharp depopulation around the 647 keV member? Does this indicate disappearance of the potential barrier between the two minima? Why is only one band of 2% intensity seen? Is part of the answer that there is still a significant pairing gap for these shapes at spin 60ħ? Why doesn't the band decay to the prolate ground-band extension rather than to the much more differently shaped oblate states? Do these bands occur in nearby nuclei, as predicted by theory? If the observed transitions represent a single cascade from where it is populated between spins 50-60ħ on down to where the band depopulates around spin 24ħ, one might expect in the E_1 vs E_2 coincidence matrix a whole succession of parallel

ridges (more than a dozen) spaced ~47 keV apart, all with the same intensity although getting wider as they go away from the diagonal. Are these higher ridges present? Again, as with the previous topics, we have much still to learn.

The last decay scheme I shall discuss, that of ^{158}Er, is being done to re-emphasize some of the points already made and to introduce the next topic, namely lifetime measurements of high-spin states. The nucleus ^{158}Er was the first one in which a second bandcrossing was observed,[67] and it was then predicted[68] to be due to the alignment of a pair of $h_{11/2}$ quasiprotons. More recent calculations[52,69,70] predict that in this nucleus oblate shapes will compete with prolate and triaxial ones along the yrast line near spin 50ħ. In fact, the first oblate shape predicted to be on the yrast line is the fully aligned 46^+ state, $\pi[(h_{11/2})^4]_{16}\nu[(f_{7/2})^3(h_{9/2})^3(i_{13/2})^2]_{30}$. Experimental evidence has been reported[71] for a change to oblate shape, however, at somewhat lower spin, ~40ħ. We have reinvestigated[72] the yrast band of ^{158}Er and confirm finding two branches feeding the 38^+ level; one is slow ($\geq$2 psec), suggesting some population of the noncollective, oblate structures predicted, and the other is fast (<1 psec), suggesting population also of the more collective prolate or triaxial structures.

The reaction used was 175-MeV ^{40}Ar (from the 88" cyclotron of LBL) on ^{122}Sn. Three targets were employed: a ~1 mg/cm^2 lead-backed target, a ~1 mg/cm^2 gold-backed one, and a target consisting of three self-supporting ^{122}Sn foils, each ~0.5 mg/cm^2 thick. The gamma rays were detected with 14 (for the lead-backed target) and 21 (for the unbacked and gold-backed targets) Compton-suppressed germanium detectors, leading to about 200 million double-coincidence events and the same number of triple-coincidence events, respectively.

A part of the spectrum (700-1400 keV) obtained in coincidence with the 1058 keV ($38^+ \rightarrow 36^+$) transition and using the unbacked targets is shown in the upper part of fig. 27. The region of the second (proton) backbend is seen and one can observe the marked drop in intensity for discrete lines above the 1058 keV gate. The five

transitions, observed in ref. 71, of 827, 1031, 1203, 1210, and 1280 keV can be seen, and in addition there is a weak 971 keV line. The lower part shows the same region gated by the same transition, but for the gold-backed target; it is clear that the 1203-1210 keV lines are missing. We believe that these are not observed because they are smeared out by Doppler shifts arising from the spread in velocity of the emitting nucleus as it slows down, and the variety of detector angles relative to the beam direction. From range-energy data,[73] the mean time to slow the recoiling ^{158}Er nucleus in gold (lead) can be estimated to be around 0.6 (1.0) psec. For the 827, 971, 1031, and 1280 keV transitions to be sharp in fig. 27 (lower) means that they must have been emitted after an interval (corresponding to their lifetime plus feeding time) 2-3 times longer than this. The fact that the 1200 keV lines disappear in that figure means that they have lifetimes (plus feeding times) shorter than the mean slowing time. If shorter than ~0.2 psec, they would be emitted before much slowing down occurred (i.e., at nearly full recoil velocity). In this case, a reasonably sharp line should appear in the summed spectrum from all the detectors after each one has been gain-adjusted for its full Doppler shift. We did not see 1200 keV lines in such a spectrum with the lead-backed target, suggesting a lifetime (plus feeding time) between 0.6 and 0.2 psec. However, at present we consider the lower limit to be tentative.

Coincidence gates on individual lines resulted in the high-spin part of the level scheme shown in fig. 28. The order in each branch has been taken from the relative intensities, and spins have been assigned from multipolarities determined by γ-γ angular correlations, assuming stretched transitions. The 971 keV transition was in agreement with expectations for a stretched quadrupole, but the two 1200 keV lines were too weak to determine reliably.

One major point of interest in these results is the nature of the highest spin state found, that decaying by the 971 keV transition. If the latter is a stretched E2 transition, as suggested, the state is the 46^+ one that is the maximally aligned state predicted by theory[56,69]; it is a band termination. That is,

all the valence particles in this configuration are aligned to their maximum spin, producing an oblate nucleus ($\gamma = 60°$). Figure 29 gives the plot of level energy (minus a rigid-rotor energy) versus spin for these high-spin states in ^{158}Er and shows the remarkable similarity for the levels of the slow branch to those of ^{156}Er (displaced 4 spin units with the two fewer neutrons), where the band termination has been seen at 42^+. Both of these states lie unusually low, which shows the favorable energy of the maximally aligned states in this region of nuclei.

The other main result of these experiments is the identification of fast- and slow-feeding components into the 38^+ state of ^{158}Er. Such components have been seen separately in neighboring nuclei[48,74,75] and have generally accepted interpretations. Among the Gd, Dy, Er, and Yb ($64 \leq Z \leq 70$) nuclei, those having neutron numbers between 82 and 88 generally have slow feeding times (>1 psec). The reason is thought to be that they have regions of non-collective behavior (oblate or spherical shapes) along the decay pathways. Such regions have relatively slow transitions (of order single-particle strength) and no smooth decay pathways. In contrast, the well-deformed rare-earth nuclei ($64 < Z < 74$; $90 < N < 110$) have fast feeding times (<<1 psec), thought to be due to the presence of rotational bands. These bands provide smooth pathways of strongly enhanced E2 transitions, and thus yield rapid deexcitation. It is therefore not so surprising that ^{158}Er, which lies on the boundary between these regions, would have both fast- and slow-feeding components. In fact, such a combination of feeding times has recently been inferred[74] from the decay curves of lower-lying states in recoil distance studies of the nearby nucleus, ^{154}Dy. The difference in the present case is that we have identified resolved lines in each of these two branches and have determined how they feed into the known yrast sequence.

We can also try to infer a bit more about the top of the yrast band (the $38^+ \rightarrow 36^+$ transition) and about the fast 1200 keV lines. The 0.6 and 0.2 ps limits mentioned above for the latter refer to their combined lifetime and feeding time; the individual level

lifetimes would have to be at least a factor of 2 shorter. In a typical rotational band the correction due to feeding from higher states amounts to a factor of around 4 for such transition energies. If we take, rather arbitrarily then, a factor of 3 for the ratio of total time observed to lifetime, the above limits correspond to $B(E2)/B(E2)_{s.p.}$ values between 20 and 50 for the 1200 keV transitions. These are only estimated limits, but indicate appreciable collectivity in this branch. On the other hand, they are less than the 150-200 single-particle units characteristic of the low-spin regions of the well-deformed nuclei and probably less than the values for the continuum γ rays in ^{158}Er and other nearby Er nuclei.[76] One should remember that these 1200 keV γ rays are very weak (1%-2% of the $4^+ \rightarrow 2^+$ transition) and could represent somewhat slower links between faster decays at both higher and lower spins. Thus, they need not be similar to the average continuum γ ray. On the other hand, the 1200 keV lifetimes are based on an assumed feeding correction and could be arbitrarily fast if all the delay is in the feeding. It will be interesting, if possible, to measure the lifetimes of the 1200 keV γ rays and the average continuum γ rays more accurately to see if a discrepancy really exists. Finally, can we set any limits on the lifetime of the 38^+ level into which the fast 1200 keV lines decay? Since all of the intensity of the 1058 keV transition (with an error of ±10%) is observed in the stopped peak for the Au- and Pb-backed target data, a crude limit is possible. Unfortunately, the 1200 keV lines account for only ~30% of the total intensity of the 1058 keV line, so that 1/3 of their contribution could be missing in the backed data and would not be noticed. However, at least two-thirds of their contribution must lie within the ~3 keV resolution of the spectrum from the Au-backed target. If we take the delay from the 1200 keV lines to be of the order of 0.6 ps (as described above), this leads to a lifetime for the 1058 keV transition of the order of 2 ps, and thus a B(E2) of ~4 s.p.u. The latter could certainly be off by a factor of 2, but not likely by a factor of 10, and so it is small, even smaller than the

value estimated for the 1200 keV lines. Thus the yrast sequence of ^{158}Er at low spin has enhancements of the order of 150 s.p.u., but by spin 20ħ (after the first bandcrossing) it drops to ~70 s.p.u.,[77] and then loses most of its collectivity (down to ~4 s.p.u.) by spin 38ħ. Presumably the nucleus is changing both shape and deformation in moving across the β-γ plain, as it most likely becomes oblate (and non-collective) at spin 46ħ. But the route it takes to get there is not clear, nor are the rates of change of the pairing or of the alignment. And while the B(E2) values are showing this marked decrease, the value of $\mathcal{J}^{(1)}$ is somewhat more constant after the second backbend; again a puzzle. We also see that in ^{158}Er a type of shape co-existence is occurring at spin 40ħ.

4. REDUCED TRANSITION PROBABILITIES AND LIFETIMES OF HIGH-SPIN STATES

Much of the previous discussion on level schemes involved deducing nuclear behavior and changes in structure from the changes in transition energies with spin, that is, involved comparisons of experimental and theoretical moments of inertia. These occurred because of variations in the pairing correlations, in the shape and deformation of the nucleus, in particle alignment, in shell effects, and perhaps in other (smaller) residual interactions. There is a very complicated interplay with many, or all, of these factors changing with spin, and although much has been learned, it is clear that it would help greatly if we could observe other characteristic nuclear properties which depend in a different way upon all the factors. It would be better still if a property is dominated by one factor, as then that factor could be isolated. This does seem to be the situation with measurements of the nuclear electric moments. The collective stretched electric quadrupole (E2) transition probabilities appear to depend mostly upon the shape and deformation of the nucleus, with little dependence upon changes in pairing. Experimentally they seem to show only temporary anomalies at bandcrossings; more gradual changes (including alignments spread over several spin changes) usually have their effects described in terms of the

(resulting) shape and deformation changes. The situation for $\Delta I = 1$ E2 transitions (rarely seen at high spin), such as those going between opposite signature rotational bands in odd-mass nuclei is somewhat more difficult, bringing in a signature dependence. And the better competing M1 transitions are considerably more complex, involving individual particle parameters as well. I shall take up examples involving only stretched E2 transitions.

The quantities of interest to be determined for the electric quadrupole transitions are their reduced transition probabilities and static quadrupole moments. The former can be obtained from lifetime measurements, and both quantities can be measured by Coulomb excitation. By a happy confluence of circumstances, Coulomb excitation has had a renaissance. This is due to the availability of very heavy-ion beams, e.g., Xe, rare earths, Pb, U (from at least two accelerators, the UNILAC at G.S.I. and the SuperHILAC at Berkeley, and perhaps others in the future), the use of parallel-plate gas avalanche counters (which are position sensitive) for particle detection in coincidence with BGO Compton-suppressed Ge detectors for the γ rays, and finally the successful development of new least-squares-fit Coulomb excitation codes, such as GOSIA, at the University of Rochester, which can handle up to 200 unknown matrix elements (E1 through E6 and M1 and M2) coupling 50 levels. The data can come from up to 50 independent experiments, plus lifetime, branching ratio, and E2/M1 mixing ratio data. The use of heavy ions, as well as lighter projectiles, allows moderately high spin states to be excited by multiple Coulomb excitation (but not as high as we can usually reach in (H.I.,xn) reactions). Another limitation is that only stable nuclei can be excited. But in the actinide region, Coulomb excitation permits the study of higher spin states than (H.I.,xn) reactions because of the dominance of fission at high spin and excitation energy with the latter. I shall not have time to discuss this subject further, but will show you a couple of examples of results in the actinides, and refer you to old classics and new reviews.[78-84)]

Figure 30[84] gives the ratio of the experimentally determined B(E2) to the rigid-rotor value (based on the $2^+ \rightarrow 0^+$ transition) for the ground band of ^{232}Th, from studies done both at G.S.I.[85] and LBL.[86] The ratios remain amazingly close to unity up to the 28^+ state, the highest measured. The dashed line marked RV indicates values obtained from attributing the increase in the ground-band moment of inertia entirely to centrifugal stretching, that is, to an increase in β^2. The dotted IBA curve assumes 12 bosons (but only s and d) outside a ^{208}Pb core and the SU(3) limit. The upper plot shows the measured g-factors for the ground-band states.[87] The cross-hatched region reflects the experimental uncertainty, but the marked increase is convincing evidence that a bandcrossing is taking place with a band containing an aligned pair of protons, probably $i_{13/2}$. However, the smoothness of the change in $\mathcal{J}^{(1)}$ with spin for ^{232}Th requires that there be a large mixing matrix element between the two bands at the crossing.

Figures 31 and 32 show for the nucleus ^{248}Cm the ratios of the transition matrix elements (the square root of the B(E2) values), experimental to rigid-rotor, and the diagonal E2 matrix elements, respectively, derived from 260 MeV ^{58}Ni and 641 MeV ^{136}Xe Coulomb excitation studies.[88] The transition matrix elements are again in very good agreement with the spheroidal rotor values, at least as high as measured ($24^+ \rightarrow 22^+$). And for the first time, static quadrupole moments have been measured to spin 20ħ, determining the prolate shape of the yrast band to that spin. They are again in agreement with values calculated from the spheroidal rotor.

The other principle method for measuring reduced electric quadrupole transition probabilities, B(E2) values, for high-spin states is by lifetime measurements from

$$B(E2) = 81.3/\tau E_\gamma^5 (1 + \alpha) \quad \text{in } e^2b^2 \tag{7}$$

where τ is the measured mean lifetime of the state (sec), E_γ is the γ-ray transition energy (keV), and α is the electron conversion

coefficient. The problem at high spins is the short lifetime. There are two main techniques available,[89] the Doppler-shift recoil distance method (RDM) and the Doppler-shift attenuation method (DSAM). The former covers the time range 10^{-9} - 10^{-12}s, and the latter goes from about 10^{-12} - 10^{-14}s. A major complication with either technique is how to take into account the feeding into the state of interest both from above in the same band, and from the "side" from normally unseen transitions from the continuum. The feeding from above is usually handled by introducing a made-up cascade to give the decay curve, or lineshape, for the transition from the highest spin state measured by the RDM, or DSAM, respectively. The side-feeding poses more of a problem, and must be fitted in a "reasonable" way as an additional parameter for each subsequent state, with only its intensity a measured quantity. However, with the greater statistics now obtainable using a multi-detector array, it may be possible to make the measurements in γ-γ coincidence with a gate on the transition in the band preceding the state of interest. This would eliminate from consideration the side-feeding into that state.

Actually, the intensity and feeding time of the side-feeding transitions are themselves of interest, as they tell us about the continuum, or at least about a section of the continuum directly next to, and feeding, the yrast or near-yrast discrete transitions under direct measurement. In transitional nuclei, between the well-deformed ones and those near closed shells, there may even be more than one side-feeding component, each with a different feeding time, which certainly complicates lifetime measurements. Examples are ^{154}Dy, which appears to have both a fast (<1 ps) and a slow (~10 ps) side-feeding from the continuum,[74] and ^{158}Er, described earlier,[72] where the ends of both components are seen as discrete-line branches into the 38^{+} state.

I would now like to describe our first DSAM measurement using HERA. This was done[90] on ^{166}Yb, and covered just the spin range where the positive-parity yrast band showed a remarkably constant

moment of inertia, $J^{(1)}_{eff}$, following the rotational relationship $E_\gamma = (4I - 2)\hbar^2/2J$ extraordinarily well, as discussed earlier. The reaction used was 180 MeV ^{40}Ar + ^{130}Te on a 1 mg/cm^2 Te target backed with a 13 mg/cm^2 gold foil. An unbacked target was also run for comparison and to obtain the side-feeding intensities. The 21 Ge detectors subtended eight different angles to the beam direction ranging from 0 to 154 degrees. Taking the average position for creation of the product nuclei to be halfway through the target, the ^{166}Yb recoils enter the gold foil with a velocity 2.2% that of light, so the Doppler shifts in the forward and backward detectors should be large.

The sum of four yrast discrete-line gates (494 + 509 + 588 + 667 keV peaks), from the 16^+ through 22^+ states, was used to produce the three background-subtracted spectra shown in fig. 33. Part a) shows the unbacked data and parts b) and c) show the coincidence γ rays in the backed-target experiment, detected in counters positioned at forward <45°> and backward <121°> angles, respectively. The lineshapes of the peaks above the 667 keV line show clearly the shoulders created by lifetimes plus feeding-times which are in the range of the mean slowing-down time in gold (0.6 ps). The use of coincidences with high-spin discrete-line gates greatly reduces the background and extraneous lines in the resulting spectra, extending considerably the range of spins at which lifetimes can be measured. We have determined the lifetimes in ^{166}Yb up to I = 34, the highest measured so far. Two comments can be made directly by inspecting the lineshapes of the top transitions. The transitions above 30 → 28 (fig. 34) have rather sharp and nearly symmetrical lineshapes. For the 36 → 34 transition the centroid of its lineshape shows a Doppler shift of only 12.5 keV (corresponding to a feeding time or delay of 0.3 ps), less than the full Doppler shift which would be 21 keV. Such data require a cascade delay in the population time distribution; that is, there must be several transitions of similar lifetime preceding this stage rather than a single long-lived isomer. The lineshapes below spin 30 have two well-defined peaks. This implies that the side-feeding into these states is different from the in-band feeding.

From the intensities of the two peaks it is concluded that the side-feeding is the slow time component. The side-feeding population also has a cascade delay, and therefore also does not seem compatible with a single isomeric transition causing the slow feeding time.

To study the lifetimes involved in the transitions from the 34^+ through 24^+ states a Doppler-shift attenuation lineshape program was developed. The model used has a rotational band with the known yrast discrete-line energies and a set of rotational transitions with the same moment of inertia preceding the highest known transition. For the present case lifetimes above spin 36 were chosen to give the best fit to the lineshape of this transition ($36^+ \rightarrow 34^+$). The subsequent decay was then allowed to proceed with the individual lifetimes of each state as free parameters. The side-feeding intensities to these states (obtained experimentally from the unbacked data) were considered to come from rotational bands with the same transition energies as the yrast sequence. These bands were controlled by a single transition moment, Q_t, which was a parameter in the fit, and for each state a new side-band with its own moment was allowed. In this way the yrast-state lifetimes and the side feeding times were fitted at each spin. The recoil velocity in the backing was considered to decrease exponentially in time, with a mean slowing-down time characteristic of ^{166}Yb in Au (0.6 picoseconds). The data were then fitted for all eight angles available in the experimental set-up. The fits obtained at forward angles for some transitions can be observed in fig. 34. The relative errors in the lifetime and feeding times obtained in such a fit are small since the number of data points exceeds the number of free parameters, particularly since eight different angles are fitted simultaneously. The dependence of the in-band lifetimes on the side-feeding lifetimes was found to be small since the two components are well separated in the experimental lineshapes observed. Therefore we believe that the largest source of uncertainty comes from systematic errors, principally the mean slowing-down value used and the assumption of an exponential slowing-down process (~20%).

There is a loss of collectivity at higher spins (as can be inferred from the decreasing B(E2) values in fig. 35) but, nevertheless, even at 34^+ the nucleus remains very collective (120 s.p.u.). The decrease in B(E2) values can result from a decreasing quadrupole deformation or an increasing triaxiality ($\gamma \neq 0$), or both, as can be seen from the relation[91,92] $B(E2) \propto \beta^2 \cos^2(30 + \gamma)$.

A decrease in B(E2), similar to that observed here around spin 30, has been seen at spins just below 20[75,93,94] in somewhat lighter nuclei (N = 88 or 90). The general reason for this difference seems clear; the lighter nuclei have calculated potential energy surfaces much softer toward shape-changes, and thus are affected at lower spins. This argument can be carried somewhat further. As mentioned earlier, shape changes in this region may be induced by the population or depopulation of specific orbitals during the alignments of particular valence nucleons.[56,95] For the lighter rare-earth nuclei, the first pair of nucleons that align are low-Ω $i_{13/2}$ neutrons which do drive towards more positive γ. However, in the well-deformed region around ^{166}Yb, the alignment of the $i_{13/2}$ neutrons does not affect the shape as much, due to the stiffness of the potential and the higher position of the Fermi level. It is not until higher rotational frequencies, where other alignments may occur, that the nucleus is driven towards the triaxial shapes preferred by those (low-Ω) single-particle orbitals.

A second alignment in ^{166}Yb is not apparent in the γ-ray energies in the spin region where the B(E2) values decrease. However, it might not show up if it occurs gradually (e.g., with a large mixing matrix element). If present it should tend to cause an increase in $\mathcal{J}^{(1)}$, which might just cancel the decrease due to the shape changes suggested by the decreasing B(E2) values. But this leads to the puzzle already mentioned; why does such an accidental cancellation over a large range of rotational angular momentum take place for a number of middle-shell nuclei at high spins?

The side-feeding transitions show longer delays than the direct feeding, suggesting either less collectivity (B(E2) ~ 60 s.p.u.) or larger moments of inertia (~25% larger) for the states involved. It

is an interesting question why (though presumably lying at somewhat higher excitation energies) they should differ so much from the yrast ones. Furthermore, a Doppler-shift analysis of the bulk of the continuum γ-ray distributions shows that the E2 bump is consistent with rotational cascades having large B(E2) values, around 150 ± 50 s.p.u.[76] These two results are not necessarily inconsistent since the unresolved cascades leading to the present high-spin yrast states represent only a small part (20 percent) of all cascades. One possible interpretation of our measurement is that by using high-spin yrast gates we sample continuum cascades that are slower than average. Indeed, if the major cooling into the yrast states is provided by statistical transitions, we must be sampling situations where they compete favorably against the collective in-band E2 transitions. For example, if these unresolved bands have larger moments of inertia, this could be a manifestation of the pairing collapse (neutrons and protons) expected at higher temperatures and spins. Another possibility is that there is a region of slower transitions in all cascades. Since, on average, there are four statistical transitions per cascade, and therefore four different rotational bands, it could be that only the last few (4-5) E2 transitions are slow, i.e., only the last band. The rotational bands close to the yrast line might be slower because they are more triaxial due to the large role played by a few aligned valence nucleons. The rest of the continuum bands (at higher excitation energies) would have to be faster--more collective. This region of higher collectivity could set in as soon as the core is substantially broken, producing larger deformations. More experiments are needed to determine which, if either, of these suggestions is correct.

To conclude this section, we can see that it now appears possible to measure reduced transition probabilities in favorable cases (good rotors) to almost as high a spin as we can produce states. This quantity gives a different insight into the structure of the states being observed than does the more usually considered moment of inertia. And, requiring calculations to reproduce both

properties simultaneously puts much more severe bounds on theory than was possible in the past.

5. CONTINUUM SPECTROSCOPY AND THE DAMPING OF ROTATIONAL MOTION

As one goes to higher and higher spins in the nucleus, the intensity of the yrast and near-yrast (discrete) transitions becomes weaker and weaker (of the order of 1% at spin 40ħ). Most of the population is in excited states ranging up to a neutron binding energy above the yrast line, and there are an enormous number of de-exciting cascades possible. So if we want to know about high-spin states, we must learn how to understand the continuum spectra. Clearly we cannot obtain the detailed information that we get from the lower-spin discrete-line studies, but we can determine the average properties, and we have actually learned quite a bit. The yrast bump (fig. 2) is typically composed predominantly of stretched E2 transitions. This conclusion comes from measurements of the angular distributions and correlations of the γ-rays[2,4,96,97] and the few conversion-electron[6] and polarization experiments[96-98] that have been performed. The highest-energy transitions in the yrast bump, those forming the upper edge, move to higher energy with an increase in the angular momentum input to the nucleus. This was first seen by comparing the spectra for a given product nucleus made with differing average angular momentum input, either by changing the bombarding energy or by changing the target-projectile combination.[1] Since then, much clearer indications of this correlation of the maximum transition energies with spin have been obtained by studying the spectra in coincidence with successive slices of the energy in a sum-spectrometer[99,100] or with successive folds of a γ-ray multiplicity filter.[101-104] This correlation and the dominant stretched E2 character of the transitions strongly suggest that rotational motion is involved.

Another type of measurement which shows more directly the collectivity of the cascades is the average transition lifetime for a certain range of transition energies. The earliest estimates came from recoil-distance Doppler-shift studies to measure the lifetimes

of the lower-spin discrete transitions[48,105-108]; the feeding times to the states being measured were also determined and gave upper limits of a few picoseconds for the dozen nuclei studied. Since this feeding involved 10-15 transitions, the individual transition, on the average, took a fraction of a picosecond. With an average γ-ray energy of ~1 MeV this indicated strongly enhanced transitions if taken to be E2. More detailed measurements[76] by DSAM gave average collectivities of 150 ± 50 s.p.u. for the continuum γ rays from about 800-1200 KeV for several erbium nuclei from mass 153 to 160. So there are a number of indications that the continuum region at high spin is made up predominantly of rotational cascades.

But we have seen that, in the discrete-line region at lower spin, the angular momentum in the nucleus is often (almost equally) divided between collective motion of the nucleus as a whole and the aligned spin of certain high-j particles. Does this behavior continue in the high-spin continuum region? To answer that, just as in the case of the discrete γ-ray studies, we must consider the changes in the values of the moments of inertia as a function of rotational frequency. Recall that the dynamic moment of inertia, $\mathcal{J}^{(2)}$, is a local value and more informative about local changes than $J^{(1)}$, which is proportional to the average value of $J^{(2)}$ from $\omega = 0$ to the ω-value at the measurement. There are two $J^{(2)}$'s; the band or collective one, measured by the width of the valley in a γ-γ correlation matrix, and the effective one, which includes all changes in angular momentum, both from collective motion and from particle alignment, $J^{(2)}_{eff} = dI_{total}/d\omega$. The latter moment can be determined from the γ-ray spectrum itself; it is just proportional to the number of transitions, dn, in the frequency interval, $\hbar d\omega$, of the spectrum

$$\frac{dn}{\hbar d\omega} = \frac{dn}{dI}\,\frac{dI}{\hbar d\omega} = \frac{1}{2}\,\frac{J^{(2)}_{eff}}{\hbar^2} \qquad (8)$$

if they are all stretched E2's (with dI = 2) <u>and</u> if the feeding from the neutron evaporation is complete at this frequency.[109] That is, all γ-ray cascades pass through this frequency. This requirement is

usually valid in the rare-earth region only for $\hbar d\omega < 0.5$ MeV, so at the higher frequencies, of greatest interest, the spectrum must be corrected for partial feeding in order to apply eq. (8). We have developed a method to make this correction (under certain constraints) by using the difference between two spectra from similar, but slightly shifted, spin distributions selected by neighboring total γ-ray energy slices from a sum spectrometer which is in coincidence with the γ-ray detector being observed.[110,111] For example, consider fig. 36. Sum slices N + 1 and N come from the populations shown at the top, yielding the two spectra given in the middle. The difference in these spectra gives a good approximation to the average of the initial spin feeding curves. The only tricky part is that we determine spectra as a function of $\hbar\omega$ rather than spin. But if we are dealing with rotational cascades, then the spin is proportional to the transition energy. Mathematically, we have for the height of a spectrum,

$$h(\omega) = \frac{dn}{\hbar d\omega} = \frac{1}{2}\frac{\mathcal{J}^{(2)}_{eff}(\omega)}{\hbar^2}\int_{I(\omega)}^{\infty} K(I')dI' \qquad (9)$$

where K(I) is the (spin) feeding curve. The γ-ray spectrum associated with a similar, but slightly shifted (ΔI), spin distribution is

$$h_{\Delta}(\omega) = \frac{1}{2}\frac{\mathcal{J}^{(2)}_{eff}(\omega)}{\hbar^2}\int_{I(\omega)-\Delta I}^{\infty} K(I')dI' \qquad (10)$$

Then the difference is

$$\Delta h(\omega) = \frac{1}{2}\frac{\mathcal{J}^{(2)}_{eff}(\omega)}{\hbar^2} K(I')\Delta I' \qquad (11)$$

If $I(\omega)$ is on average a monotonic function of ω, and remembering that $\frac{dI}{d\omega} = \frac{\mathcal{J}^{(2)}}{\hbar}$

$$\Delta h(\omega) = \frac{1}{2\hbar} F(\omega)\Delta I \qquad (12)$$

where $F(\omega)$ is the feeding curve as a function of frequency, rather than spin. Therefore $J^{(2)}_{eff}$ can now be obtained through the "corrected" spectrum $H(\omega)$,

$$\frac{J^{(2)}_{eff}}{\hbar^2} = 2H(\omega) = 2h(\omega)\,\frac{\int_0^{\infty}\Delta h(\omega')d\omega'}{\int_{\omega}^{\infty}\Delta h(\omega')d\omega'} \qquad (13)$$

Consider the NaI spectra shown in fig. 37. These are for 185 MeV ^{40}Ar on lead-backed targets of ^{124,122,120,118}Sn, which at the highest spins consist primarily of the 4n products, ^{160,158,156,154}Er. These[112] were taken in coincidence with a sum spectrometer and correspond to a slice of the latter's spectrum from 25-27.5 MeV. They have been unfolded with their detector's response function and have had their statistical component subtracted. The large (multiple) peak around $\hbar\omega$ = 0.3 MeV in each spectrum contains the known first backbend ($\nu\, i_{13/2}$) in these nuclei, as well as the blocked BC alignment and the second one in the yrast band ($\pi\, h_{11/2}$ for the heavier nuclei). All four spectra show a fall-off above $\hbar\omega \approx 0.6$ MeV due to incomplete feeding. But even without making the correction for incomplete feeding discussed in the preceding paragraph, it can be seen, particularly in the ^{156,154}Er spectra, that there is a minimum in the spectra ($J^{(2)}_{eff}$) at ~0.5 MeV and then an increase which is cut-off finally by the lack of feeding at the highest frequencies (spins). If we make the feeding correction, we get the spectra of fig. 38, where[111] now clearly all show the minimum at 0.5-0.6 Mev followed by a distinct rise in $J^{(2)}_{eff}$. What does this mean? We think it means that in the low-energy peak the nuclei exhaust the possibilities of aligning the high-j orbitals in the valence shell, and so have a more difficult time to add angular momentum. This leads to the observed minimum. The subsequent increase in the moment of inertia above $\hbar\omega \approx 0.5$ MeV indicates that a new source of angular momentum has been tapped by the nuclei at the higher frequency. This can most likely only come from an increase in deformation or from new alignments. The necessary large increase in deformation is not expected theoretically for the heavier isotopes

until much higher spins, if at all. And although a deformation increase may contribute for the lighter, softer Er nuclei, it is not likely to be the main cause, as such large deformations would contribute to a marked increase in $J^{(2)}_{coll}$. This would appear as a narrowing of the valley-ridge structure in γ-γ correlation plots, and does not appear to occur. The values of $J^{(2)}_{coll}$ for ^{160}Er so determined are shown as thin horizontal dashes in fig. 38, and indicate no increase (although, unfortunately, they are not known quite high enough). But CSM[61,113,114] calculations do indicate that the low-Ω orbitals from the $i_{13/2}$ and $h_{9/2}$ protons in the next shell in these nuclei do fall rapidly with increasing frequency and reach the Fermi surface at values around 0.6-0.7 MeV (without change in deformation). We believe this is the origin of the high-energy bump observed in these nuclei. If true, we might expect it to occur at a somewhat lower frequency for ytterbium isotopes, as they have two protons more and so start with their Fermi surface closer to the steeply falling $i_{13/2}$ and $h_{9/2}$ proton orbitals. Indeed, fig. 39 shows this to be the case; the NaI spectrum for ^{162}Yb, corrected for feeding, rises earlier and more steeply than that of its isotone, ^{160}Er, but about the same as for ^{166}Yb. The latter behavior also indicates that this is a proton effect.

If the above reasoning is essentially correct, then all nuclei might be expected to likewise show two, more or less separated bumps in their feeding-corrected spectra corresponding to alignments first in their valence shell, and then at higher frequencies, from the shell above. To observe this, four product nuclei ranging in mass from 86 to 136 were studied in the same way.[115] Figure 40 shows normalized, unfolded, statistical-component-subtracted NaI spectra from the reaction of 170 MeV ^{40}Ar on ^{82}Se in coincidence with the different sum slices indicated in the insert. Figure 41 shows a typical difference spectrum (the peaks at low energy are not statistical fluctuations but are from changes in the reaction channel, with discrete lines from ^{118}Te increasing and those from ^{117}Te decreasing), with the integration region for the feeding

correction indicated by the arrows. The upper part of the figure indicates the percentage of stretched E2 transitions as a function of E_γ, and so shows the lower limit of applicability of the method (where the percentage of E2 transitions falls below 90-100%). Two corrected spectra are shown in fig. 42. They correspond to different sum slices and are consistent up to their end-points which involve a correction factor of 4.

Figure 43 shows the values of $\mathcal{J}^{(2)}_{eff}$ so determined as a function of $\hbar\omega$. It can be seen that all four nuclei have a minimum between $\hbar\omega$ = 0.7-0.9 MeV and then show a significant increase in the value of $\mathcal{J}^{(2)}_{eff}$. In addition, it might be mentioned that CSM calculations do show particle crossings from the shell above in each of these cases at about the right frequencies. So it appears that the unique-parity, high-j orbitals from the shell above do fall to the Fermi surface with increasing rotational frequency, permitting a new sequence of alignments or band crossings to take place at values of $\hbar\omega \geq 0.6$ MeV. This results in a marked increase in $\mathcal{J}^{(2)}_{eff}$, and seems to be a general phenomenon, at least in the mass range 90 to 170 that has been studied.

The discussion so far has suggested that continuum states seem to be rotational states and that they behave much as low-energy rotational states do with a similar mixture of collective motion and alignments. In what ways are they different? Consider again the relation between E_γ and spin for a good rotor

$$E_\gamma(I \rightarrow I - 2) = \frac{\hbar^2}{2\mathcal{J}}(4I - 2) \qquad (2b)$$

For a constant moment of inertia, such a spectrum is a series of equally spaced lines as shown in fig. 44, and no two gamma rays have the same energy. Then, in a two-dimensional $E_\gamma(1) - E_\gamma(2)$ array, the diagonal is zero and the pairs of discrete lines form rows of points (ridges) parallel to the diagonal. (The distance between the ridges across the diagonal is $8\hbar^2/\mathcal{J}^{(2)}_{coll}$, and so far this is our only method for determining this quantity in the continuum.) Figure 45 shows such a two-dimensional correlation matrix for ^{166}Yb from pairs of Ge

detectors. There is indeed a diagonal valley and several ridges can be seen, as well as the horizontal and vertical stripes that come from coincidences with the strongest discrete lines in the spectrum. This is one of the better examples of a valley known so far. But the valley is not very deep, becoming even shallower at larger E_γ, and disappearing completely above $E_\gamma \approx 1.2$ Mev, as do the ridges. This fading out of the rotational features at higher γ-ray energies was a great disappointment in the initial γ-γ correlation studies of a few years ago. But it indicates clearly that the bands in the continuum are not those of a good rigid rotor. A minimum requirement is that they involve a distribution of transition energies (moments of inertia) at a given spin. And it is not sufficient that there be many bands, each with its own different, but constant, moment of inertia. The individual bands themselves must have the distribution in transition energies in order to fill in the valley. In the last few years techniques have been developed to measure the width and depth of the valley, and then using simple models one can determine the transition-energy spread.[116-119]

One method[116,117] was to vary a gate width, W, and look for a change in the dip in the coincident spectrum when those two widths became comparable. The analysis involved the coincident spectra for pairs of contiguous gates of various widths from 20-200 keV and at different median energies in the spectrum. The members of each pair, as shown schematically in fig. 46, are normalized to the same height ($d_1 = d_2$), and the spectra are subtracted as in fig. 46b. The variation of H/W vs W is first analyzed to give the full-width at half-maximum, FWHM, of the assumed Gaussian spread in transition energies. Then the ratio H/d is analyzed to give, almost independently, the filling in of the valley due to another wider component (or components) of the spread. Figure 47 shows actual NaI detector data for 100 keV gates with a common boundary at 840 keV for ^{160}Er as the product nucleus. The top spectrum is for the higher gate; the bottom shows both the experimental and calculated difference spectra; the latter uses the FWHM value for the transition-energy spread

determined by the H/W vs W plot for this median energy. The FWHM values scatter around 100 keV for boundary energies varying from 960 to 1200 keV. However, 85% of the population does not appear to contribute to the valley, as indicated by its small depth. Presumably this larger part of the population has a larger spread in transition energies which is what makes it hard to observe but fills in the valley. However, another experimental evaluation of the transition-energy spread,[118] this time for ^{168}Yb and done with Compton-suppressed Ge detectors, also gave values from 75-110 keV, but used a different model for the comparison calculations and did not find it necessary to include a wider component. Thus the experimental situation is a little fuzzy at present (but see below).

On the other hand the theoretical picture is getting somewhat clearer. Last year an explanation was made that involved the idea of rotational damping.[120] The idea has two basic ingredients. First, as the excitation energy, E*, above the yrast line (or more accurately, above an energy, U_0, (~1 MeV) above the yrast line) increases, the level density goes up very rapidly, and at some point the levels are so close together that the residual interactions mix them over an interval that itself grows with the excitation energy (as $E^{*3/2}$ in the model of ref. 120). Second, the individual basic rotational bands that mix have different transition energies at the same spin, that is, different moments of inertia. As a result, the decay from a mixed state has a distribution of transition energies, a transition-energy spread (not the same as the mixing interval), that fills in the valley and smooths out the ridges if it is large enough. But both features are needed; in the absence of the mixing of states, the distribution of moments of inertia would broaden the ridge, but not fill the valley inside a limit given by the largest moment of inertia. And if there is mixing but only one moment of inertia, then there is no effect on the valley or ridges.

In this model, the transition-energy spread increases at first with excitation energy, and then at still higher excitation decreases. The authors have made estimates of this spread by ascribing the distribution in the moments of inertia of the initial

rotational bands to differences in particle alignment. In the rare-earth region around spin 40ħ they estimate values of ~100 keV, in striking agreement with the two different experiments. However, some very recent calculations[121] indicate that there are also contributions to the transition-energy spread due to shape fluctuations, particularly at higher excitation, that were not included in the earlier calculation. It is not settled yet, but these shape fluctuations might be the origin of a wider energy spread. Finally, we must consider more carefully in what part of the γ-ray cascades damping is most likely to occur, that is, to show its effects. In the cascades following neutron evaporation, the cooling statistical transitions compete best with the rotational transitions when the latter have, on average, small transition energies at lower spin. On average, then, the high-spin, high-energy rotational transitions will have a higher excitation energy above the yrast line than the low-spin, low-energy ones. (This is why we see the discrete lines only at lower spins; at higher spins the population is spread over a much larger range of excitation energy.) Thus the high-spin transitions should be more highly damped, as the mixing increases with temperature, and the effects of damping should be most visible with the higher-energy transitions.

In the last few months we have repeated the γ-γ correlation study on ^{160}Er, but using the Ge detectors of HERA, and trying to evaluate the effect on the coincident γ-ray spectrum of requiring a gate having a particular energy and width.[119] There is always one transition, the gate, that must be missing from this (coincident) spectrum. In the case of a single, undamped cascade, one sharp transition (the gate) is indeed missing, but with a γ-ray spread the missing transition is distributed over an energy related to the width of this spread, producing a "dip" in the spectrum, an example of which is shown in fig. 48. Two gated spectra are shown in this figure--the lighter one is the full projection of the coincidence matrix from (mainly) ^{159}Er and ^{160}Er, and the darker spectrum is coincident with a narrow gate (24 keV width) at 1.1 MeV. The dip, resulting from the narrow gate, is obvious. For gates above γ-ray

energies of 1.3 MeV, this dip disappears completely. However, it can be reasonably well identified between 0.8 and 1.3 MeV where its width is ~90 keV and its intensity drops from ~30% to ~5% of one transition with increasing E_γ. (Note that the full coincident spectrum represents 20-25 transitions.) The intensity pattern of this dip is very much like that of the resolved lines, which, in this spectrum, also become too weak to be observed somewhere between 1.2 and 1.3 MeV. This is an argument that the dip is a rather "cold" effect. Rather cold, undamped bands (having somewhat different moments of inertia), would give widths around 100 keV, in reasonable accord with the 90 keV observed.

On the other hand, this narrow dip is a weak feature (~30% of one transition) already at γ-ray energies around ~0.8 MeV (spins 20-35$\hbar$), and, so to explain the spectra, the bulk of the population must have a considerably larger spread in the γ-ray energies even there. Only this larger spread occurs above ~1.3 MeV (spin ~50$\hbar$). From the relationship between E_γ (or spin) and temperature, it is likely that this larger spread arises from the highest temperature region, and thus is most likely to be a damping effect. The width of this broad component is difficult to measure. Limits have been known for some time. It must be considerably greater than 100 keV in order to produce a dip too broad to be observed in fig. 48. On the other hand, sum-energy gates and multiplicity gates <u>do</u> show correlations of $\bar{E}_\gamma$ with I, which require this width to be less than ~500 keV. Figure 49 illustrates two methods by which we try to measure this width. Figure 49a shows a hypothetical feeding curve, which is just taken to be constant over the upper half of the spin range. This could occur, approximately, if a heavy-ion reaction was used that limited the maximum angular momentum to ~60$\hbar$, and the lower edge was defined by selecting a minimum total γ-ray energy or multiplicity. Since each fed spin decays through all those below itself, such a feeding curve produces a spectrum like the lighter solid line in fig. 49b. We assume here that all moments of inertia are equal and constant so that E_γ is strictly proportional to spin. The spectrum in coincidence with a gate in the feeding region, G_H, is illustrated

by the heavy solid line in fig. 49b (the dip associated with the gate width is ignored). Only spins above the γ-ray energy of G_H can contribute to the spectrum, so that, with our assumptions, it will not continue to rise below G_H. If it does so, then E_γ is not strictly proportional to spin, and we will assume that in this region of E_γ (1.0-1.5 MeV; 40-60ħ) the main cause is a spread in the γ-ray energies emitted by each rotational state. Then the energy range below G_H over which the spectrum continues to rise is a rough measure of the width of this spread in energies. Figure 50a shows such a spectrum with the gate energy G_H = 1.4 MeV indicated. The distance from the gate to the intersection of the lines in fig. 50a is 350 keV, from which we estimate that the FWHM of the γ-ray spread from each rotational state is around 250 keV. (The main difference between these numbers comes because the spread is involved twice: $E_\gamma \rightarrow I \rightarrow E_\gamma$.) Between 1.0 and 1.5 MeV, there seems to be an increase in this spread from ~160 to ~280 keV, but this is not very clear.

Another way to evaluate the width involves a second lower gate, G_L, whose coincident spectrum is also illustrated in fig. 49b (dashed line). If there is no γ-ray spread, all the feeding above G_H should contribute equally to both gates. Thus a subtraction of the spectrum coincident with G_H from that coincident with G_L should be zero above G_H. The data for G_H = 1.22 and G_L values of 0.94, 0.98 and 1.02 MeV (gate widths 44 keV) are shown in fig. 50b. The indicated half-width at half-maximum is 125 keV, from which we estimate the FWHM of the spread to be 180 keV at 1.22 MeV, reasonably consistent with the above estimates. Neither of these methods is very reliable. The experimental problems are least serious and 15-20% uncertainties in the quantities measured are reasonable. The interpretation depends on feeding patterns and moment-of-inertia variations which we do not know, so we estimate overall uncertainties at 30-40%. If we associate this broad component with a transition-energy spread, then the present indications are that between 40 and 60ħ it is in the range 150-300 keV, probably increasing with E_γ(spin).

It is clear that we do not yet understand much about the damping of rotational bands in nuclei at modest temperatures, other than that it probably occurs and is responsible for the filling in of the (diagonal) valley. We have learned enough to make some plausible arguments, but we have much to do to solve this new and interesting problem in high-spin studies (as is true with several other of the topics I have discussed with you). I hope these examples of "unfinished" studies will leave you with the feeling that, although we have learned a great deal about nuclear structure in the last few years from in-beam γ-ray spectrosocpy and other techniques, these are exciting times and there is much more to understand about the behavior of nucleons in a nucleus, about this complex not-so-many-particle quantal system. It shows analogies with larger systems (pairing, liquid-drop behavior), but also differences (no sharp phase changes, pair alignments) due to the small number of active particles. New and more ingenious techniques, equipment, and theories, as well as better use of old ones, will help us solve these puzzles, but, in the process, we will surely uncover new questions.

Since, courtesy of the airline strike, I am the final speaker, coming even after the summary speaker,I would like to thank, on behalf of the other invited speakers as well as myself, Dr. E. Maqueda and the organizers of this IX Workshop on Nuclear Physics, Drs. E. Ventura, H.M. Sofia, and A.O. Macchiavelli, for the opportunity to come here, speak to you, and see this laboratory and its beautiful, new accelerator. We are grateful for the great kindness and hospitality shown us, and wish TANDAR and its people good hunting in nuclear physics and buena suerte.

6. ACKNOWLEDGEMENTS

I would like to thank all the wonderful people who during the past 2-3 years have contributed so much to the work at LBL that I have described: J.C. Bacelar, E.M. Beck, M.A. Deleplanque, Th. Døssing, J.E. Draper, E.L. Dines, J.L. Egido, B. Herskind, A. Holm, A.O. Macchiavelli, H. Mühry, S.B. Patel, P.O. Tjøm. My thanks go to M.K. Lee for his unfailing help with our electronics,

and to R. Belshe for his expert and beautiful work on our computer programming, to P. Conant for her typing of these lectures, and especially to my partner F.S. Stephens.

This work was supported by the Director, Office of Energy Research, Division of Nuclear Physics of the Office of High Energy and Nuclear Physics of the U.S. Department of Energy under Contract DE-AC03-76SF00098.

7. REFERENCES

1) Simon, R.S., Banaschik, M.V. Diamond, R.M., Newton, J.O. and Stephens, F.S., Nucl. Phys. A290, 253 (1977).

2) Simon, R.S., Diamond, R.M., El Masri, Y., Newton, J.O., Sawa, P. and Stephens, F.S., Nucl. Phys. A313,209 (1979).

3) Newton, J.O., Sie, S.H. and Dracoulis, G.D., Phys. Rev. 40, 625 (1978).

4) Deleplanque, M.A., Byrski, Th., Diamond, R.M., Hübel, H., Stephens, F.S. Herskind, B. and Bauer, R., Phys. Rev. Lett. 41, 1105 (1978).

5) Feenstra, S.J., Ockels, W.J., van Klinken, J., deVoigt, M.J.A. and Sujkowski, Z. Phys. Lett. 69B, 403 (1977).

6) Feenstra, S.J., van Klinken, J., Pijn, J.P., Janssens, R., Michel, C., Steyaert, J., Vervier, J., Cornelis, K., Huyse, M. and Lhersonneau, G., Phys. Lett. 80B, 183 (1979).

7) Horn, D., Häuser, O., Faestermann, T., McDonald, A.B., Alexander, T.K., Beene, J.R. and Herrlander, C.J., Phys. Rev. Lett. 39, 389 (1977).

8) Grosse, E., Balanda, A., Emling, H., Folkmann, F., Fuchs, P., Piercey, A.B., Schwalm, D., Simon, R.S., Wollersheim, H.J., Evers, O. and Ower, H., Phys. Scr. 24, 337 (1981).

9) Bohr, Aa., Mottelson, B.R. and Pines, D., Phys. Rev. 110, 936 (1958).

10) Burde, J., Dines, E.L., Shih, S., Diamond, R.M. , Draper, J.E., Lindenberger, K.H., Schück, C. and Stephens, F.S., Phys. Rev. Lett. 48, 530 (1982).

11) Johnson, A., Ryde, H., Sztarkier, J., Phys. Lett. 34B, 605 (1971).

12) Stephens, F.S. and Simon, R.S., Nucl. Phys. A183, 257 (1972).

13) Garrett, J.D. and Gaardhøje, J.J., XIV Masurian Summer School on Nuclear Physics (Mikolajki, Poland, August, 1980).

14) Garrett, J.D., Andersen, O., Gaardhøje, J.J., Hagemann, G.B., Herskind, B., Kownacki, J., Lisle, J.C., Riedinger, L.L., Walus, W., Roy, M., Jonsson, S., Ryde, H., Guttormsen, M. and Tjøm, P.O., Phys. Rev. Lett. 47, 75 (1981).

15) Garrett, J.D., Phys. Scr. T5, 21 (1982).

16) Bes, D.R., Broglia, R.A. and Nilsson, B., Phys. Lett. 40B, 328 (1972).

17) de Voigt, M.J.A., Dudek, J. and Szymanski, Z., Rev. Mod. Phys. 55, 949 (1983).

18) Bentsson, R. and Garrett, J.D., "Collective Phenomena in Atomic Nuclei," International Review on Nuclear Physics, Vol. 2 p. 193 (World Scientific Pub., Singapore, 1984).

19) Diamond, R.M. and Stephens, F.S., Nature 310, 457 (1984).

20) Hamamoto, I., Treatise on Heavy-Ion Science, Vol. 3 p. 313 (Plenum Pub., New York, 1985).

21) Garrett, J.D. Hagemann, G.B. and Herskind, B., "Recent Nuclear Structure Studies in Rapidly-Rotating Nuclei," Annual Review of Nuclear and Particle Science, Vol. 35 (Annual Review Inc., Palo Alto, 1986).

22) (a) Diamond, R.M. and Stephens, F.S., "The High Resolution Ball" (proposal, unpublished, 1981).
(b) Diamond, R.M., "The Berkeley High-Resolution Ball," Instrumentation for Heavy-Ion Nuclear Research, p. 259 (Harwood Academic Pub., New York, 1985).

23) Twin, P.J., Nolan, P.J., Aryaeinejad, R., Love, D.J.G., Nelson, A.H. and Kirwan, A., Nucl. Phys. A409, 343e (1983).

24) Beck, E.M., Bacelar, J.C., Deleplanque, M.A., Diamond, R.M. and Stephens, F.S., to be published, 1986.

25) Walus, W., Roy, N., Jonsson, S., Carlen, L., Ryde, H., Hagemann, G.B., Herskind, B., Garrett, J.D., Chen, Y.S., Almberger, J. and Leander, G., Phys. Scr. 24, 324 (1981).

26) Bengtsson, R. and Frauendorf, S., Nucl. Phys. A314, 27 (1979).

27) Bengtsson, R. and Frauendorf, S., Nucl. Phys. A327, 139 (1979).

28) Jonsson, S., Roy, N., Ryde, H., Walus, W., Kownacki, J., Garrett, J.D, Hagemann, G.B., Herskind, B., Bengtsson, R. and Åberg, S., Nucl. Phys. A449, 537 (1986).

29) Chapman, R., Lisle, J.C., Mo, J.N., Paul, E., Simcock, A., Willmott, J.C., Leslie, J.R., Price, H.G., Walker, P.M., Bacelar, J.C., Garrett, J.D., Hagemann, G.B., Herskind, B., Holm, A. and Nolan, P.J., Phys. Rev. Lett. 51, 2265 (1983).

30) Bacelar, J.C., Diebel, M., Ellegaard, C., Garrett, J.D., Hagemann, G.B., Herskind, B., Holm, A., Yang, C.X., Zhang, J.Y., Tjøm, P.O., Lisle, J.C., Nucl. Phys. A442, 509 (1985).

31) Recht, J., Agarwal, Y.K., Blume, K.P., Guttormsen, M., Hübel, H., Kluge, H., Maier, K.H., Maj, A., Roy, N., Decman, D.J., Dudek, J. and Nazarewicz, W., Nucl. Phys. A440, 366 (1985).

32) Schück, C., Bendjaballah, N., Diamond, R.M., Ellis-Akovali, Y., Lindenberger, K.H., Newton, J.O., Stephens, F.S., Garrett, J.D. and Herskind, B., Phys. Lett. 142B, 253 (1984).

33) Price, H.G., Lister, C.J., Varley, B.J., Gelletly, W. and Olness, J.W., Phys. Rev. Lett. 51, 1842 (1983).

34) Pakkanen, A., Chung, Y.H., Daly, P.J., Faber, S.R., Helppi, H., Wilson, J. Chowdhury, P., Khoo, T.L., Ahmad, I., Borggreen, J. and Grabowski, Z.W., Phys. Lett. 122B, 1530 (1982).

35) Simpson, J., Riley, M.A., Cresswell, J.R., Forsyth, P.D., Howe, D., Nyako, B.M., Sharpey-Schafer, J.F., Bacelar, J.C., Garrett, J.D., Hagemann, G.B., Herskind, B. and Holm, A., Phys. Rev. Lett. 53, 648 (1984).

36) Hamamoto, I., Phys. Scr. T5, 10 (1983).

37) Frauendorf, S., Nucl. Phys. A409, 243c (1983).

38) Bohr, Aa. and Mottelson, B.R., Phys. Scr. 24, 71 (1981).

39) Tanabe, K. and Sugawara-Tanabe, K., Nucl. Phys. A390, 385 (1982).

40) Zhang, J.Y. and Åberg, S., Nucl. Phys. A390, 314 (1982).

41) Mutz, U. and Ring, P., J. Phys. G10, L39 (1984).

42) Schmid, K.W., Grummer, F. and Faessler, A., Phys. Rev. C29, 291 (1984).

43) Broglia, R.A., Diebel, M., Frauendorf, S. and Gallardo, M., Phys. Lett. 166B, 252 (1986).

44) Bacelar, J.C., Holm, A., Diamond, R.M., Beck, E.M., Deleplanque, M.A., Draper, J., Herskind, B. and Stephens, F.S., to be published, 1986.

45) Egido, J.L., private communciation, June, 1986.

46) Stephens, F.S., Deleplanque, M.A., Diamond, R.M. and Macchiavelli, A.O., Phys. Rev. Lett. 54, 2584 (1985).

47) Diamond, R.M., Stephens, F.S., Kelly, W.H and Ward, D., Phys. Rev. Lett. 22, 546 (1969).

48) Sunyar, A.W., Der Mateosian, E., Kistner, O.C., Johnson, A., Lumpkin, A.H. and Thieberger, P., Phys. Lett. 62B, 283 (1976).

49) Diamond, R.M., Symons, G.D., Quebert, J.L., Maier, K.H., Leigh, J.R. and Stephens, F.S., Nucl. Phys. A184, 481 (1972).

50) Ragnarsson, I. and Bengtsson, T., Nucl. Phys. A447, 251c (1986).

51) Bengtsson, T. and Ragnarsson, I., Phys. Scr. T5, 165 (1983).

52) Dudek, J. and Nazarewicz, W., private communication, 1985.

53) Patel, S.B., Stephens, F.S., Bacelar, J.C., Beck, E.M., Deleplanque, M.A., Diamond, R.M. and Draper, J.E., Phys. Rev. Lett. 57, 62 (1986).

54) Baktash, C., Schutz, Y.H., Lee, I.Y., McGowan, F.K., Johnson, N.R., Halbert, M.L., Hensley, D.C., Fewell, M.P., Courtney, L., Larabee, A.J., Riedinger, L.L., Sunyar, A.W., der Mateosian, E., Kistner, O.C. and Sarantites, D.G., Phys. Rev. Lett. 54, 978 (1985).

55) Ragnarsson, I., Bengtsson, T., Nazarewicz, W., Dudek, J., Leander, G.A., Phys. Rev. Lett. 54, 982 (1985).

56) Chen, Y.S., Frauendorf, S. and Riedinger, L.L., Phys. Lett. 171B, 7 (1986).

57) Frauendorf, S. and May, F.R., Phys. Lett. 125B, 245 (1983).

58) Riley, M.A., Simpson, J., Araeinjad, R., Cresswell, J.R., Forsyth, P.D., Howe, D., Nolan, P.J., Nyako, B.M. and Sharpey-Schafer, J.F., Phys. Lett. 135B, 275 (1984).

59) Jonsson, S., Roy, N., Ryde, H., Walus, W., Kownacki, J., Garrett, J.D., Hagemann, G.B., Herskind, B., Bengtsson, R., Åberg, S., Nucl. Phys. A449, 537 (1986).

60) Polikanov, S.M., Druin, V.A., Karnaukhov, V.A., Mikheev, V.L., Pleve, A.A., Skobelev, N.K., Subbotin, V.G., Ter-Akop'yan, G.M. and Fomichev, V.A., J. Exptl. Theor. Phys. (USSR) 42, 1464 (1962); trans. Sov. Phys. JETP 15, 1016 (1962).

61) Andersson, G., Larsson, S.E., Leander, G., Møller, P., Nilsson, S.G., Ragnarsson, I., Åberg, S., Bengtsson, R., Dudek, J., Nerlo-Pomorska, B., Pomorski, K. and Szymanski, Z., Nucl. Phys. A268, 205 (1976).

62) Åberg, S., Phys. Scr. 25, 23 (1982).

63) Dudek, J. and Nazarewicz, W., Phys. Rev. C31, 298 (1985).

64) Nyako, B.M., Creswell, J.R., Forsyth, P.D., Howe, D., Nolan, P.J., Riley, M.A., Sharpey-Schafer, J.F., Simpson, J., Ward, N.J. and Twin, P.J., Phys. Rev. Lett. 52, 507 (1984).

65) Twin, P.J., Nelson, A.H., Nyako, B.M., Howe, D., Cranmer-Gordon, H.W., Elenkov, D., Forsyth, P.D., Jabber, J.K., Sharpey-Schafer, J.F., Simpson, J. and Sletten, G., Phys. Rev. Lett. 55, 1380 (1985).

66) Twin, P.J., Nyako, B.M., Nelson, A.H., Simpson, J., Bentley, M.A., Cranmer-Gordon, H.W., Forsyth, P.D., Howe, D., Mokhtar, A.R., Morrison, J.D., Sharpey-Schafer, J.F. and Sletten, G., to be published, 1986.

67) Lee, I.Y., Aleonard, M.M., Deleplanque, M.A., El Masri, Y., Newton, J.O., Simon, R.S., Diamond, R.M. and Stephens, F.S., Phys. Rev. Lett. 38, 1454 (1977).

68) Faessler, A. and Ploszajczak, M., Phys. Lett. 76B, 1 (1978).

69) Dudek, J. and Nazarewicz, W., Phys. Rev. C31, 298 (1985) and private communication, March, 1984.

70) Tanabe, K. and Sugawara-Tanabe, K., Phys. Lett. 135B, 353 (1984).

71) Simpson, J., Riley, M.A., Creswell, J.R., Forsyth, P.D., Howe, D., Nyako, B.M., Sharpey-Schafer, J.F., Bacelar, J.C., Garrett, J.D., Hagemann, G.B., Herskind, B. and Holm, A., Phys. Rev. Lett. 53, 649 (1984).

72) Tjøm, P.O., Diamond, R.M., Bacelar, J.C., Beck, E.M., Deleplanque, M.A., Draper, J.E. and Stephens, F.S., Phys. Rev. Lett. 55, 2405 (1985).

73) Northcliffe, L.G. and Schilling, R.F., Nucl. Data A7, 233 (1970).

74) Azgui, F., Emling, H., Grosse, E., Michel, C., Simon, R.S., Spreng, W. and Wollersheim, H.J., Nucl. Phys. A439, 573 (1985).

75) Emling, H., Grosse, E., Kulessa, R., Schwalm, D. and Wollersheim, H.J., Nucl. Phys. A419, 187 (1984).

76) Hübel, H., Diamond, R.M., Aguer, P., Ellegaard, C., Fossan, D.B., Kluge, H., Schück, C., Shih, S., Stephens, F.S. and Smilanski, U., Z. Phys. A304, 2251 (1982).

77) Oshima, M., Johnson, N.R., McGowan, F.K., Baktash, C., Lee, I.Y., Schutz, Y., Ribas, R.V. and Wells, J.C., Phys. Rev. C33, 1988 (1986).

78) Alder, K., Bohr, Aa., Huus, T., Mottelson, B.R. and Winther, Aa., Rev. Mod. Phys. 28, 432 (1956).

79) Alder, K. and Winther, Aa., Coulomb Excitation (Academic Press, New York, 1966).

80) Alder, K. and Winther, Aa., Electromagnetic Excitation, Theory of Coulomb Excitation with Heavy Ions (North-Holland, Amsterdam, 1975).

81) McGowan, F.K. and Stelson, P.H., Nuclear Spectroscopy and Reactions, C, Cerny, J., editor (Academic Press, New York, 1974).

82) Newton, J.O., The Electromagnetic Interaction in Nuclear Spectroscopy, Hamilton, W.D., editor, pp. 237-282 (North-Holland, Amsterdam, 1975).

83) deBoer, J., Treatise on Heavy-Ion Science, Vol. 1, pp. 293-352 (Plenum Press, New York, 1984).

84) Cline, D., "Nuclear Shapes Studied by Coulomb Excitation," Annual Review of Nuclear and Particle Science, Vol. 35 (Annual Review, Inc., Palo Alto, 1986).

85) Ower, H., Elze, T.H., Idzko, J., Stelzer, K., Grosse, E., Emling, H., Fuchs, P., Schwalm, D., Wollersheim, H.J., Kaffrell, N. and Trautmann, M., Nucl. Phys. A398, 421 (1982).

86) Guidry, M.W., Butler, P.A., Colombani, P., Lee, I.Y., Ward, D., Diamond, R.M., Stephens, F.S., Eichler, E., Johnson, N.R. and Sturm, R., Nucl. Phys. A266, 288 (1976).

87) Häuser, O., Gräf, H., Grodzins, L., Jaeschke, E., Metag, V., Habs, D., Pelte, D., Emling, H., Grosse, E., Kulessa, R., Schwalm, D., Simon, R.S. and Keinonen, J., Phys. Rev. Lett. 48, 383 (1982).

88) Czosnyka, T., Cline, D., Hasselgren, L., Wu, C.Y., Diamond, R.M., Kluge, H., Roulet, C., Hulet, E.K., Lougheed, R.W. and Baktash, C., Nucl. Phys, in press.

89) Alexander, T.K. and Forster, J.S., Adv. in Nucl. Phys. 10, 199 (1978).

90) Bacelar, J.C., Holm, A., Diamond, R.M., Beck, E.M., Deleplanque, M.A., Draper, J., Herskind, B. and Stephens, F.S., to be published, 1986.

91) Bohr, Aa., Mottelson, B.R., Nuclear Structure, Vol. II (Benjamin, New York, 1975).

92) Ring, P., Hayashi, A., Hara, K., Emling, H. and Grosse, E., Phys. Lett. 110B, 423 (1982).

93) Pakkanen, A., Chung, Y.H., Daly, P.J., Faber, S.R., Helppi, H., Wilson, J., Chowdhury, P., Khoo, T.L., Ahmad, I., Borggreen, J. Grabowski, Z.W. and Radford, D.C., Phys. Rev. Lett. 48, 1530 (1982).

94) Fewell, M.P., Johnson, N.R., McGowan, F.K., Hattula, J.S., Lee, I.Y., Baktash, C., Schutz, Y., Wells, J.C., Riedinger, L.L., Guidry, M.W. and Pancholi, S.C., Phys. Rev. C31, 1057 (1985).

95) Zhang, J.Y. and Åberg, S., Nucl. Phys. A390, 314 (1982).

96) Vivien, J.P., Schutz, Y., Beck, F.A., Bozek, E., Byrski, T., Gehringer, C. and Merdinger, J.C., Phys. Lett. 85B, 325 (1979).

97) Trautmann, W., Sharpey-Schafer, J.F., Andrews, H.R., Haas, B., Häuser, O., Taras, P. and Ward, D., Phys. Rev. Lett. 43, 991 (1979).

98) Hübel, H., Diamond, R.M., Stephens, F.S., Herskind, B. and Bauer, R., Z. Phys. A297, 237 (1980).

99) Tjøm, P.O., Espe, I., Hagemann, G.B., Herskind, B. and Hillis, D.L., Phys. Lett. 72B, 439 (1978).

100) Körner, H.J., Hillis, D.L., Roulet, C.P., Aguer, P., Ellegaard, C., Fossan, D.B., Habs, D., Neiman, M. Stephens, F.S. and Diamond, R.M., Phys. Rev. Lett. 43, 490 (1979).

101) Hagemann, G.B., Broda, B., Herskind, B., Ishihara, M., Ogaza, S. and Ryde, H., Nucl. Phys. A245, 166 (1975).

102) Sarantites, D.G., Barker, J.H., Halbert, M.L., Hensley, D.C., Dayras, R.A., Eichler, E., Johnson, N.R. and Gronemeyer, S.A., Phys. Rev. C14, 2138 (1976).

103) Deleplanque, M.A., Lee, I.Y., Stephens, F.S., Diamond, R.M. and Aleonard, M.M., Phys. Rev. Lett. 40, 629 (1978).

104) Hillis, D.L., Garrett, J.D., Christensen, O., Fernandez, B., Hagemann, G.B., Herskind, B., Back, B.B. and Folkmann, F., Nucl. Phys. A325, 216 (1979).

105) Kutschera, W., Dehnhardt, D., Kistner, O.C., Kump, P., Povh, B. and Sann, H.J., Phys. Rev. C5, 1658 (1972).

106) Newton, J.O., Stephens, F.S. and Diamond, R.M., Nucl. Phys. A210, 19 (1973).

107) Rud, N., Ward, D., Andrews, H.R., Graham, R.L. and Geiger, J.S., Phys. Rev. Lett. 31, 1421 (1973).

108) Bochev, B., Karamyan, S.A., Kutsarova, T. and Subbotin, V.G., Yad. Fiz. 22, 665 (1975) as given in Sov. J. Nucl. Phys. 22, 343 (1975).

109) Simon, R.S., Banaschik, M.V., Colombani, P., Soroka, D.P., Stephens, F.S. and Diamond, R.M., Phys. Rev. Lett. 36, 359 (1976).

110) Deleplanque, M.A., Körner, H.J., Kluge, H., Macchiavelli, A.O., Bendjaballah, N., Diamond, R.M. and Stephens, F.S., Phys. Rev. Lett. 50, 409 (1983).

111) Deleplanque, M.A., Diamond, R.M., Stephens, F.S., Macchiavelli, A.O., Døssing, Th., Draper, J.E. and Dines, E.L., Nucl. Phys. A448, 495 (1986).

112) Deleplanque, M.A., Macchiavelli, A.O., Diamond, R.M., Stephens, F.S., Dines, E.L. and Draper, J.E., Phys. Rev. Lett. 51, 1854 (1983).

113) Leander, G., Chen, Y.S. and Nilsson, B.S., Phys. Scr. 24, 164 (1981).

114) Frauendorf, S., Phys. Scr. 24, 349 (1981).

115) Macchiavelli, A.O., Muehry, H., Deleplanque, M.A., Diamond, R.M., Stephens, F.S., Dines, E.L. and Draper, J.E., Nucl. Phys. A443, 538 (1985).

116) Stephens, F.S. Proceedings of the Second International Conference on Nucleus-Nucleus Collisions (North-Holland, Amsterdam, 1985).

117) Draper, J.E., Dines, E.L., Deleplanque, M.A., Diamond, R.M. and Stephens, F.S., Phys. Rev. Lett. 56, 309 (1986).

118) Bacelar, J.C., Hagemann, G.B., Herskind, B., Lauritzen, B., Holm, A., Lisle, J.C. and Tjøm, P.O., Phys. Rev. Lett. 55, 1858 (1985).

119) Stephens, F.S., Draper, J.E., Egido, J.L., Bacelar, J.C., Beck, E.M., Deleplanque, M.A. and Diamond, R.M., to be published, 1986.

120) Døssing, T., Nuclear Structure 1985, p. 379 (Elsevier Science Pub., Amsterdam, 1985); Lauritzen, B., Broglia, R.A. and Døssing, T., to be published

121) Egido, J.L., private communication, 1986

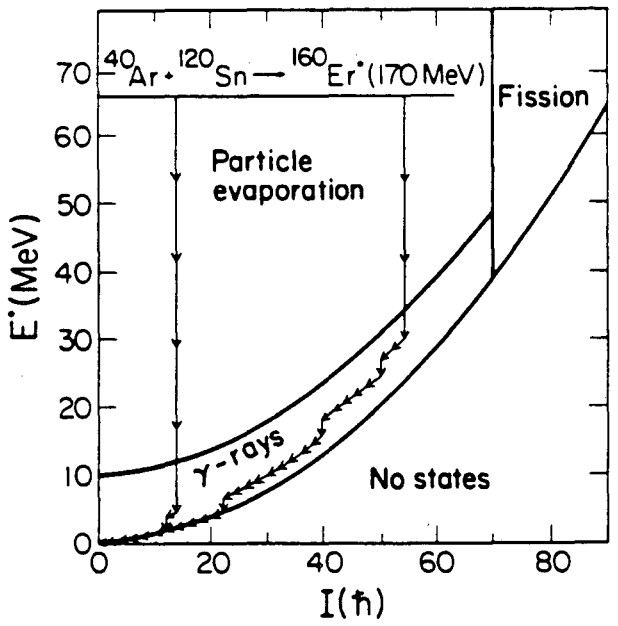

FIGURE 1 Decay modes in excitation energy-spin space for the (typical) reaction indicated. Long arrows indicate neutron emission, short arrows are γ-rays.

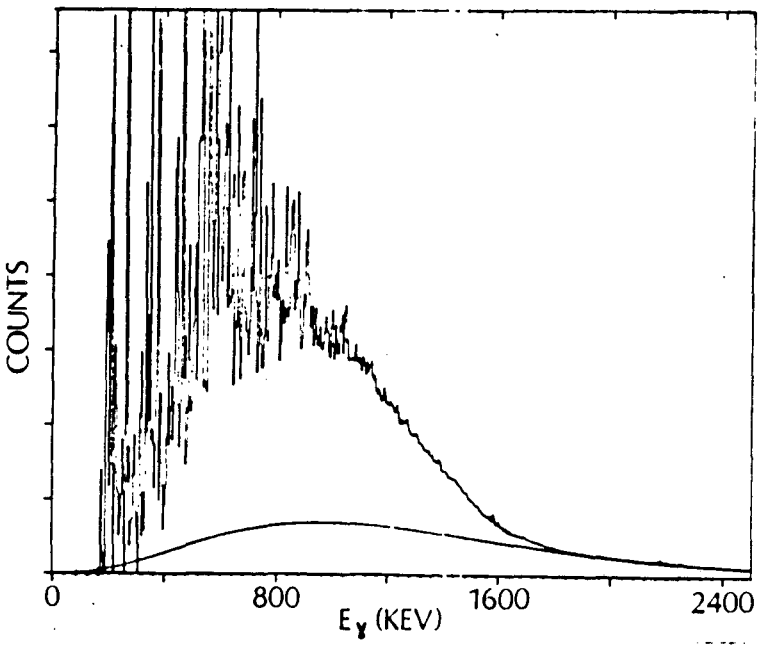

FIGURE 2 Total projection of unfolded Ge coincidence spectrum for 180 MeV ^{40}Ar on Sn^{124}. Curve for statistical component drawn in as $E_\gamma^3 \exp(-E_\gamma/T)$.

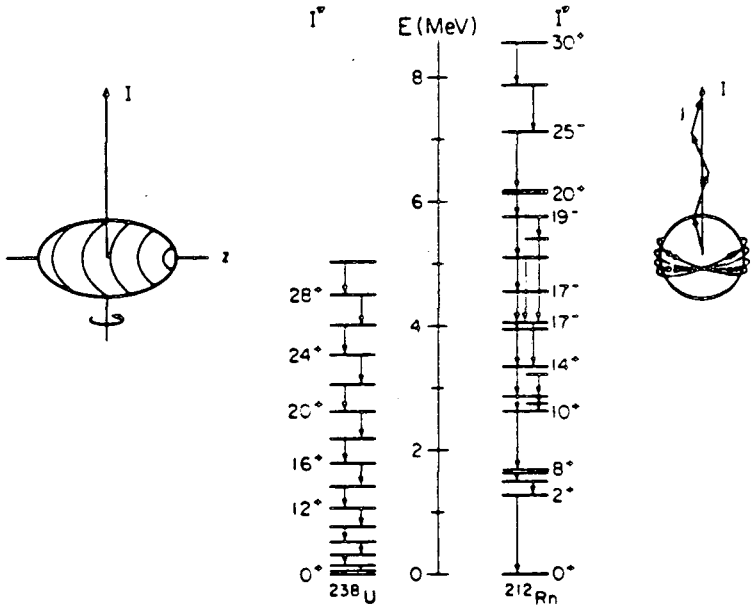

FIGURE 3 Level schemes for ^{238}U and ^{212}Rn, illustrating collective rotation and aligned-particle motion, respectively (refs. 7,8).

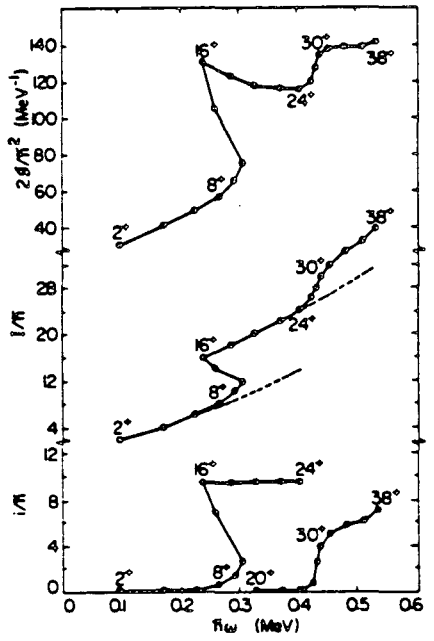

FIGURE 4 Plots of (top) twice the moment of inertia, (middle) the total spin, (bottom) the aligned spin vs. the rotational frequency ($E_\gamma/2$) for the yrast sequence in ^{158}Er (ref. 10)..

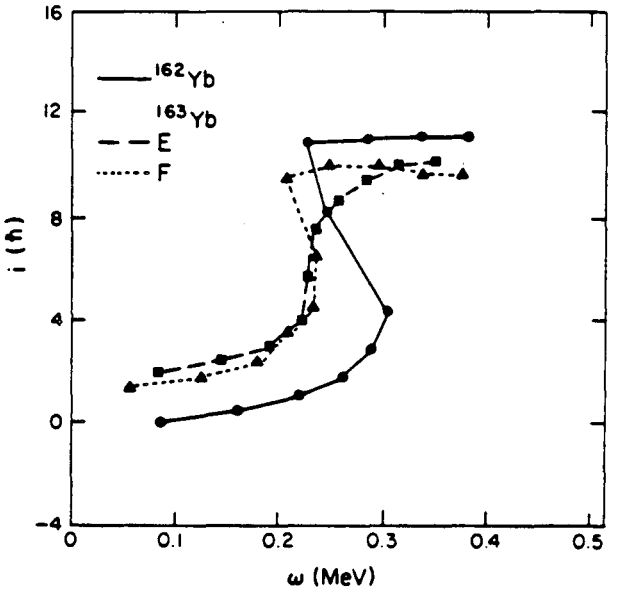

FIGURE 5 Aligned spin vs rotational frequency for yrast sequence in ^{162}Yb and for negative-parity odd quasiparticle bands in ^{163}Yb (ref. 13).

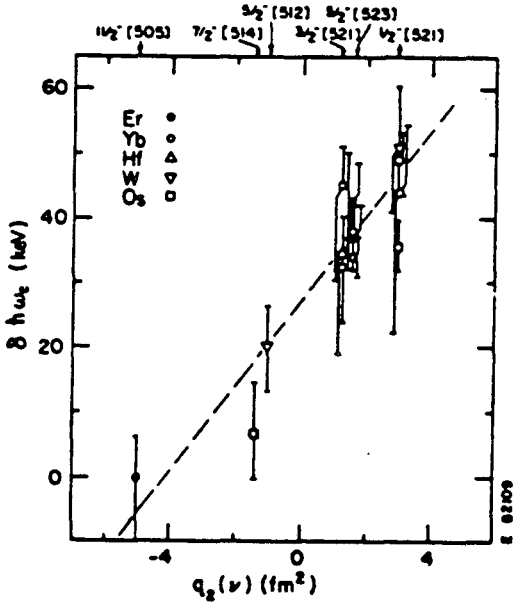

FIGURE 6 Shift in crossing frequency, $\delta\hbar\omega$, between the odd-neutron and neighboring even-even nucleus vs the quadrupole moment of the odd-neutron orbit, $q_2(\nu)$. The odd-neutron configuration is given by its Nilsson quantum numbers at the top (ref. 15).

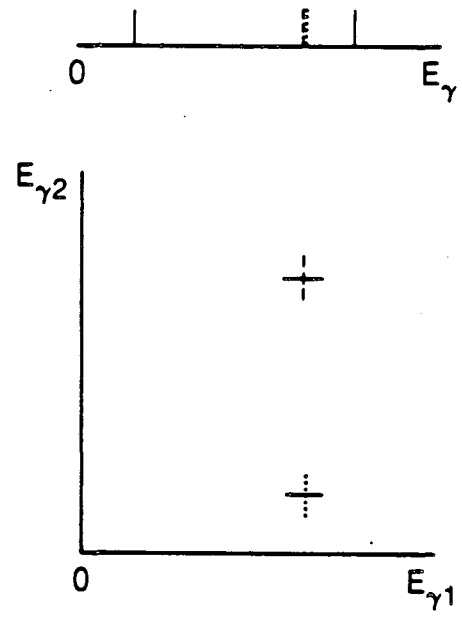

FIGURE 7 Overlapping lines in singles spectrum (top) are resolvable in the doubles spectrum through their different coincidence partners (bottom).

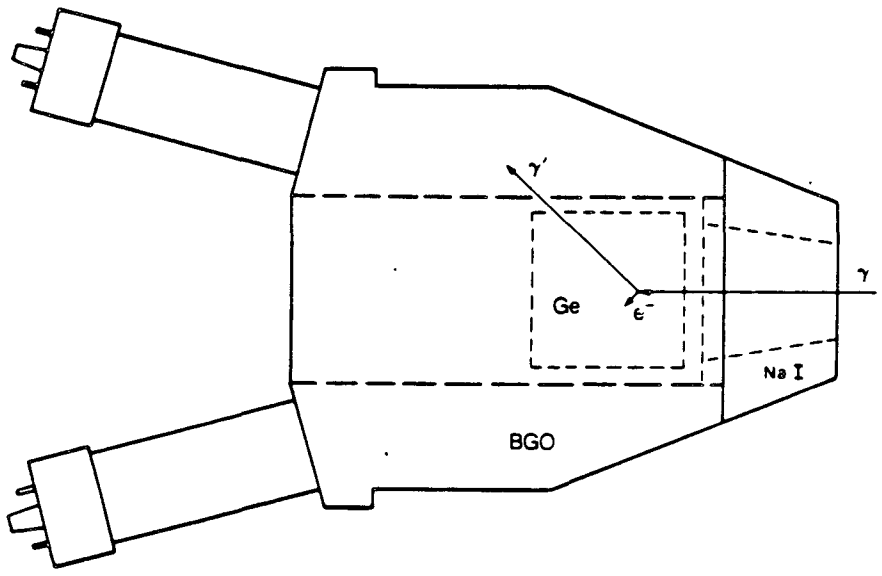

FIGURE 8 Outline of cylindrical BGO Compton-suppression shield showing 5 x 5 cm Ge detector inside, two of six photomultiplier tubes on back surface, and NaI cap at front.

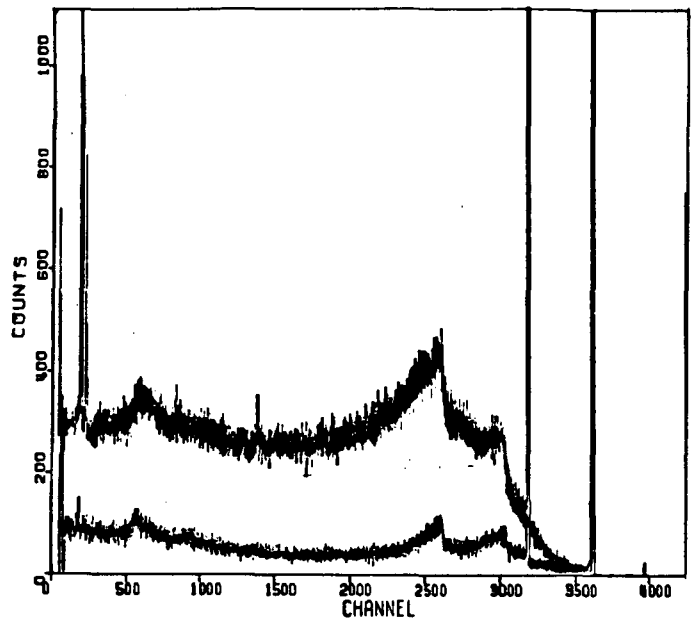

FIGURE 9 Spectra of ^{60}Co taken with bare 20% Ge detector and with Compton-suppressed one (with NaI cap). Peaks go up 12 times the figure height.

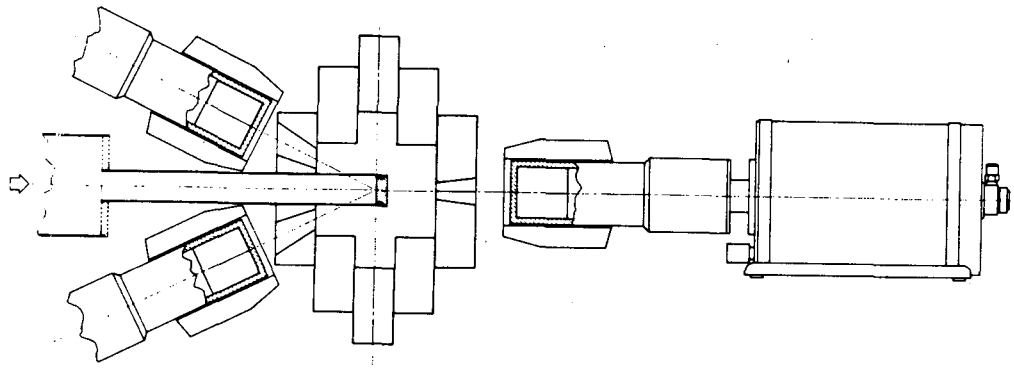

FIGURE 10 Vertical cut through HERA showing one Ge detector in each ring and central BGO ball. Not shown are photomultiplier tubes and NaI caps.

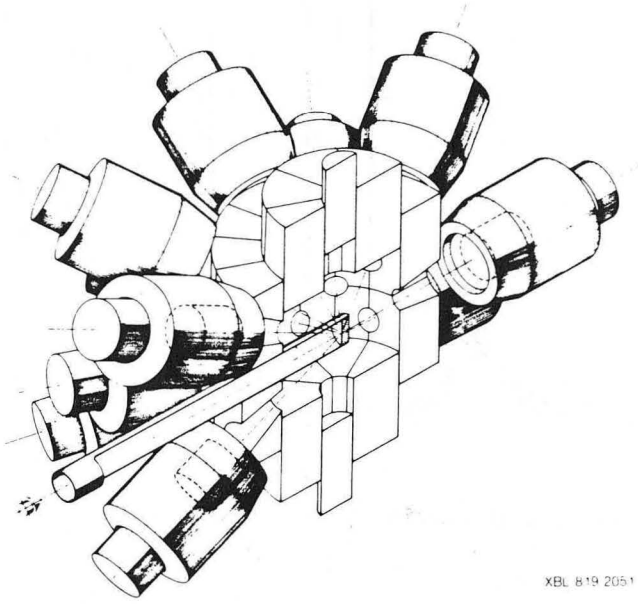

FIGURE 11 Perspective view of one-half the system.

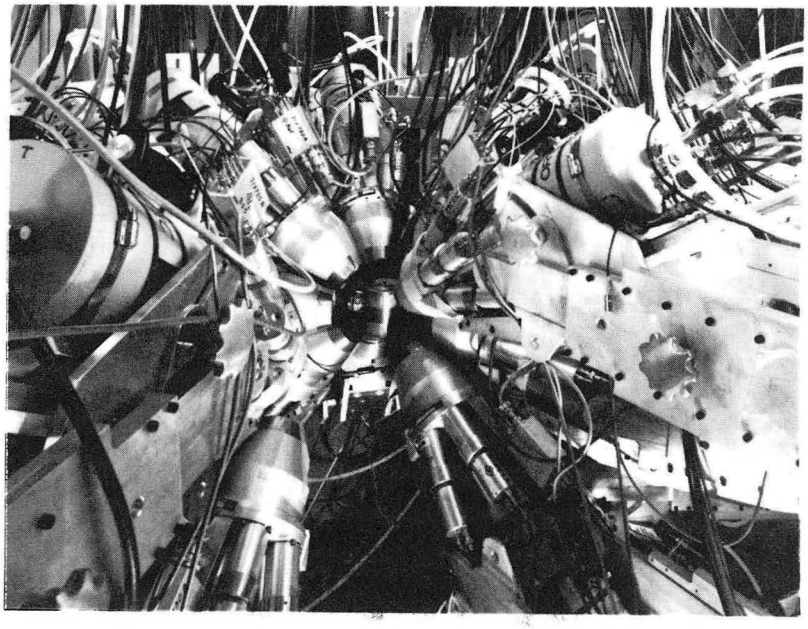

CBB 853-2061

FIGURE 12 Photograph of 15 Compton-suppressed Ge modules (without NaI caps) in place around target chamber. Six more modules are pulled back toward camera to allow access.

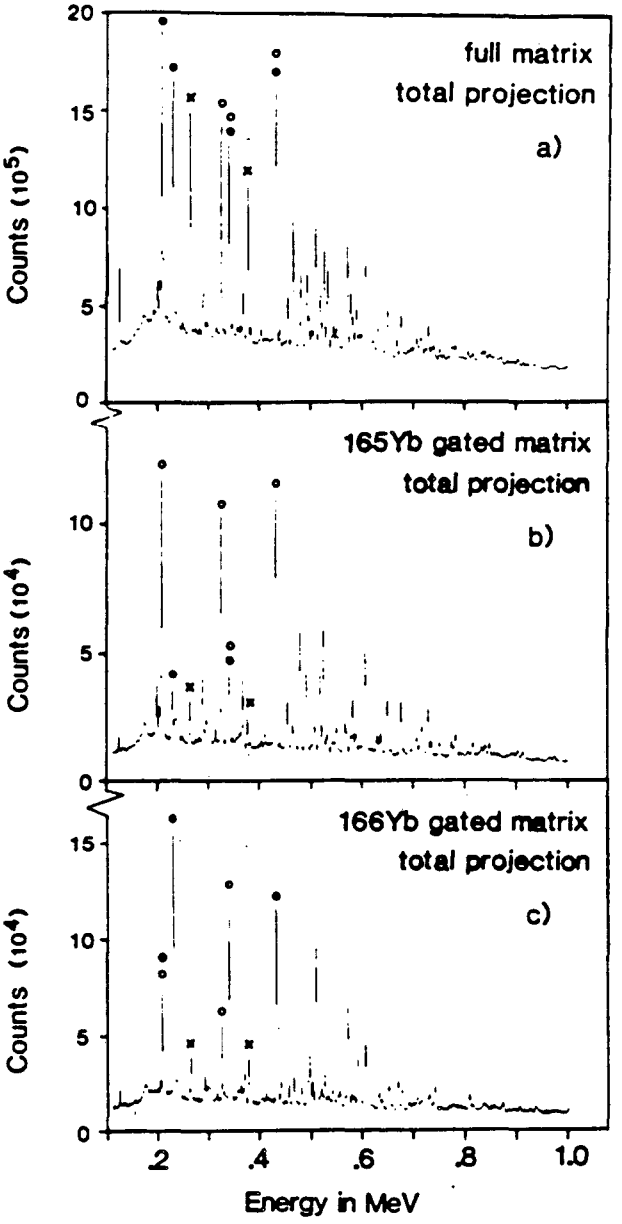

FIGURE 13 Full projections of the two-dimensional γ-coincidence spectra from $^{130}Te(^{40}Ar,xn)^{166-164}Yb$: a) from full matrix; b) from gated matrix in coincidence with discrete lines in ^{165}Yb; c) from gated matrix in coincidence with discrete lines in ^{166}Yb. The strongest lines in ^{165}Yb are marked by open circles, those in ^{166}Yb by full circles, and those in ^{164}Yb by crosses (ref. 24).

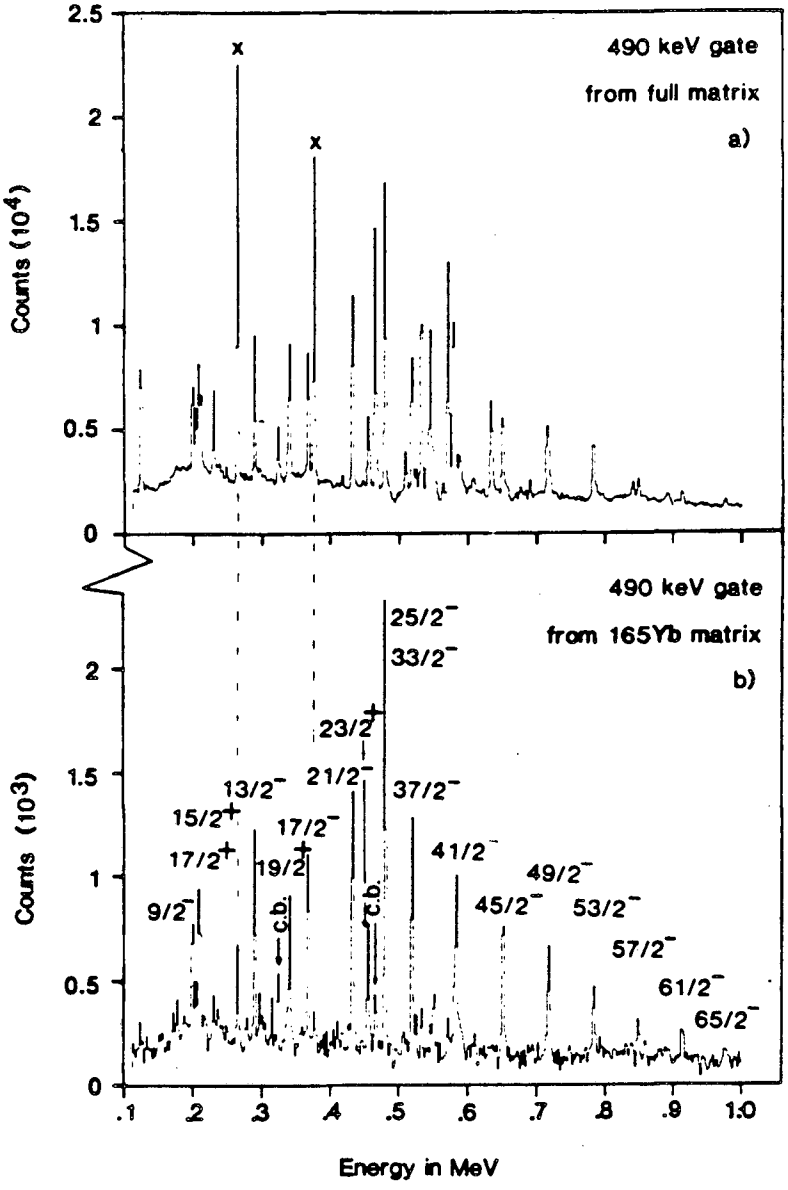

FIGURE 14 Background-subtracted spectra in coincidence with 490 keV ($29/2^- \rightarrow 25/2^-$) transition of ^{165}Yb; a) projection from full matrix (the gate is contaminated by a transition of same energy in ^{164}Yb, whose strongest lines are indicated by crosses); b) projection from gated matrix in coincidence with discrete lines in ^{165}Yb. Only the main transitions in ^{165}Yb in coincidence with the 490 keV gate are labeled with their initial spin; c.b. stands for cross-band transition (ref. 24).

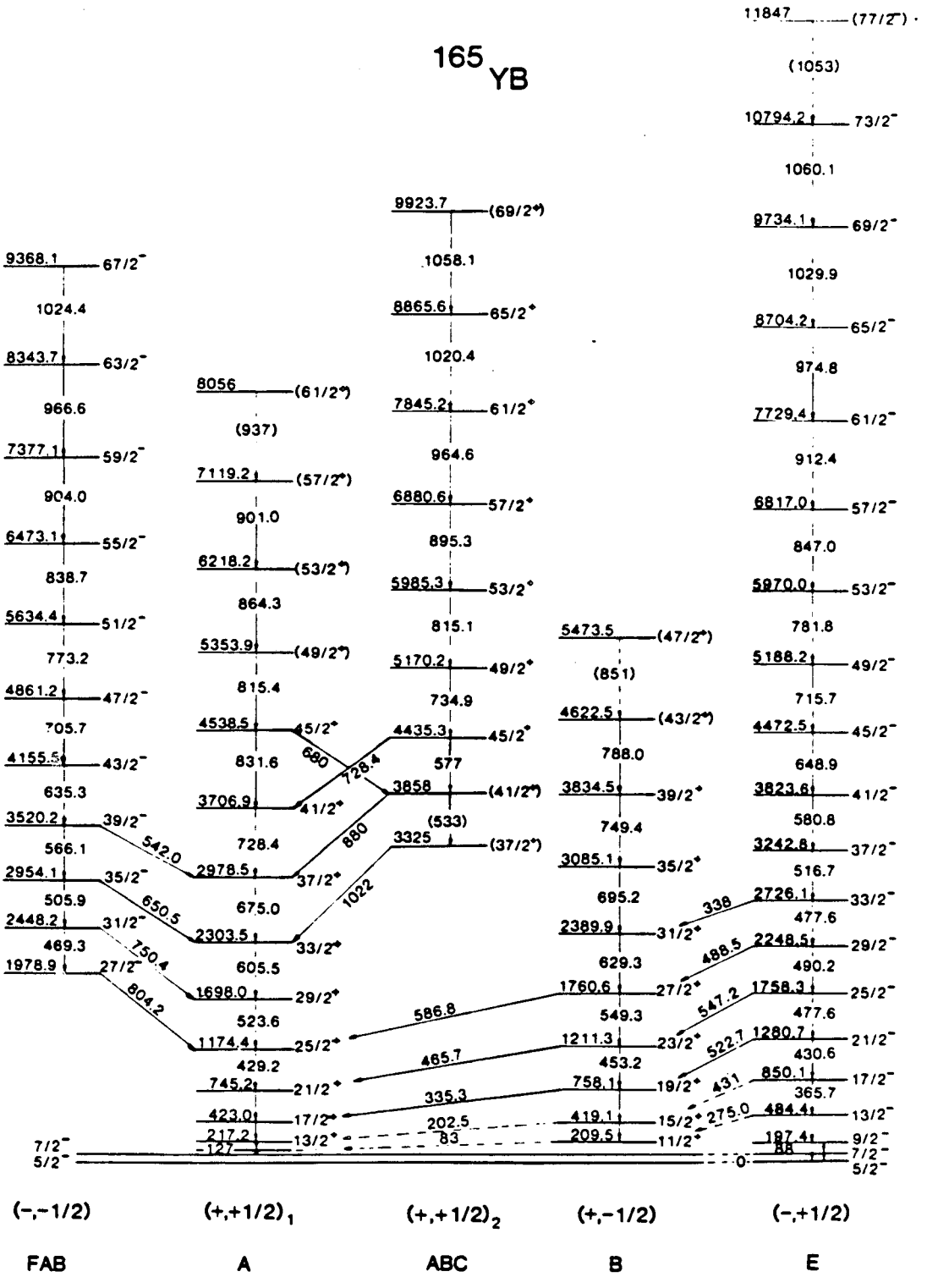

FIGURE 15 Level scheme of ^{165}Yb (ref. 24).

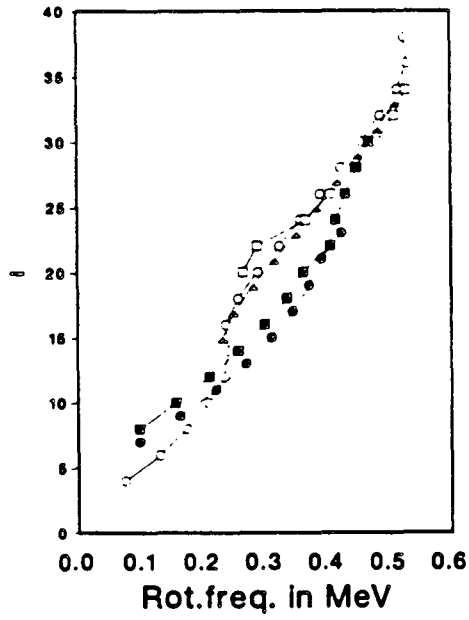

FIGURE 16 Angular momentum I vs rotational frequency for high-spin bands in ^{165}Yb. Full squares represent A band, open squares the ABC band, full circles the B band, open circles the E (EAB after first backbend), and full triangles the FAB band (ref. 24).

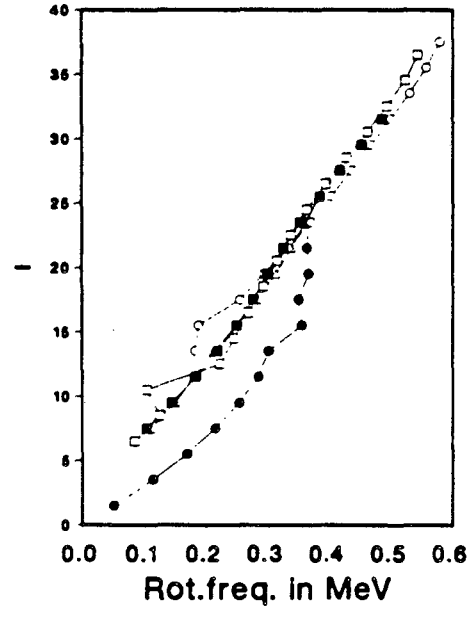

FIGURE 18 Angular momentum I vs rotational frequency for high-spin bands in ^{166}Yb. Full circles mark the paired ground band, open circles the AB band, open squares the AE band, full squares the AF band, and open triangles the BE band (ref. 24).

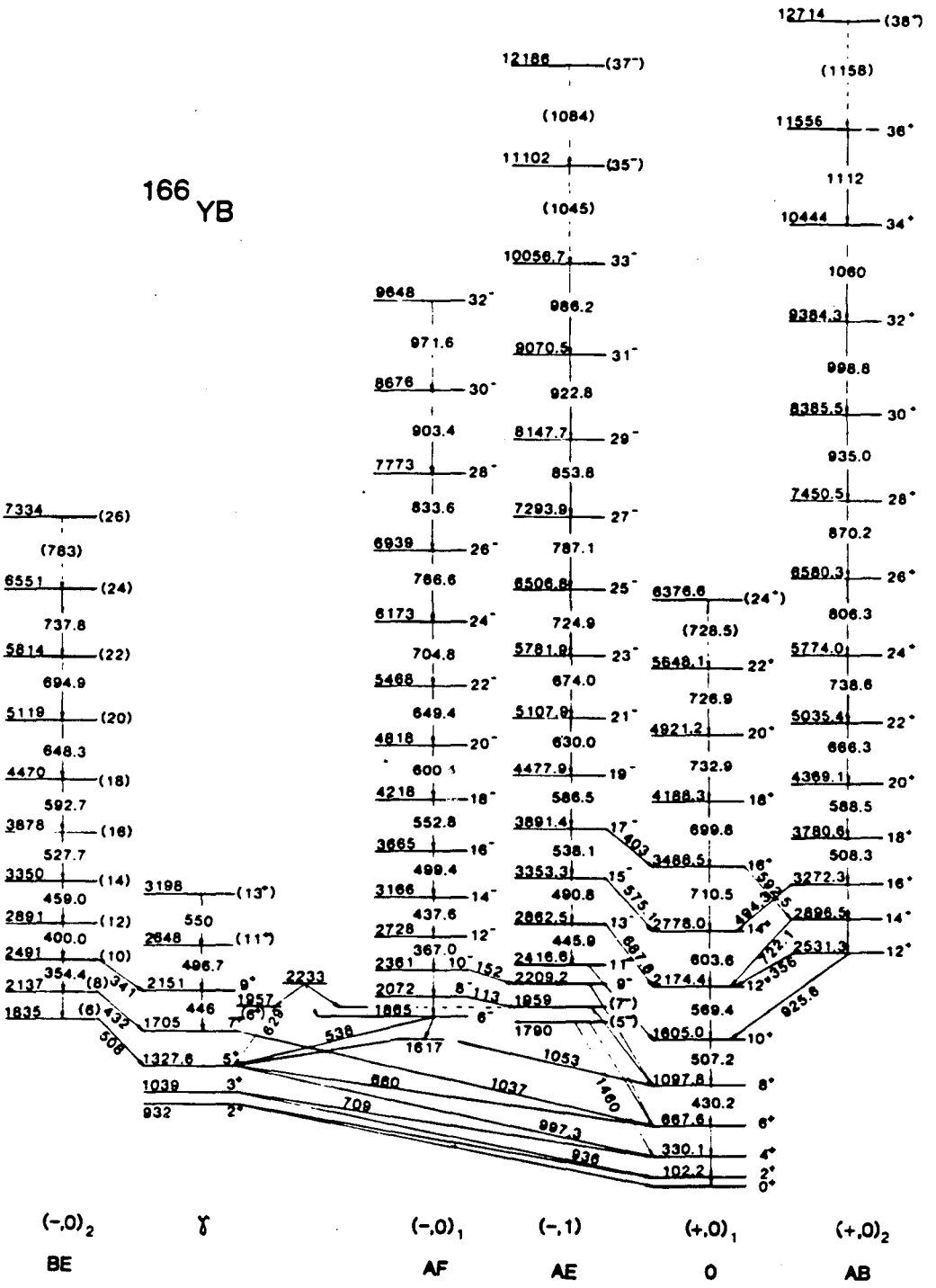

FIGURE 17 Level scheme of ^{166}Yb (ref. 24).

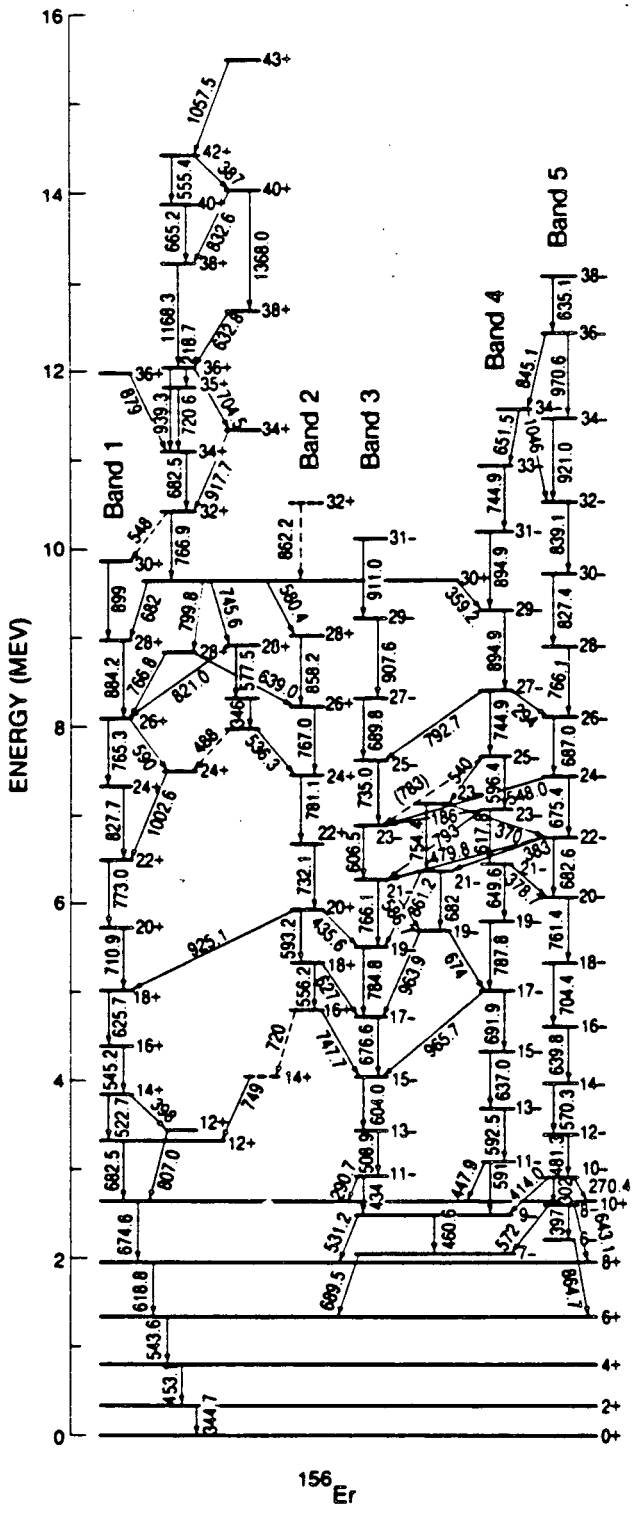

FIGURE 20 Level scheme of ^{156}Er (ref. 46).

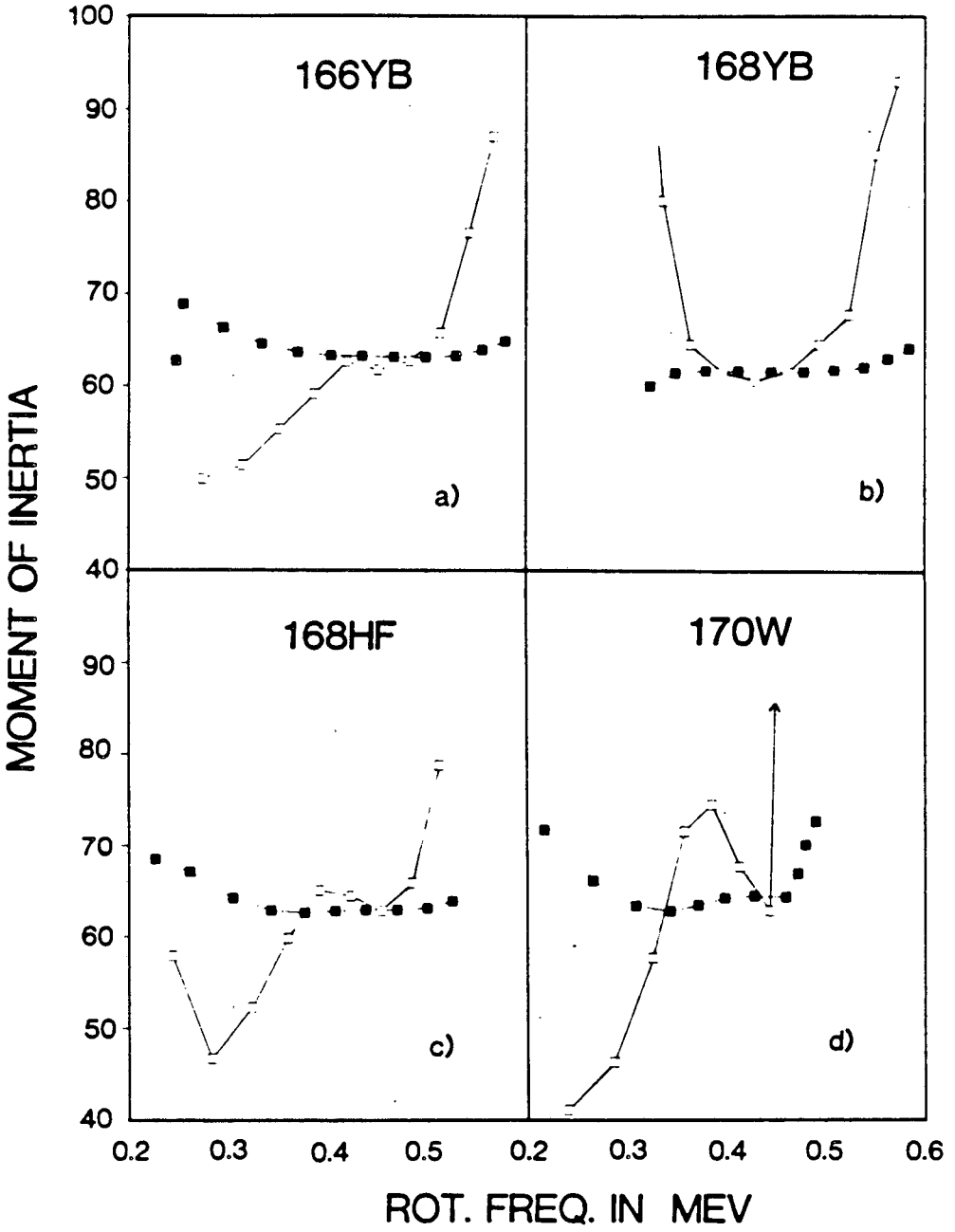

FIGURE 19 Kinematic $\mathcal{J}^{(1)}$ (full squares) and dynamic $\mathcal{J}^{(2)}$ (open squares) moments of inertia in units of $\hbar^2$ MeV^{-1} vs rotational frequency $\hbar\omega$. Data for ^{166}Yb, ^{168}Yb, ^{168}Hf, ^{170}W are taken from refs. 24,30,29,31 respectively.

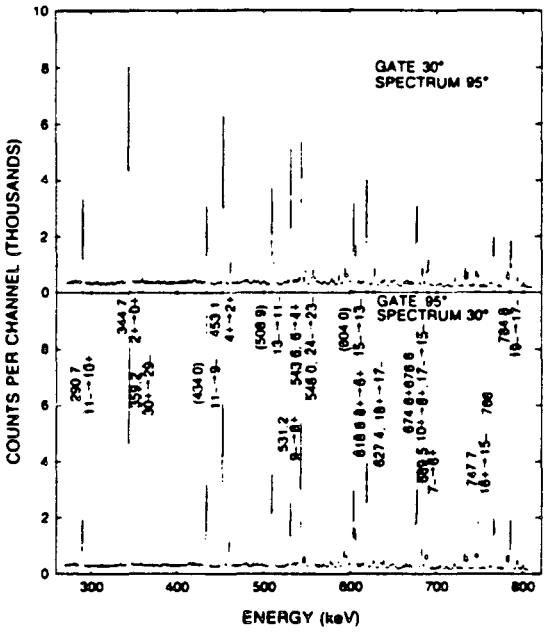

FIGURE 21 Projections on the x (30°) and y (95°) axes of the summed coincidences with three γ rays; 434, 509, and 604 keV (ref. 46).

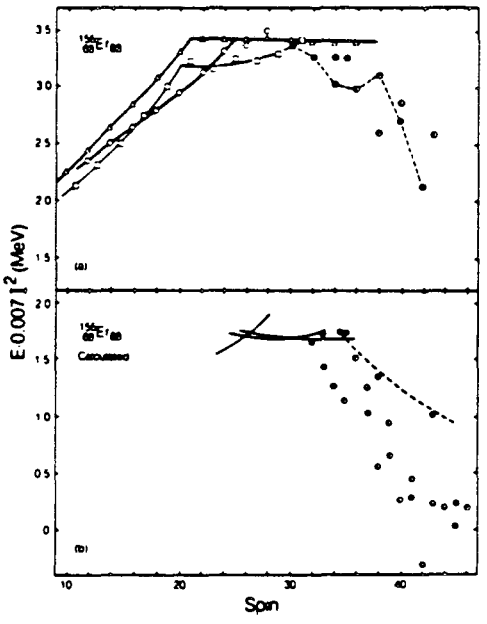

FIGURE 22 Comparison of a) experimental (ref. 46) and b) calculated (ref. 52) energy levels in ^{156}Er, with an average rigid-rotor energy subtracted. Lines connect levels that seem to be related as bands, with the dashed line in a) following the proposed terminating band.

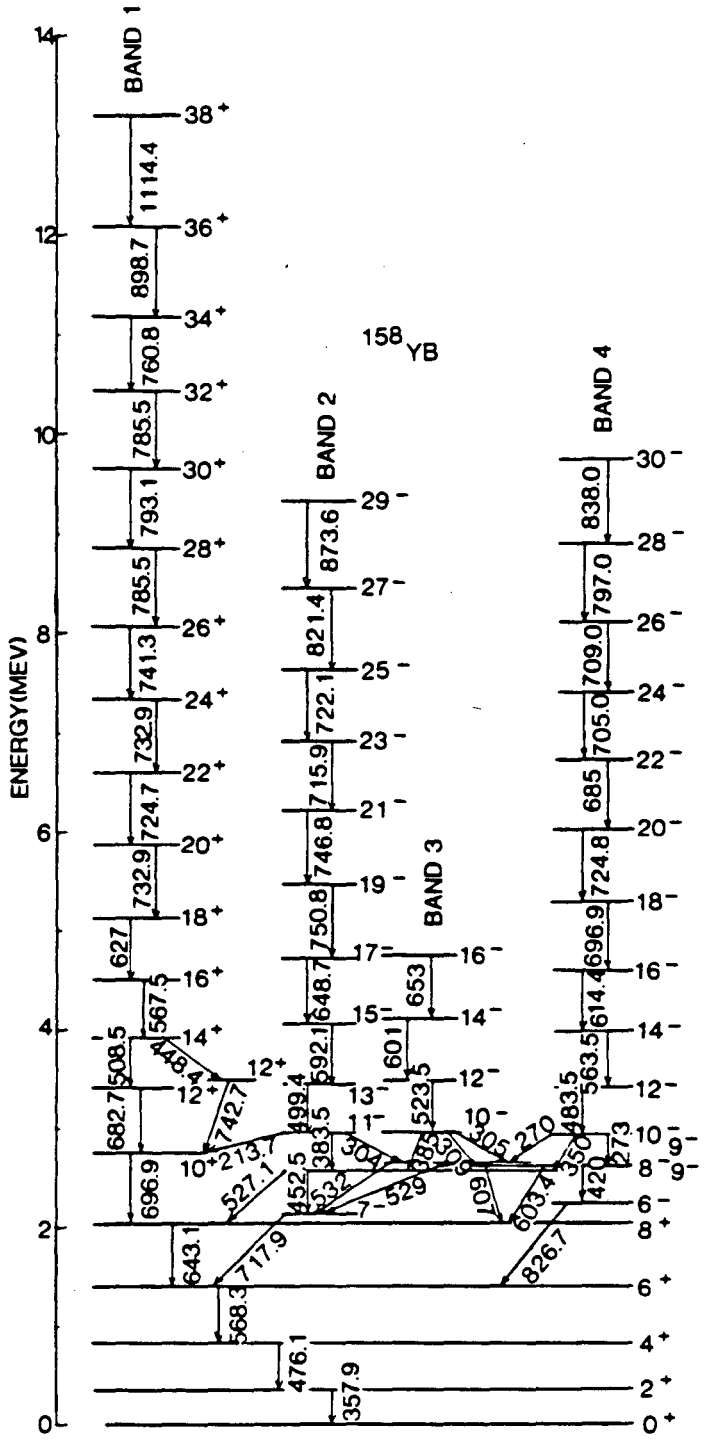

FIGURE 23 Level scheme of ^{158}Yb (ref. 53).

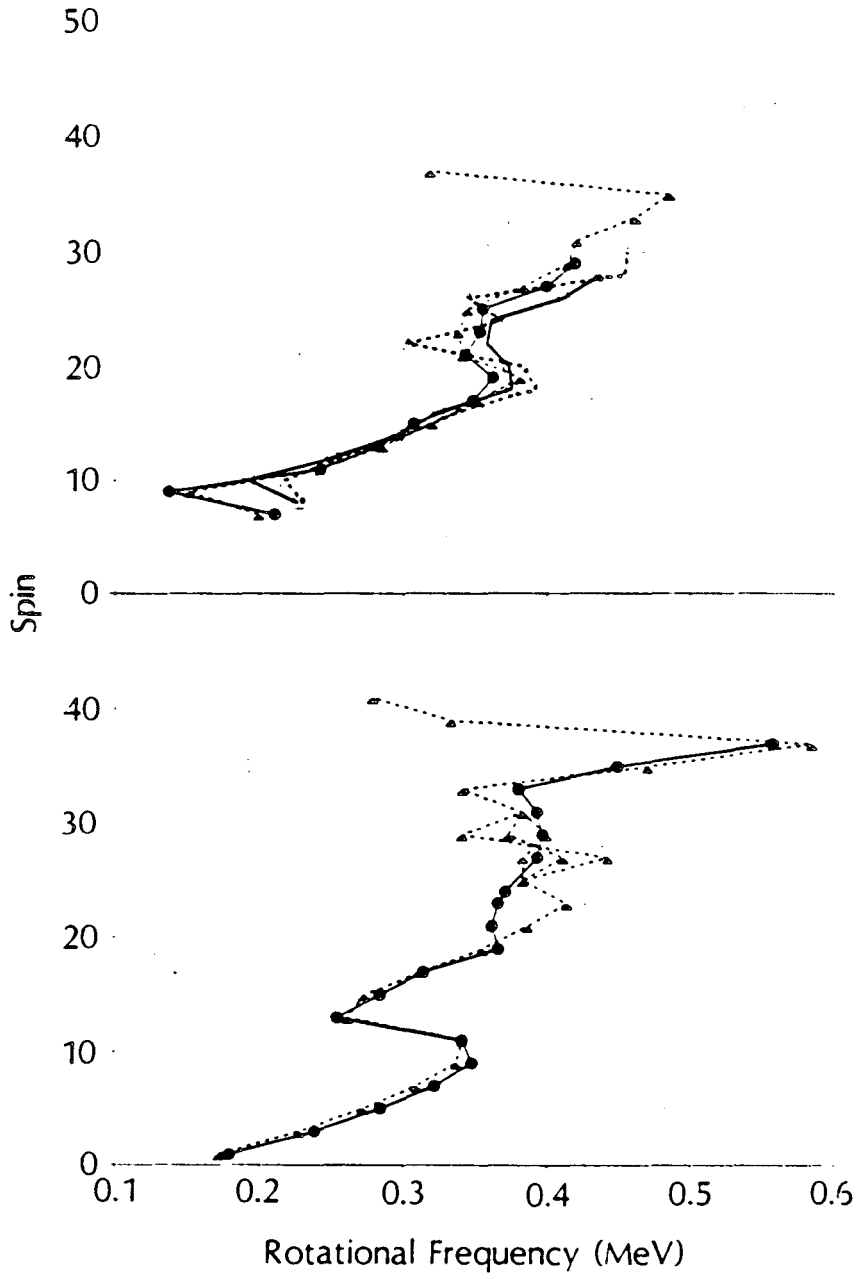

FIGURE 24 Plots of spin $(I_i + I_f)/2$, vs rotational frequency for (bottom) the yrast sequences, band 1, in ^{158}Yb (circles) and ^{156}Er (triangles), and (top) the AE (open symbols) and AF (closed symbols) sequences in the two nuclei (ref. 53).

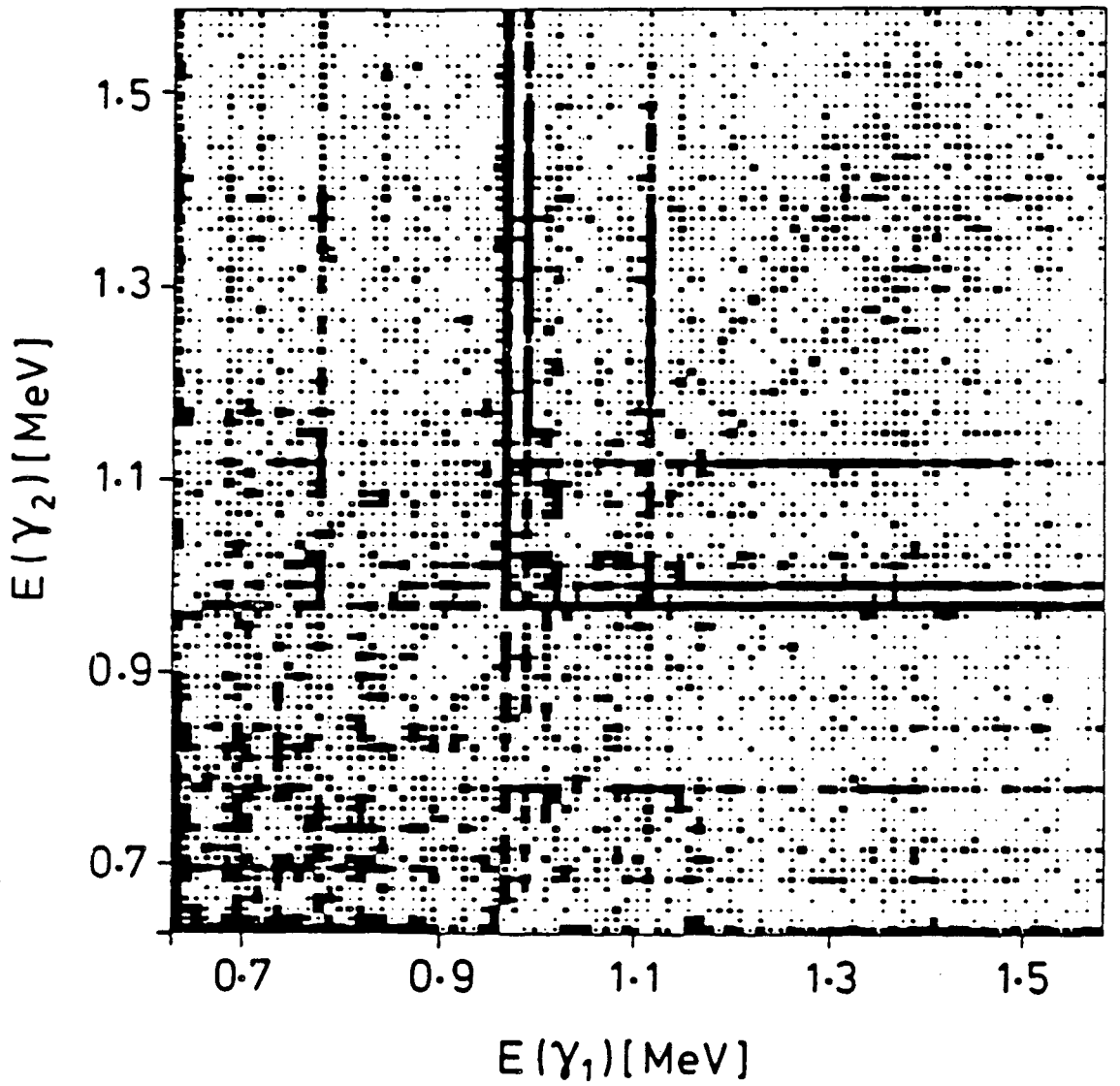

FIGURE 25 Plot of $E(\gamma_1)$ - $E(\gamma_2)$ coincidence matrix in ^{152}Dy following the reaction of 205 MeV ^{48}Ca on ^{108}Pd. The data, taken with Compton-suppressed Ge detectors, have been corrected for the response function and efficiency of the detectors, and have had uncorrelated events subtracted (ref. 64).

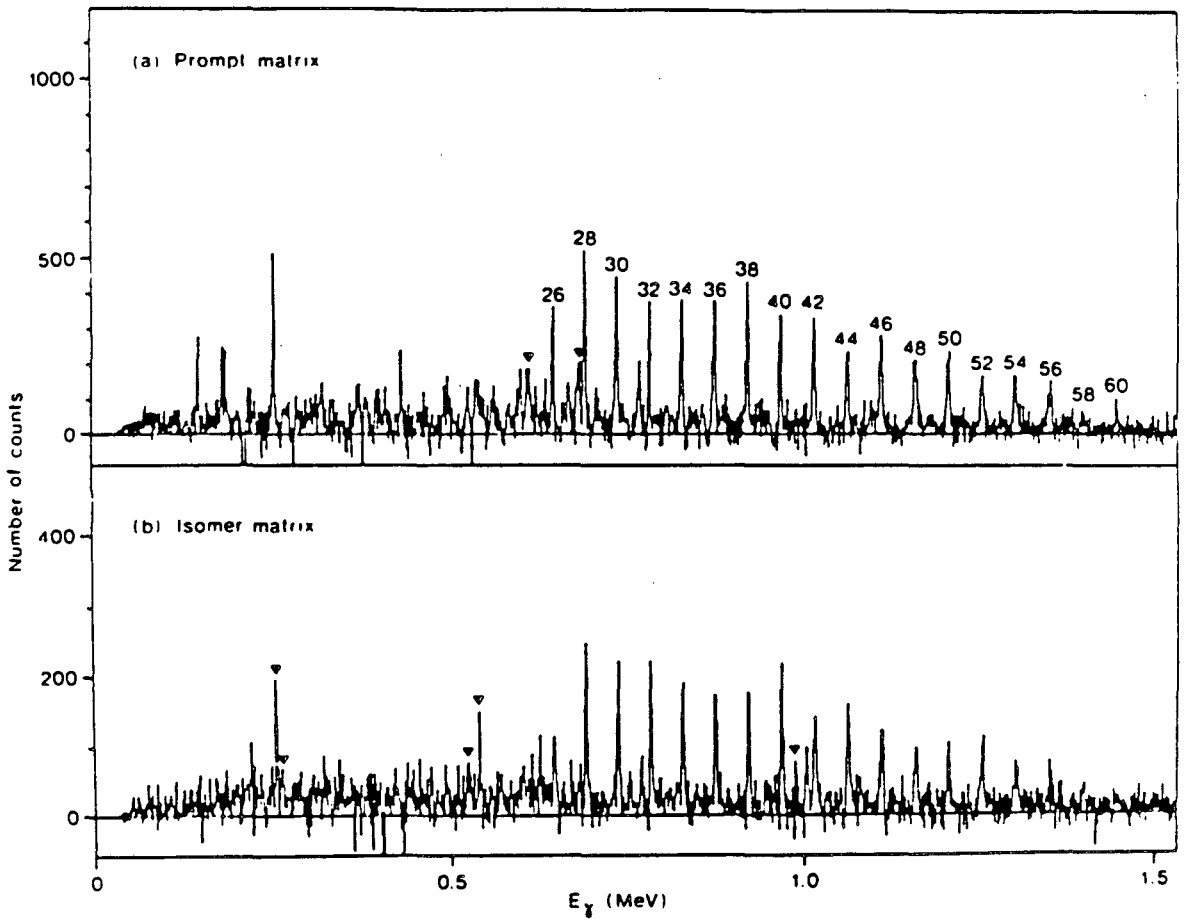

FIGURE 26 Gamma-ray spectra in ^{152}Dy obtained by summation of gates set on most members of the superdeformed band: a) from the "prompt" matrix; b) from the "isomer" matrix. (▼) indicates ground-band transitions $2^+ \rightarrow 0^+$ and $6^+ \rightarrow 4^+$ in a) and transitions between yrast oblate states ranging from 25^- to the isomeric 17^+ (ref. 66).

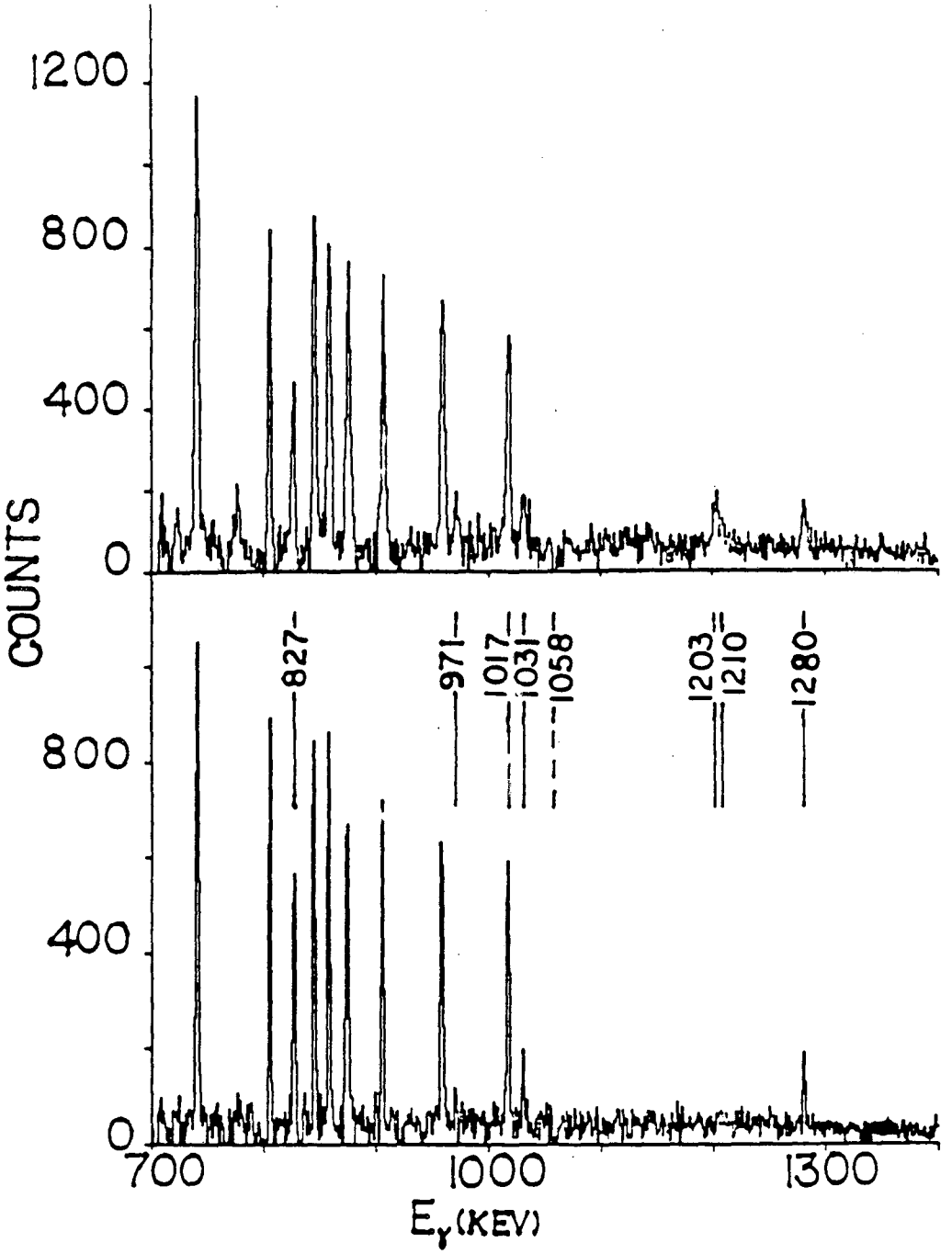

FIGURE 27 Gamma-ray spectrum in coincidence with 1058 keV, $38^+ \rightarrow 36^+$ yrast transition with (top) self-supporting target, and (bottom) gold-backed target (ref. 72).

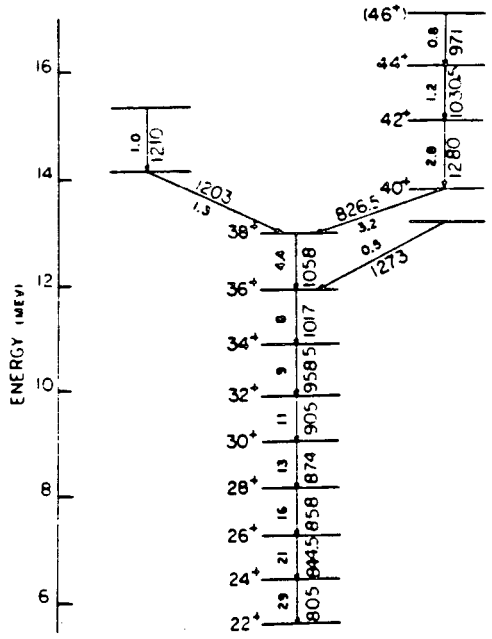

FIGURE 28 Top of the level scheme for the yrast band in ^{158}Er (ref. 72).

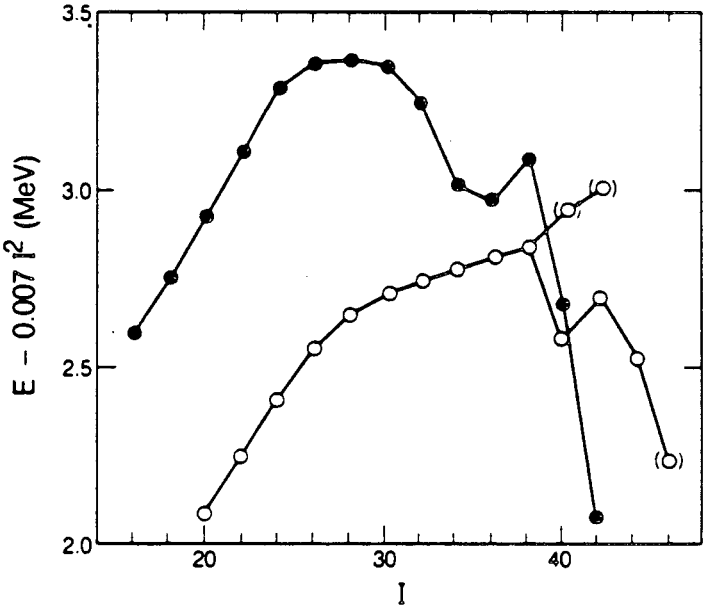

FIGURE 29 Plot of level energy minus rigid-rotor energy vs spin for yrast states in ^{156}Er (full circles) and ^{158}Er (open circles) (ref. 72).

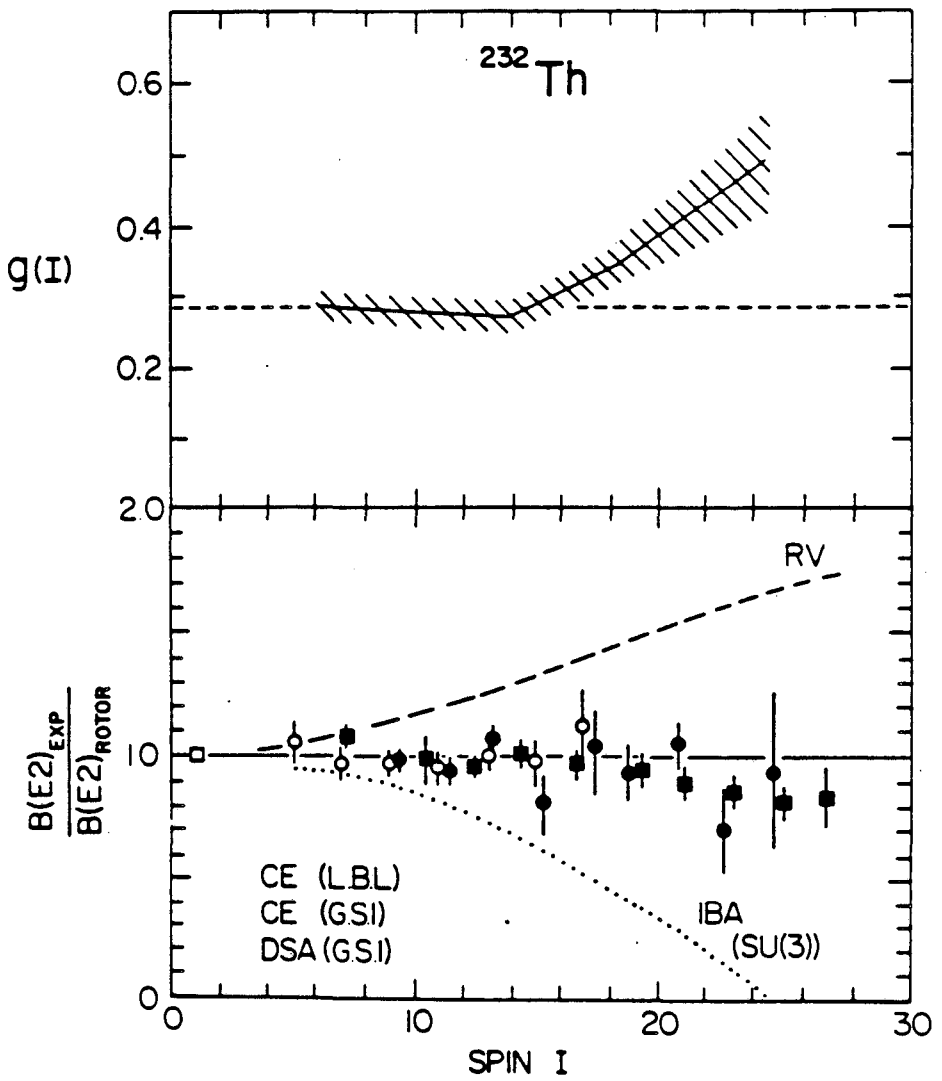

FIGURE 30 Experimental B(E2) values for ^{232}Th ground band normalized to rigid-rotor values derived from the 2 → 0 transition. The dashed line shows Rotation-Vibration model calculations that result from attributing deviations in level energies to centrifugal stretching, and the dotted line is an IBA-1 calculation assuming 12 bosons beyond the ^{208}Pb core and the SU(3) limit. The upper plot shows the measured g-factors for the ground-band states. The cross-hatched region reflects the experimental uncertainty (ref. 84).

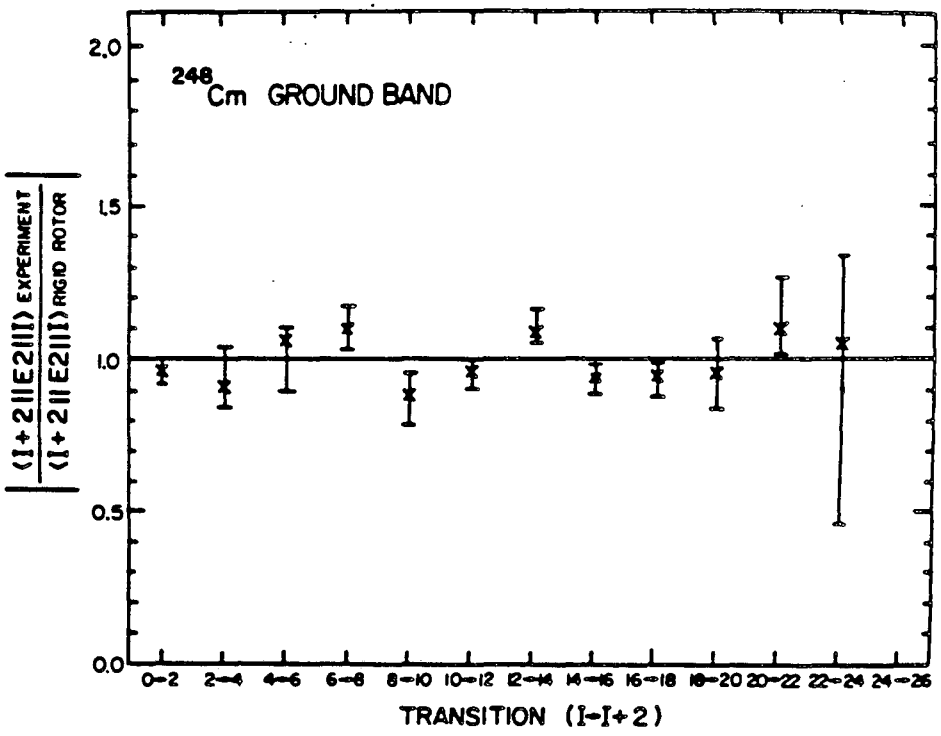

FIGURE 31 Experimental transition matrix elements for ^{248}Cm ground band normalized to rigid-rotor values derived from the B(E2; $0^+ \rightarrow 2^+$) (ref. 88).

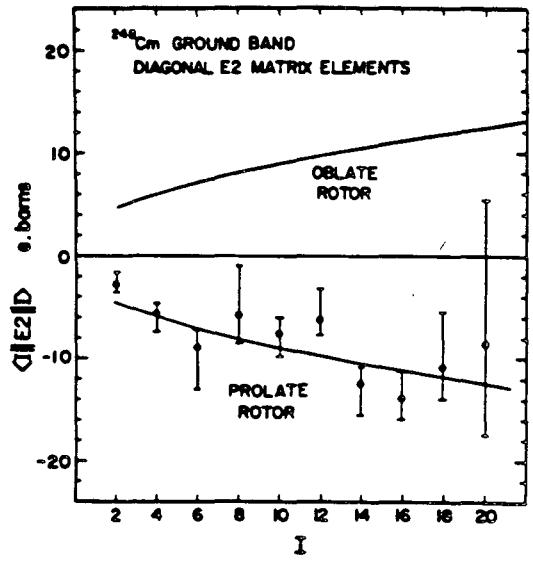

FIGURE 32 Diagonal E2 matrix elements for ^{248}Cm ground-band states. The curves indicate the prolate and oblate values calculated from the rigid-rotor transition elements shown in fig. 31 (ref. 88).

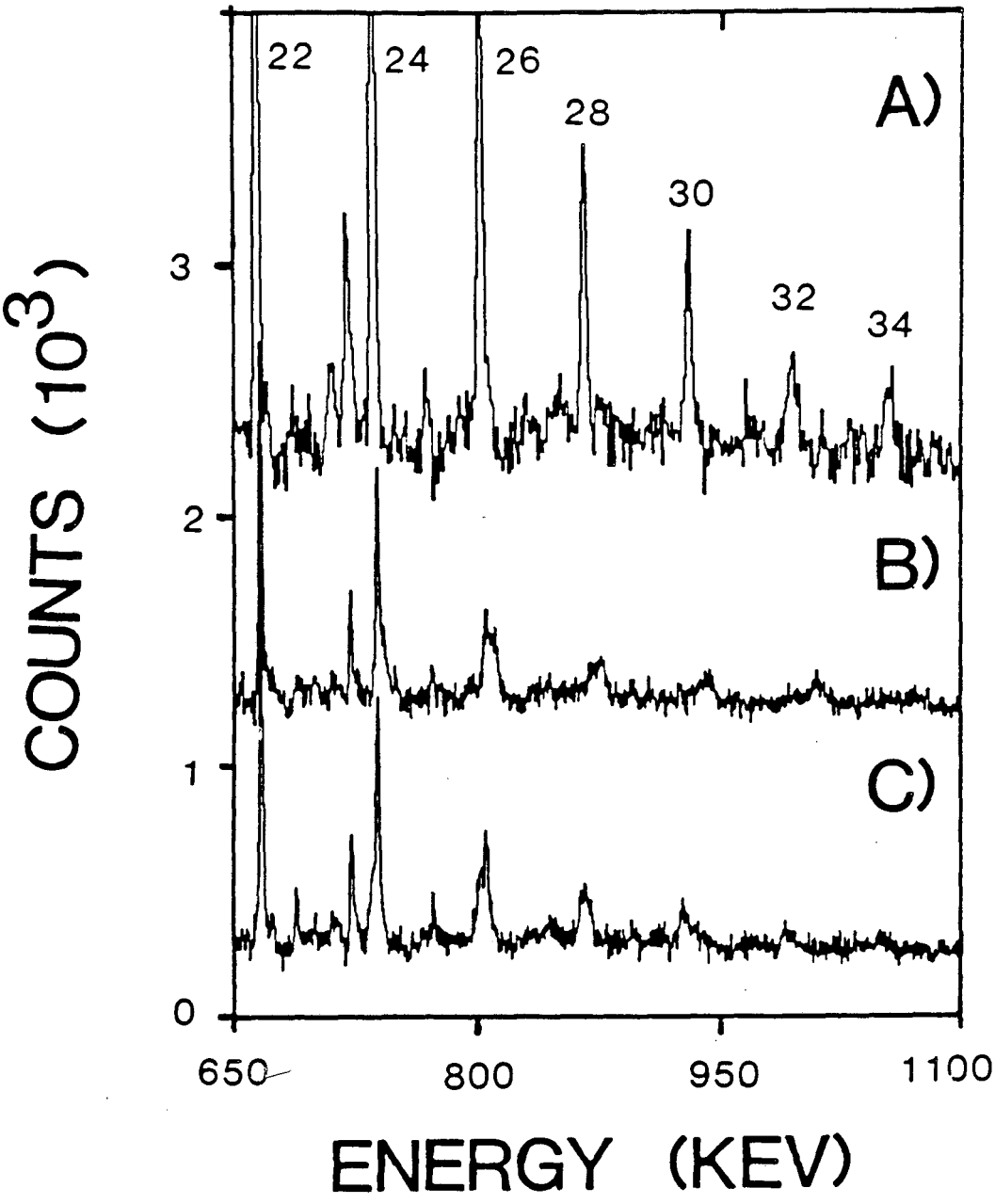

FIGURE 33 Summed ^{166}Yb spectra gated by transitions from 16^+, 18^+, 20^+, and 22^+ yrast states: A) with unbacked target (1000 counts offset); with gold-backed target and detectors at B) <45°> angle (1000 counts offset), and C) <121°> angle to the beam direction (ref. 90).

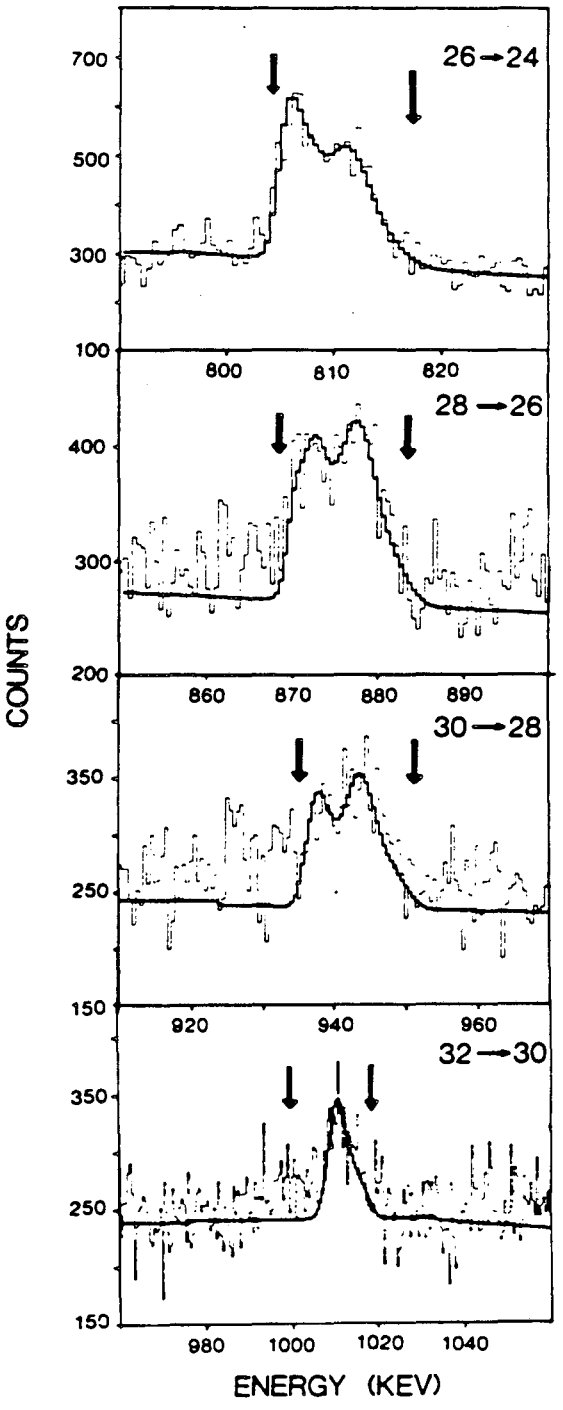

FIGURE 34 Fits to some of peaks shown in fig. 33B. The stopped (left arrow), and fully shifted (right arrow) positions are shown for each peak (ref. 90).

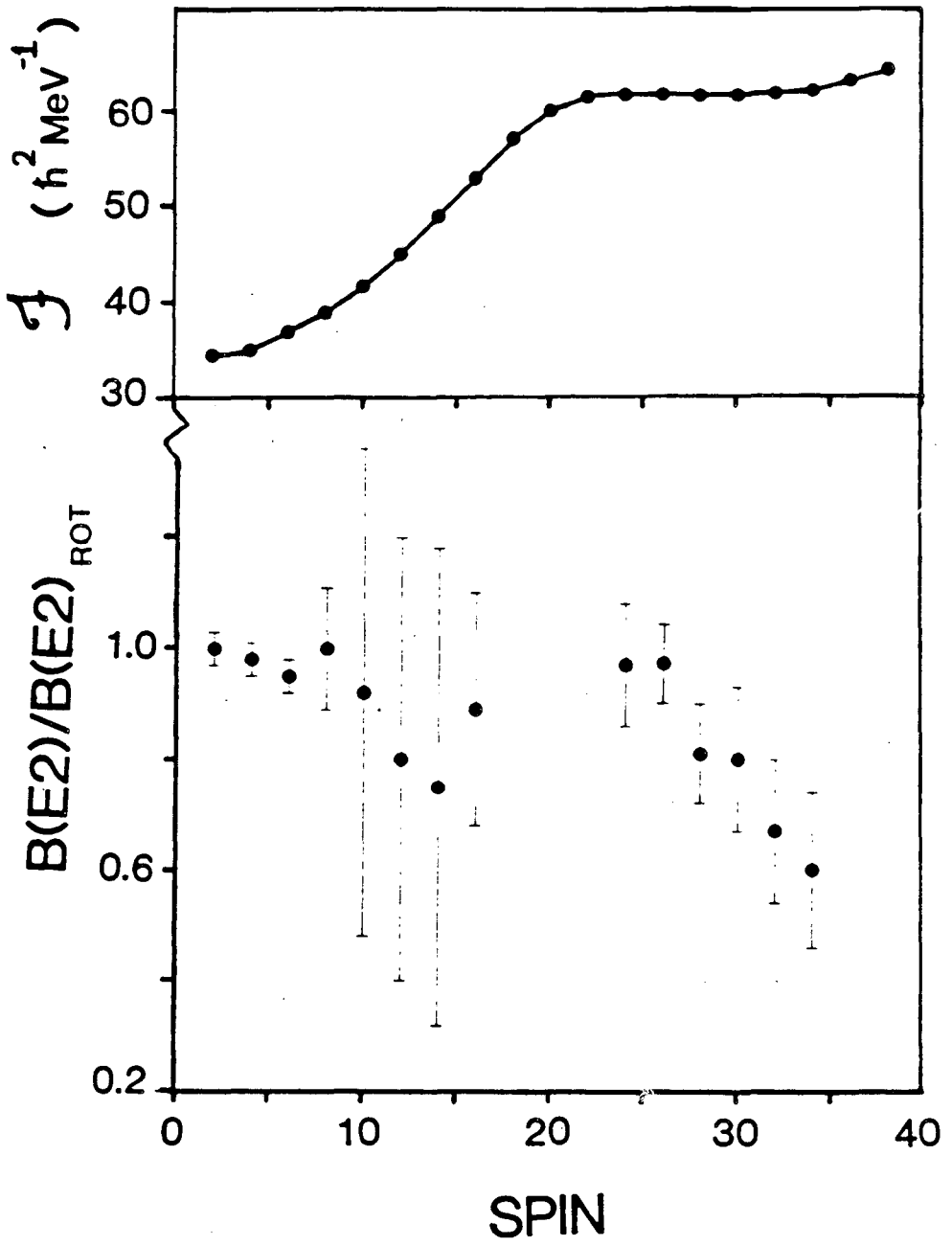

FIGURE 35 Values of B(E2)/B(E2)$_{rot}$ and (top) moment of inertia vs spin are shown for ^{166}Yb yrast states. The low spin (<20$^+$) data for the B(E2)'s are from ref. 77; the moment of inertia data are from ref. 24.

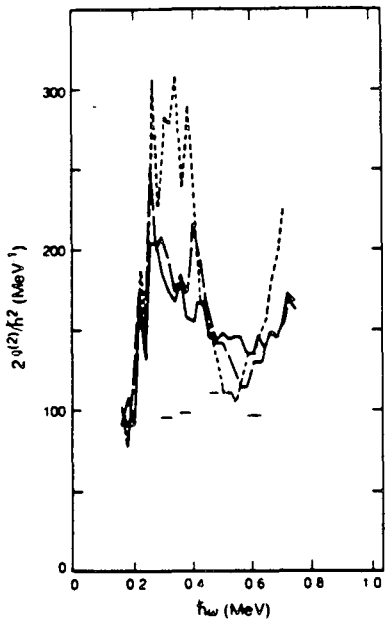

FIGURE 38 Feeding-corrected spectra in coincidence with high-spin sum-spectrometer slices for ^{160}Er (solid line), ^{158}Er (long-dashed line), ^{156}Er (short-dashed line). The thin dashes indicate values of $J^{(2)}_{band}$ for ^{160}Er extracted from γ-γ correlation data (ref. 111).

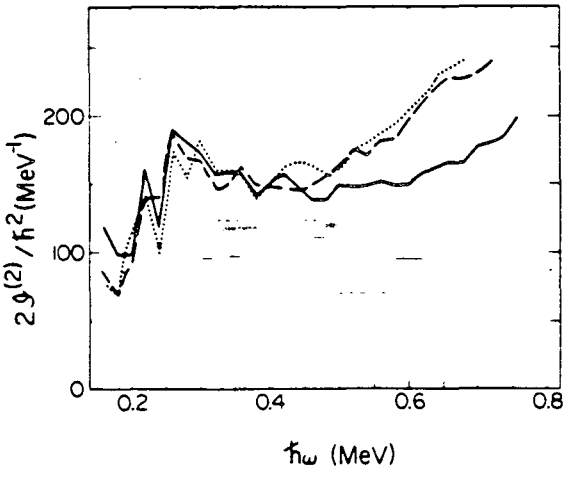

FIGURE 39 Plots of $2J^{(2)}_{eff}/J^2$ vs $\hbar\omega$ from NaI spectra after unfolding, subtracting the statistical component, and then correcting for partial feeding. The curves are for compound nuclei made by 185 MeV ^{40}Ar on: ^{124}Sn (thick solid line), ^{126}Te (dotted line), ^{130}Te (thick dashed line). Also shown are the values of $J^{(2)}_{band}$ for ^{124}Sn (thin solid lines) and and ^{130}Te (thin dashed lines) targets (ref. 110).

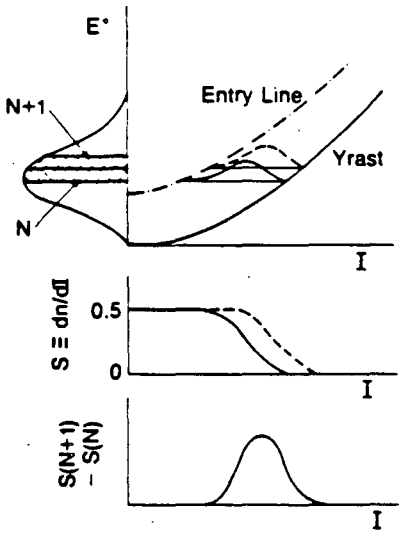

FIGURE 36 Schematic illustration of the feeding-correction method: (top) two neighboring sum-energy slices (N and N + 1) sample the two similar, but slightly shifted, spin-feeding distributions shown; from the difference in their associated spectra (middle) we obtain a curve (bottom) close to the average of the initial spin-feeding curves (ref. 115).

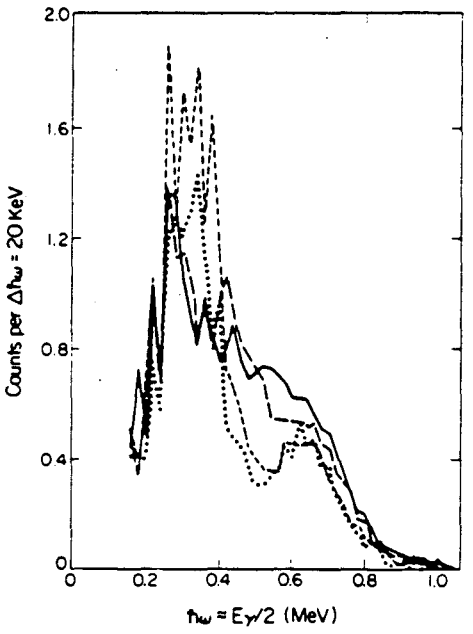

FIGURE 37 Sodium-iodide γ-ray spectra (after unfolding and subtracting a statistical component) for $^{124}Sn + ^{40}Ar$ (solid line), $^{122}Sn + ^{40}Ar$ (long-dashed line), $^{120}Sn + ^{40}Ar$ (short-dashed line), $^{118}Sn + ^{40}Ar$ (dotted line) (ref. 112).

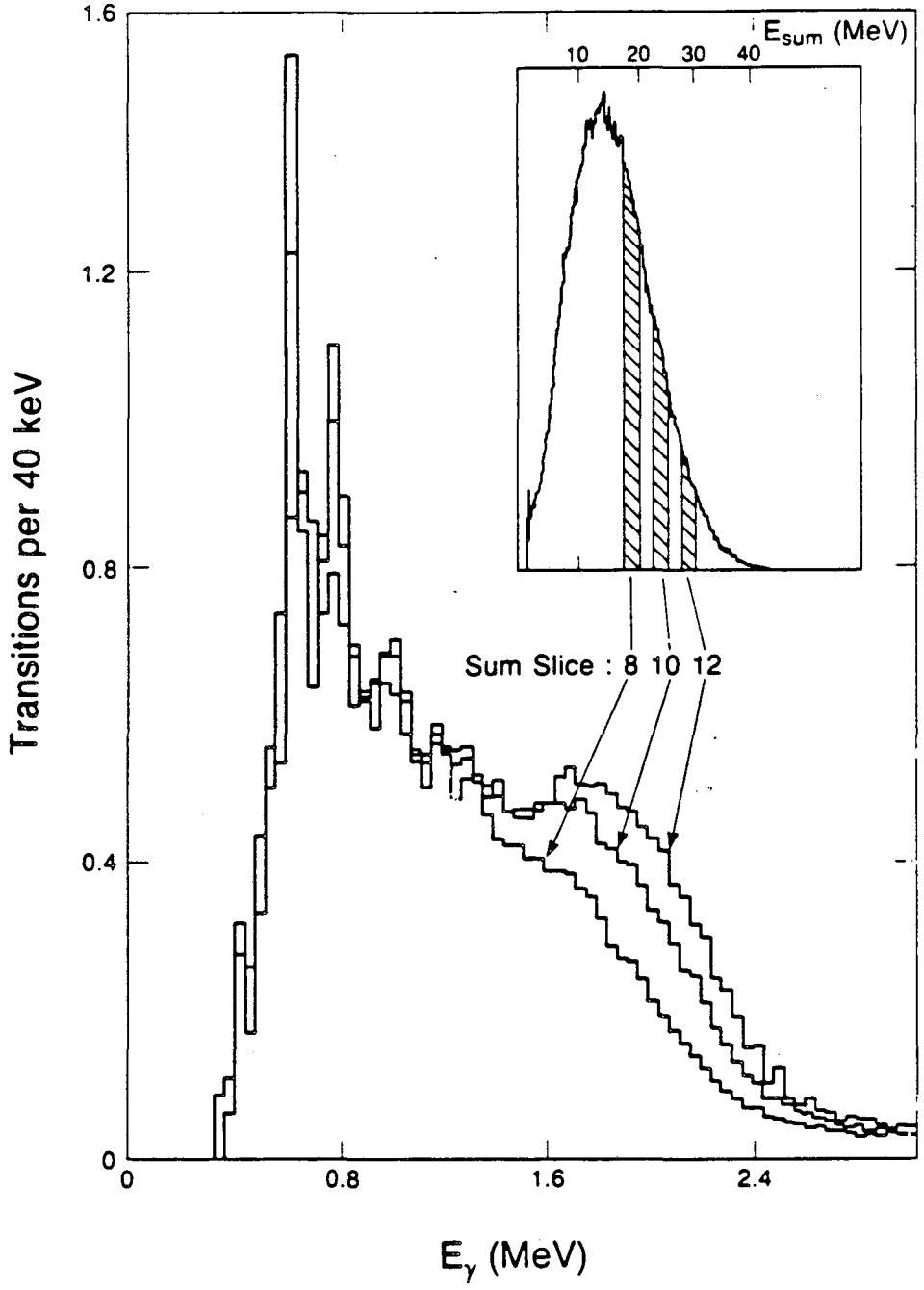

FIGURE 40 Normalized unfolded spectra for the reaction $^{40}Ar + ^{82}Se$ in coincidence with different sum slices as shown in insert. The slices are 2.5 MeV wide and are numbered starting from 0 MeV (ref. 115).

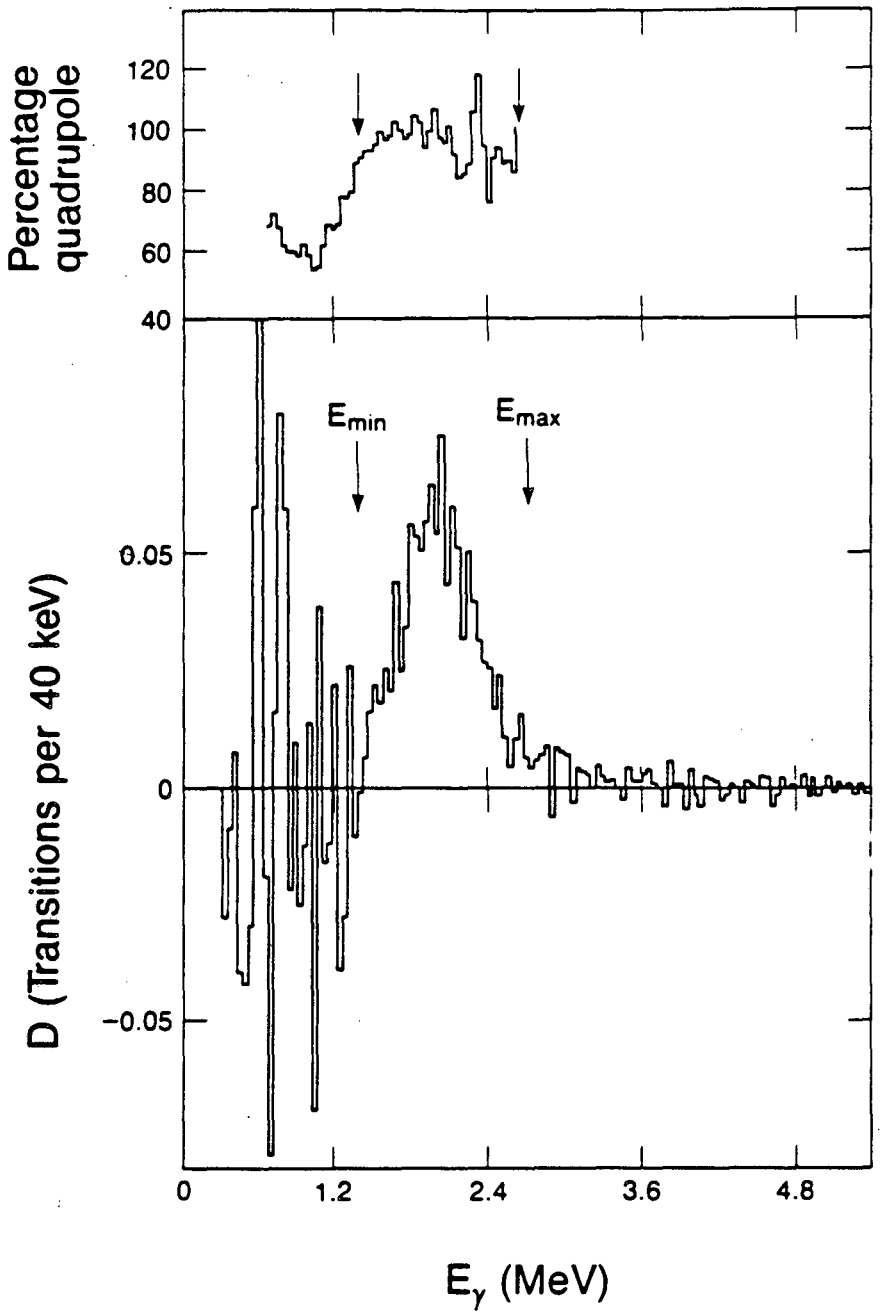

FIGURE 41 A typical difference spectrum (from the spectra in fig. 40) used to generate the feeding correction factor. The integration region (E_{min},E_{max}) is indicated by the arrows. On top the angular distribution results are shown as the percentage of stretched quadrupole transitions.

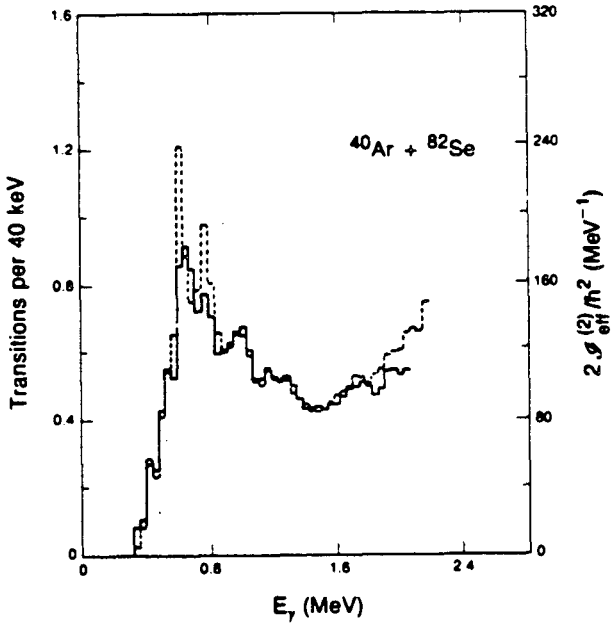

FIGURE 42 Feeding-corrected spectra from fig. 40 (slice 8, full line, and slice 10, dashed line). The results are plotted up to a correction factor of 4 and the moment of inertia scale is only relevant for $E_\gamma > 1.2$ MeV.

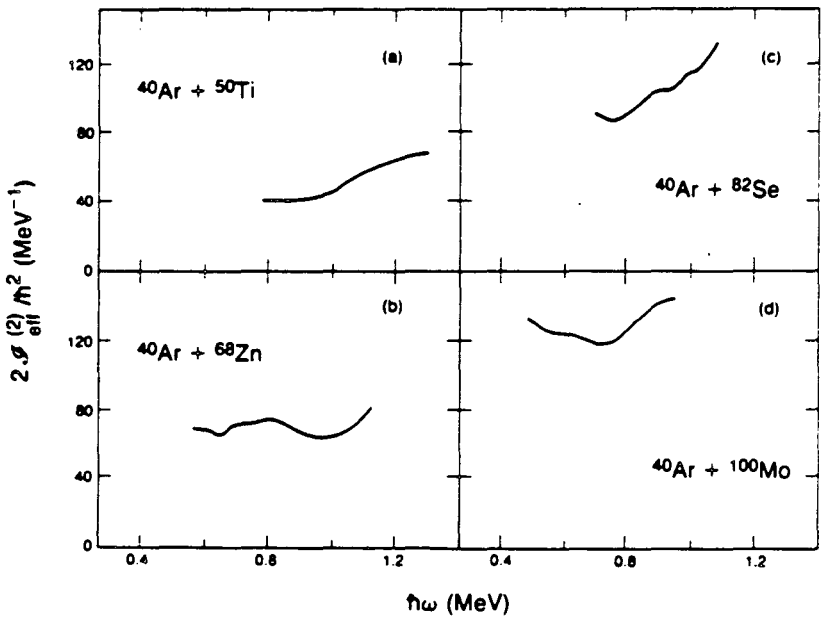

FIGURE 43 Values of $\mathcal{J}^{(2)}_{eff}$ for the product of the indicated reactions (ref. 115).

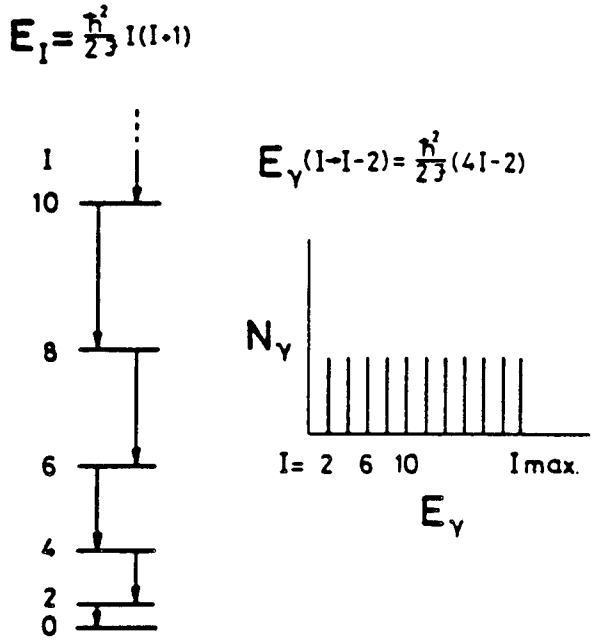

FIGURE 44 A schematic rotational band (left), and the resulting γ-ray spectrum from an initial state of spin I_{max} (right).

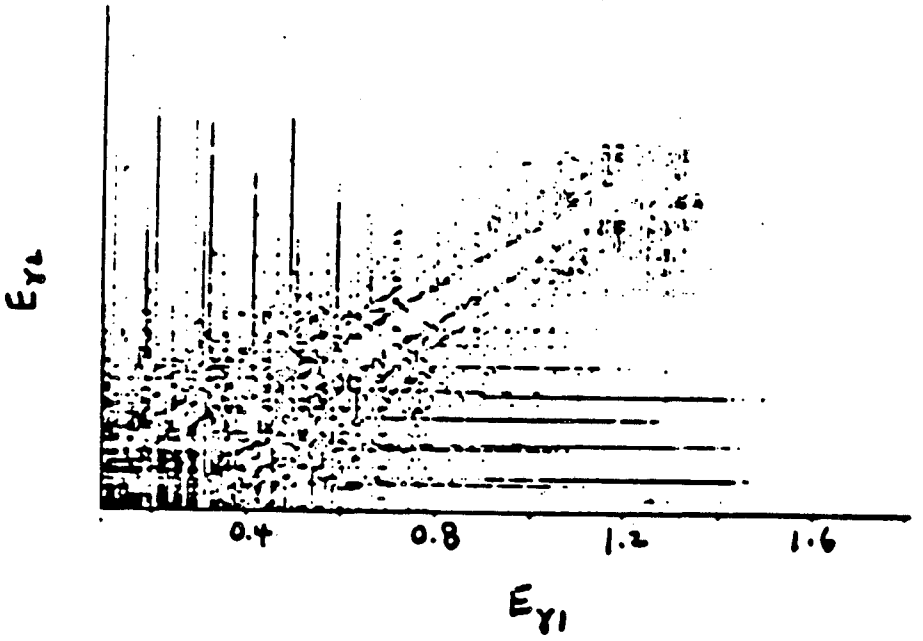

FIGURE 45 Plot of $E_\gamma(2)$ vs $E_\gamma(1)$ for ^{166}Yb coincidences after subtracting ucorrelated components. The diagonal valley and three pairs of ridges can be seen, as well as "stripes" involving coincidences with the strongest discrete transitions.

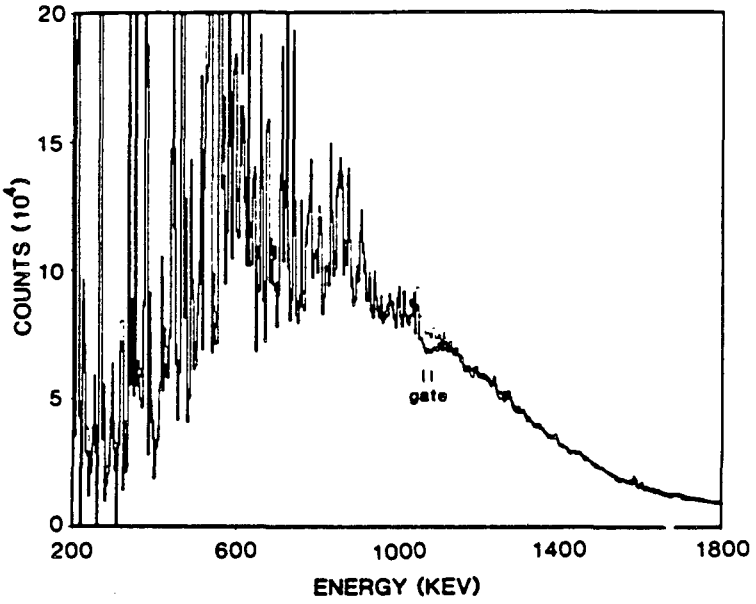

FIGURE 48 Spectra from $^{124}Sn(^{40}Ar,xn)^{160,159}Er$. The lighter line is the full projection of all coincidences, whereas the darker one is coincident with the narrow gate indicated. The original two-dimensional matrix had been unfolded first (ref. 119).

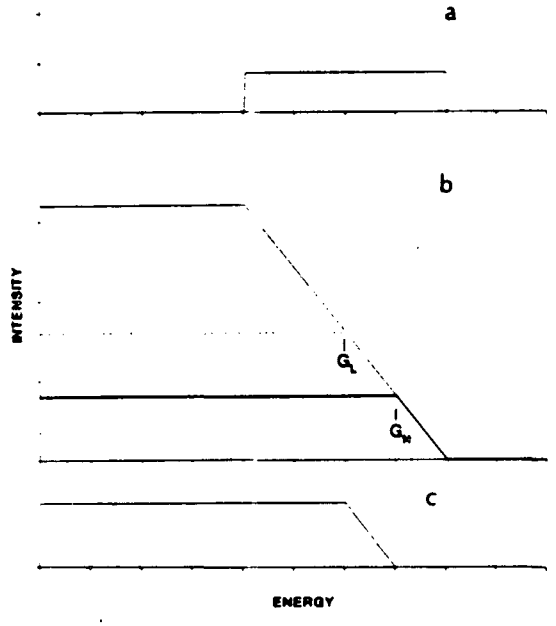

FIGURE 49 Schematic illustration of a) a plausible feeding curve following a heavy-ion fusion reaction, b) the spectra coincident with gates G_H (heavy line) and G_L (dashed line), and c) the difference of the two gated spectra (ref. 119).

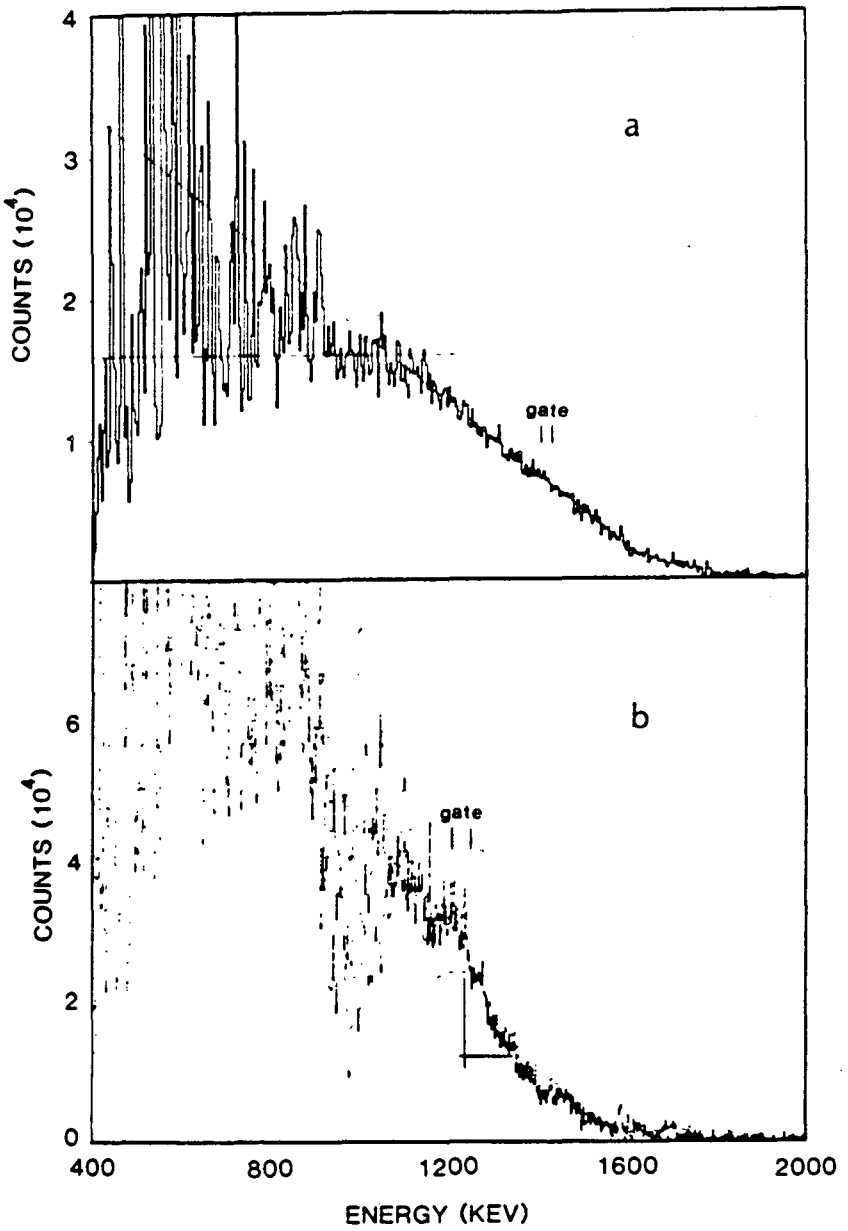

FIGURE 50 a) The Ge spectrum (see caption to fig. 48, but the matrix here also had the statistical transitions subtracted) coincident with a gate at 1.4 MeV. The lines (to guide the eye) indicate the two regions of the spectrum (see text). b) The difference between spectra gated at 0.94, 0.98, or 1.02 MeV and one gated at 1.22 MeV. The dashed line indicates an estimated removal of the narrow dip, and the solid lines are the gate position (vertical) and the half-height level (horizontal) (ref. 119).

This report was done with support from the Department of Energy. Any conclusions or opinions expressed in this report represent solely those of the author(s) and not necessarily those of The Regents of the University of California, the Lawrence Berkeley Laboratory or the Department of Energy.

Reference to a company or product name does not imply approval or recommendation of the product by the University of California or the U.S. Department of Energy to the exclusion of others that may be suitable.

LAWRENCE BERKELEY LABORATORY
TECHNICAL INFORMATION DEPARTMENT
UNIVERSITY OF CALIFORNIA
BERKELEY, CALIFORNIA 94720